

# POLITECNICO DI TORINO

DIPARTIMENTO DI INGEGNERIA MECCANICA E AEROSPAZIALE

## Master Degree in Biomedical Engineering



## Arrhythmia Detection based on Photoplethysmography

**Supervisor**

Prof. Gabriella OLMO

**Tutor**

Ing. Alessandro GUMIERO

**Candidate**

Cristina CIPPITELLI

Matricola 242993

**Academic Year**

2018 - 2019





# List of Acronyms

<b>AC</b>	Alternating Current
<b>AF</b>	Atrial Fibrillation
<b>ANC</b>	Adaptive Noise Cancellation
<b>AV</b>	Atrio-Ventricular
<b>CVI</b>	Chronic Venous Insufficiency
<b>DC</b>	Direct Current
<b>BCU</b>	Body Control Unit
<b>BLE</b>	Bluetooth Low Energy
<b>BPM</b>	Beats Per Minute
<b>ECG</b>	Electrocardiogram
<b>FIR</b>	Finite Impulse Response
<b>FN</b>	False Negative
<b>FP</b>	False Positive
<b>HR</b>	Heart Rate
<b>HRL</b>	High Reliability Level
<b>HRV</b>	Heart Rate Variability
<b>IBI</b>	Inter Beat Interval
<b>ICT</b>	Information and communication technologies
<b>ILR</b>	Implantable Loop Recorder
<b>LED</b>	Led Emitting Diode
<b>LRL</b>	Low Reliability Level
<b>LOA</b>	Limit Of Agreement

<b>MRL</b>	Medium Reliability Level
<b>NIR</b>	Near-Infrared
<b>NSR</b>	Normal Sinus Rhythm
<b>PCA</b>	Principal Component Analysis
<b>PPG</b>	Photoplethysmography
<b>PPI</b>	Peak to Peak Interval
<b>PSD</b>	Power Spectral Density
<b>PVB</b>	Premature Ventricular Beat
<b>PVC</b>	Premature Ventricular Contraction
<b>PWB</b>	Pulse Wave Begin
<b>PWD</b>	Pulse Wave Duration
<b>PWE</b>	Pulse Wave End
<b>PWV</b>	Pulse Wave Velocity
<b>RIIV</b>	Respiratory Induced Intensity Variations
<b>SA</b>	Sino-Atrial
<b>SNR</b>	Signal to Noise Ratio
<b>SpO2</b>	Peripheral blood Oxygen Saturation
<b>TN</b>	True Negative
<b>TP</b>	True Positive
<b>VF</b>	Ventricular Fibrillation
<b>VT</b>	Ventricular Tachycardia
<b>WBAN</b>	Wireless Body Area Network
<b>WBAS</b>	Wireless Body Area Sensor

# Contents

<b>I</b>	<b>Introduction</b>	<b>15</b>
	<b>Project Aim</b>	<b>17</b>
<b>1</b>	<b>Telehealth</b>	<b>19</b>
1.1	Wearable Body Area Sensors . . . . .	22
1.1.1	Application of Wearables in Telehealth . . . . .	23
<b>2</b>	<b>Theoretical Framework</b>	<b>25</b>
2.1	Cardiovascular System . . . . .	25
2.1.1	Heart's Electrical Conduction System . . . . .	26
2.1.2	Arrhythmia . . . . .	28
2.1.3	Arrhythmia Diagnosis in Clinic . . . . .	35
2.2	Photoplethysmography . . . . .	36
2.2.1	Light Propagation Principles . . . . .	37
2.2.2	PPG Modes and the Importance of Wavelength . . . . .	41
2.2.3	The PPG Signal . . . . .	44
2.2.4	Factors affecting the Quality of the Signal . . . . .	45
2.2.5	Photoplethysmography Applications . . . . .	47
<b>3</b>	<b>State of the Art</b>	<b>51</b>
<b>II</b>	<b>Materials and Methods</b>	<b>55</b>
<b>4</b>	<b>Data and Acquisition</b>	<b>58</b>
4.1	Subjects and Databases . . . . .	58
4.2	Acquisition System . . . . .	59
4.2.1	Bio2Bit Move . . . . .	61
4.2.2	BioToBit HI . . . . .	66
<b>5</b>	<b>Implemented Algorithm</b>	<b>67</b>
5.1	PPG Signals Pre-Processing . . . . .	67
5.2	Feature Extraction . . . . .	70
5.2.1	Morphological Feature Extraction . . . . .	70
5.2.2	Segment Feature Extraction . . . . .	75

5.3	Motion Analysis . . . . .	78
5.4	HR Estimation . . . . .	80
5.5	Arrhythmia Detection . . . . .	81
5.6	Reliability Level Computation . . . . .	82
<b>III</b>	<b>Results</b>	<b>87</b>
<b>6</b>	<b>HR Estimation and Reliability Level Classification</b>	<b>89</b>
6.1	Performance Metrics . . . . .	89
6.2	Performance Assessment . . . . .	92
<b>7</b>	<b>Arrhythmia Detection</b>	<b>99</b>
7.1	Performance Metrics . . . . .	99
7.2	Performance Assessment . . . . .	100
<b>IV</b>	<b>Conclusions and Future Works</b>	<b>105</b>

# List of Figures

1.1	Components of telehealth . . . . .	19
1.2	Wearable sensors classification [1] . . . . .	22
1.3	A Wireless Body Area Network scheme [2] . . . . .	23
2.1	Pulmonary and Systemic circulation [3] . . . . .	25
2.2	Cardiac conduction system [4] . . . . .	26
2.3	ECG signal with characteristic time durations [5] . . . . .	27
2.4	Different type of PVCs, detected through 12-lead ECG [6] . . . . .	32
2.5	Different types of Ventricular Tachycardia and Ventricular Fibrillation, detected through 12-lead ECG [6] . . . . .	34
2.6	Electrode Placement in 12-lead ECG [7] . . . . .	35
2.7	Holter Monitor Set-up [8] . . . . .	36
2.8	Light-Matter interactions [9] . . . . .	37
2.9	Basic anatomy structures of the skin [10] . . . . .	40
2.10	Absorption and molar extinction coefficients of main biological tissue constituents at 500 to 1100 nm window wavelengths [11] . . . . .	41
2.11	Placement of the LED and photo-detector in transmittance and reflectance mode [12] . . . . .	42
2.12	Propagation of light of different wavelength in the tissues [13] . . . . .	42
2.13	Origin of PPG waveform according to [14]. (a) Artery is in the diastole phase with the smallest compression of the capillary bed. (b) Systole phase with slightly compressed capillaries because of elastic external boundary. (c) Strongly compressed capillary bed in the case of external contact. . . . .	44
2.14	PPG Waveform [15] . . . . .	44
2.15	Pulse wave characteristic of the pulse wave AC component [16] . . . . .	45
2.16	Families of factors that influence PPG signal [11] . . . . .	46
2.17	Block diagram of an adaptive filter with an accelerometer [17] . . . . .	47
3.1	Wearable PPG-based devices [17–19] . . . . .	51
3.2	Types of PVCs in the PPG signals: a) with premature pulse $PVC_2$ b) without premature pulse $PVC_1$ [20] . . . . .	53
3.3	Algorithm’s Block Diagram . . . . .	57
4.1	Signals Acquisition System . . . . .	59

4.2	Main Bio2Bit BLE Application screen . . . . .	60
4.3	Bio2Bit BLE Application - Vital Configuration section . . . . .	61
4.4	<i>Bio2Bit Move</i> and accessories for board housing and for its positioning on the wrist . . . . .	61
4.5	<i>Bio2Bit Move</i> Hardware block diagram . . . . .	62
4.6	Position of the sensors used and the main components on the <i>Bio2Bit Move</i> board . . . . .	63
4.7	Time Slot Timing Diagram. . . . .	64
4.8	HI Hardware Signal Polarity . . . . .	66
5.1	Pre-Processing Block Diagram . . . . .	67
5.2	Signals obtained at each pre-processing phase . . . . .	68
5.3	Spectral Estimation of the PPG signals, before and after the pre-processing phase. . . . .	69
5.4	Low-Pass FIR Filter Design . . . . .	69
5.5	Morphological Feature Extraction's Block Diagram . . . . .	73
5.6	Peak and valley detection. The detection of the peaks in the ECG reference signal has been performed through the <i>peakdetection</i> function of MATLAB . . . . .	74
5.7	Morphological Feature Extracted from the pulse . . . . .	74
5.8	Movement Indices trend respect to <i>ACC</i> and <i>AC</i> green signal . . . . .	79
5.9	Motion analysis process over the signal <i>S#1</i> . Segment considered too noisy to be used are marked with a red asterisk. . . . .	79
5.10	Motion analysis phase block diagram . . . . .	80
5.11	HR estimation block diagram . . . . .	81
5.12	ECG and filtered PPG signal with correspondent PVC Count annotation (reported as a text for illustrative scope). Detected peaks and valleys are marked and the PVC's typology is indicated below the corresponding pulse. . . . .	82
5.13	Arrhythmia Detection block diagram . . . . .	83
5.14	Segment Features behaviour respect to the <i>AC<sub>G</sub></i> signal . . . . .	85
6.1	Motion Analysis and <i>HR<sub>FINAL</sub></i> ( <i>BPM<sub>est</sub></i> ) Estimation process over signal <i>S#1</i> . . . . .	94

6.2	Scatter plot between $BPM_{true}$ (the ground-truth HR values) and $BPM_{est}$ (the associated estimates over the 8 signal of the Subjects). The fitted line was $y = 0,9994x + 2,9736$ , where x indicates the ground-truth heart rate value, and y indicates the associated estimate. The $R^2$ value measure the goodness of fit and was 0.8256. The Pearson correlation coefficient was 0.909. . . . .	94
6.3	The Bland-Altman plot of the estimation results on the 8 Subjects' signal. The LOA was $[-11.76, 5.90]$ BPM and the mean of the difference was -2.93. . . . .	95
6.4	Reliability results on the Subject 6 (randomly chosen) respect to the HR Error in BPM performed. Discarded Segment are also shown, along with the threshold and the $Dev_{ACC}$ used to determine if the movement's amount was too big. . . . .	96
6.5	Perfusion Index changes respect to the quality of the PPG signal. . . .	98
7.1	Screen employed for the arrhythmia detection evaluation. . . . .	99
7.2	Screen employed for the arrhythmia detection evaluation. . . . .	100
7.3	Trend of the Morphological Features with respect to the PPG signal . . . .	101
7.4	Trend of the Segment Features with respect to the PPG signal . . . .	102
7.5	Low quality PPG signal often leads to FN and PVCs detection. Five out of six FN detections are due to the artefacts present in the PPG signal. . . . .	102
7.6	Typical cases in which a FP PVC is detected. . . . .	103
7.7	Algorithm behaviour in segment 9 of signal D#10 and segment 11 of signal D#11. . . . .	103
7.8	Multiform PVCs in ECG signal, along with the correspondent detected PVC type in the PPG signal, are highlighted in different colours for different database signals. . . . .	104

# List of Tables

4.1	Main MultiLED LRTB GVTG Characteristics for a <i>Forward Current</i> of 20 mA . . . . .	65
4.2	Main Photodiode BPW34 Characteristics . . . . .	65
5.1	Parameters and Threshold employed in the different algorithm step. . .	86
6.1	3x3 Confusion Matrix for classification problem . . . . .	92
6.2	SNR before and after the preprocessing phase for both the red and green PPG signals. . . . .	92
6.3	Average Absolute Errors and Relative Percentage Errors on the 8 Subjects' signal without apply the Motion Analysis algorithm. This means that there are not discarded segment. SD denotes the standard deviation. . .	93
6.4	Average Absolute Errors and Relative Percentage Errors on the 8 Subjects' signal applying the Motion Analysis algorithm. The total percentage of discarded segments is 4.59%. SD denotes standard deviation . . . . .	93
6.6	3x3 Confusion Matrix of Reliability Level classification performance . .	96
6.5	Reliability Level results for the 8 subjects. SD denotes standard deviation.	97
7.1	2x2 Confusion Matrix for the evaluation of PVCs detection . . . . .	100



# Abstract

This work aims to design an algorithm which will be embedded into the Bio2Bit Move (a STMicroelectronics prototype) in order to develop a Telemedicine application. In particular, the algorithm estimates the heart rate in real time and detects the ventricular extrasystoles on the photoplethysmographic signal, which is acquired through the reflection mode at green light. Alarms about arrhythmia events could be stored or sent to other devices such as smartphone or laptop through the Bluetooth Low Energy (BLE) module embedded in the board, and if it is necessary, they are sent to the doctor. The wearable device is capable of acquire green and red photoplethysmography (PPG) and 3-axis accelerometer signals, among others. The pulsatile component of the PPG (AC component) is related to the cardiac synchronous variations in the blood volume with each heartbeat, and unlike the ECG, which is the clinical standard in the detection of arrhythmias, it allows a continuous monitoring for long periods of time. Holter and Event Monitor allows a continue monitoring but only for some days moreover, they are not so comfortable to wear and they are not accessible to all. Instead, PPG used in reflectance mode allow to perform the measure in almost any body site. The 3-axis accelerometer signal is used in order to implement a motion analysis system, which allow to discard too noisy time windows. Since in some point the PPG quality is low, even if the accelerometer do not register any movements, a reliability level estimation, based on two features (one taken from the accelerometric signal and one from the green PPG signal itself), is implemented. Heart Rate estimation, computed using green PPG, leads to an Average Absolute Error of 2.25 BPM and a Relative Percentage Error of 3.36%. The arrhythmia detection is performed using Physionet MIMIC Database. The searched Premature Ventricular Contractions (PVC) are very common and they are usually benign and do not require treatment but sometimes, they are related to heart diseases or may also trigger more severe arrhythmia such as Ventricular Tachycardia, Ventricular Fibrillation and Atrial Fibrillation. In order to assess the PVC severity it is necessary to investigate the number of PVC events, if they occur with a particular rhythmic pattern, if they form a couplet (two consecutive PVC) or triplet (three consecutive PVC) or if they originate from multiple foci. Two morphological features are used to assess if a beat is a PVC but also others are investigated. The performed PVC detection shows a Sensitivity of 90.10%, Specificity of 99.3% and Accuracy of 98.83%.



# Part I

## Introduction



# Project Aim

The purpose of this work is to create an embedded system, acting as a Body Area Network. The device should allow real-time arrhythmia detection and be able to store and download the detected alarms, in order to send them to a specialist, who provides for a more accurate analysis and decides if further investigations are needed. This, it will be possible thanks to the *Bio2Bit Move*, a wearable device prototype developed by STMicroelectronics. The board, plugged in an adjustable wrist strap, transmit and download signals and alarms via Bluetooth Low Energy, which allows significant power consumption savings. Arrhythmia detection is carried out using the photoplethysmographic signal at green wavelength, under reflectance mode. This allows to make non-invasive monitoring in almost any part of the body, enabling in this way, the continuous monitoring of the cardiac condition over a long period of time, as opposed to the devices currently used in clinic for arrhythmia's diagnosis (ECG, Holter Monitor, Event Monitor).

Since the photoplethysmographic set-up requires only a few opto-electronic components, it is possible to reduce the costs of the device compared to those equipped with ECG electrodes. The board is also capable of acquiring, among other signals, photoplethysmography at red wavelength and accelerometer data, which enable to evaluate the impact of noise on the measure, and allow to filter the artefact or otherwise, to assess the estimation's reliability.

The arrhythmia analysis is focused on finding Premature Ventricular Beats (PVBs). They are very common among the population and, although they are usually benign, when their frequency is high, multiform premature contraction occurs or under some other conditions, it is necessary to better evaluate the clinical situation. Since PVBs are sporadic in most patients, a continuous long-term monitoring by means of the *Bio2Bit Move*, would be more suitable than the methods currently used and would allow the doctor to determine, if necessary, the best clinical investigations to be carried out. The PVBs detection is performed using the morphology of the signal: this allows to discriminate beats with different shapes and to establish if the ectopic beats recur following a specific pattern or not.

The design of a comfortable, low-cost and accessible device, allows therefore to perform an arrhythmia telescreening on a large part of the population. In this way, everyone will access to an appropriate clinical evaluation and it will be possible to establish the real need for further medical examinations. This is important not only for reducing the number of unnecessary visits, but also because it will be easier to establish the most suitable diagnostic and treatment path for each patient.



# Chapter 1

## Telehealth

Telehealth deals with clinical health care, patient and professional instruction, public health and health management. All these services are provided remotely, thanks to the use of Information and Communication Technology (ICT).

Telemedicine and Telecare are two Telehealth subfields that deal with the delivery of clinical care outside of traditional health-care facilities, without taking into account administrative and educational health services [21].

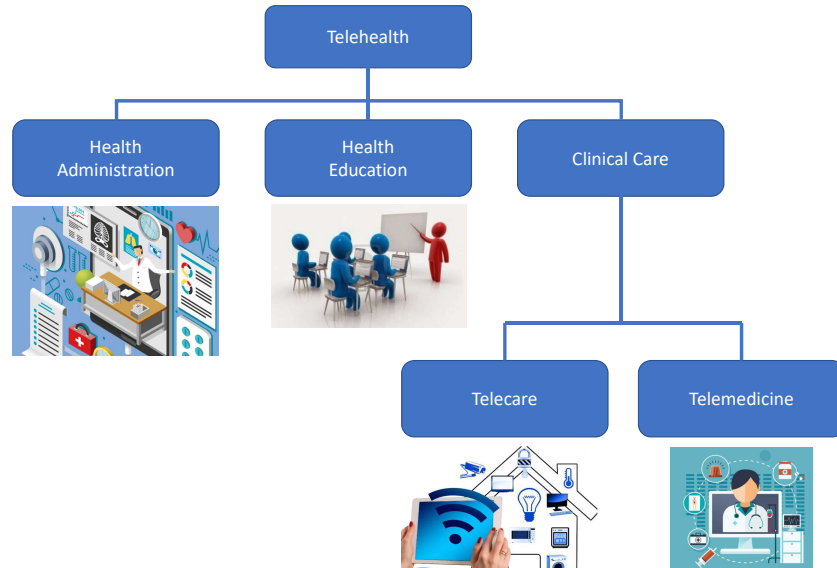


**Figure 1.1:** Components of telehealth

The 104 definitions of the word "Telemedicine" reviewed in 2007 [22] indicate confusion about the term but also that is a fast-growing sector. According to the European Commission, telemedicine can be defined as:

"The provision of healthcare services, through the use of ICT in situations where the health professional and the patient (or two health professional) are not in the same location. It involves secure transmission of medical data and information, through text, sound, images or other forms needed for the prevention, diagnosis, treatment and follow-up of patients" [23].

Telemedicine should not to be confused with "Telecare", whose main focus is the use of ICT in order to provide remote care to patients, allowing them to keep living in their own homes [24].

Telemedicine and Telecare services can be delivered asynchronously (store-and-forward method) or synchronously (real-time methods) and according to European Commission, can be generally divided in:

- **Teletriage:** it is the process of identifying the patient's state of health, associating his/her symptoms with a level of urgency and providing advice via phone by trained professionals, to ensure safe, timely and appropriate management of patient's problems [25]. Not only teletriage is beneficial for patients as a powerful tool in case of urgencies or uncertainties but, from the point of view of healthcare institutions, it also helps to reduce healthcare system's costs, by avoiding inappropriate emergency visits [24].
- **Teleconsultation:** it is the communication at distance through ICT in order to perform a diagnose, treat a patient in a remote location, obtain a second opinion from a specialist or develop innovative treatment approaches. Teleconsultation provides easy and affordable access to medical services for everyone in particular, for people living in rural and remote areas, where there is sometimes a lack of health personnel, and for individuals with physical disabilities, who have greater difficulty in organizing hospital visits. Therefore, teleconsultations help to save time and reduce transport costs for patients [26].
- **Telesurgery:** it can be performed in the form of telementoring or telepresence surgery. In the first case, the surgeon, who is operating, is supported by a remote specialist, who provides interactive assistance through video and audio connections. In the second case, the surgeon is not in the same place as the patient but operates on it, thanks to the use of a wireless network and computerized robotic technologies that link the surgeon's movements to a scale-down movement produced by a small machine [27]. This technology limits the shortage of surgeons, allows timely and high-quality surgical intervention and avoids long-distance journeys, often risky for the patient.

- **Telediagnosis:** it is the determination of the nature of a diseased condition, at a remote location, on the basis of clinical data and information transmitted through ICT. Telediagnosis by medical experts helps distant healthcare operators to assess patients health and to provide them appropriate treatments [28]. Telediagnosis can also be performed during telescreening or telemonitoring and therefore is not limited to diagnosing a patient in a remote location as does the teleconsultation. Furthermore, telediagnosis should not be confused with teletriage, since the former involves identification and diagnosis of the symptoms described by the subject, while the latter only assesses the urgency of patient's health status.
- **Telescreening:** it consists of carrying out a remotely medical investigation in order to identify the possible presence of a disease in subjects without signs or symptoms, or with pre-symptomatic or unrecognized symptomatic disease. Not to be confused with telediagnosis, telescreening is more focused on the identification and subsequent follow-up of a pathology that can be suspicious. The application of telemedicine on screening procedures provides an optimization of healthcare professional's time and resources and operate a greater coverage of the population's potential disease [24].
- **Telemonitoring:** it is included in the telecare scope and it can be described in five stages:
  1. Data acquisition through a sensor.
  2. Data transmission from patient to physician by telephone or a networked system.
  3. Data integration with other information regarding the patient's state.
  4. Data examination.
  5. Data storage.

Thanks to telemonitoring services, patients can actively manage their diseases and furthermore, it is possible to improve continuity of care and prevention of future episodes in the context of chronic disease control [29, 30].

Telemedicine and Telecare aims to guarantee access, equity, quality and cost-effectiveness in both developed and less economically developed countries. However, it is important to clarify that these technologies are not intended to replace traditional medicine, but only to provide support, in order to improve health care and ensure a better assistance to citizens.

## 1.1 Wearable Body Area Sensors

Recent progresses in miniaturized electronics are promoting a rapid growth of wearable technologies [31]. In particular, the application of such wearable technologies to health care enables a continuous monitoring in the patient's daily-life environment that allows:

- early-stage detection;
- remote monitoring of chronic disease and drug's administration;
- management of medical emergencies;
- impact and evolution monitoring of the clinical treatment or intervention;
- cost savings.

As a first approximation, wearable sensors are small electronic devices which can be placed close to, or implanted within, the human body [32]. A first classification of Wearable Body Area Sensors (WBAS) could be done dividing them based on the contact with the body. In Figure 1.2 a more detailed categorization is shown.

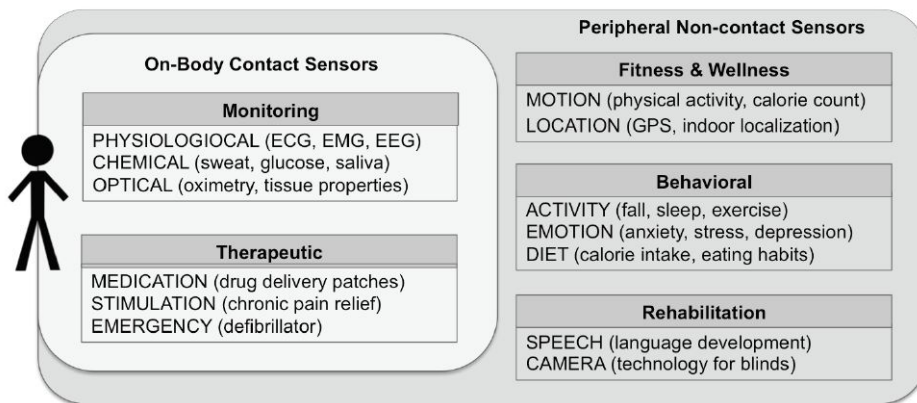


**Figure 1.2:** Wearable sensors classification [1]

Nowadays, it is no longer sufficient to design standalone wearable devices but it becomes vital to create a Wireless Body Area Network (WBAN), able to communicate physiological data in the immediate proximity of the human body. Informations are transmitted to a gateway device, also called Body Control Unit (BCU), which can be a smartphone or any portable device that gathers collected information and forwards it to the cloud or server centers [2]. In order to communicate with the wearable sensors, the BCU comprises short-range communication technology such as Bluetooth but at the same time, it is provided with heterogeneous networks, such as Wi-Fi and GSM, used to send the data to the cloud or medical server. Gateway devices can also store

data, run some pre-processing algorithms, evaluate relevant clinical alarms and send data intermittently to remote servers [1].

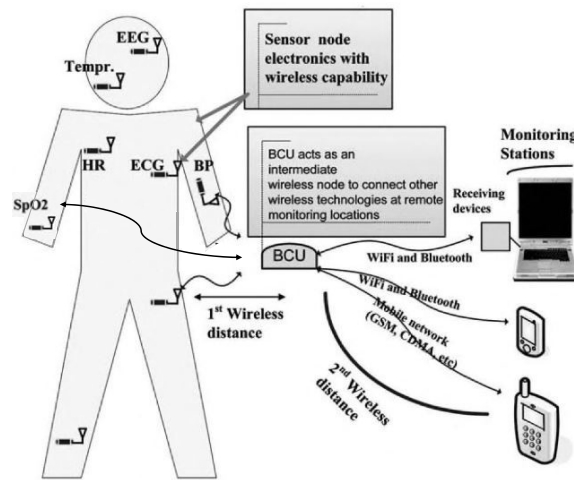


**Figure 1.3:** A Wireless Body Area Network scheme [2]

### 1.1.1 Application of Wearables in Telehealth

There are a lot of potential applications for telemedicine and telecare using wearable devices. In this Section, a few examples of solutions that were clinically evaluated, are reported below.

#### Remote Monitoring of Patients with Heart Failure

Heart failure (HF) is a chronic and progressive condition associated with high morbidity, mortality and health care costs. The basic manifestations of HF are dyspnea (paroxysmal at night or during exercise), orthopnea, edema of the lower limbs and asthenia, which may limit exercise tolerance and lead to pulmonary edema and peripheral edema [33]. HF is difficult to manage because it can have different comorbidities and requires significant changes in lifestyle. The patient often has to monitor his/her symptoms, take different drugs and check the weight to monitor the state of water retention. Early identification and treatment, along with better coordination of care, management of comorbidity conditions and better self-organization of the patient, can help preventing re-hospitalization, reduce mortality, and provide more effective solutions about the healthcare's administration [34]. Actions have therefore directed to better monitor the patient with chronic HF at home. The disease management includes structured telephone support, telemonitoring or remote monitoring of device that can measure Heart Rate (HR), Heart Rate Variability (HRV), Electrocardiogram (ECG), patient mobility and intra-thoracic impedance. The use of implantable devices such as cardiac pacemakers,

implantable cardioverter-defibrillators and implantable hemodynamic monitors has been demonstrated to enhance the prognosis of HF at home, which may enable for preventive measures to be taken [35].

### **Automatic Detection of Fall Among the Elderly**

Falls are one of the biggest risks that elderly and fragile population has to face. After a fall, many people cannot get up and if there is a loss of consciousness or cognitive deficits are present, it is not even possible to activate a user-operable wearable alarm device. A prolonged time lying down in the ground can carry important medical and physiological consequences and to avoid this, wearable devices capable of automatically detecting falls have been developed. They are usually based on impact, position and tilt sensors, and accelerometers, along with suitable control algorithms performed in a micro controller [36].

# Chapter 2

## Theoretical Framework

### 2.1 Cardiovascular System

The cardiovascular system consists of the heart and a closed system of vessels divided into arteries, veins and capillaries, which are responsible of blood transport throughout the body in order to provide nourishment, regulate body temperature, pH, water content of cells and to help in fighting diseases. The circulatory system can be divided into a pulmonary circulation and a systemic circulation. The first one is responsible to carry deoxygenated blood from the right ventricle to the lungs (through the pulmonary artery), in order to be oxygenated and then brought back, via the pulmonary veins, to the left atrium of the heart. Once in the left atrium, oxygenated blood is pumped into left ventricle through the mitral valve, goes into the aorta and is then distributed across the body thanks to the systemic circulation, before returning again to the pulmonary one.

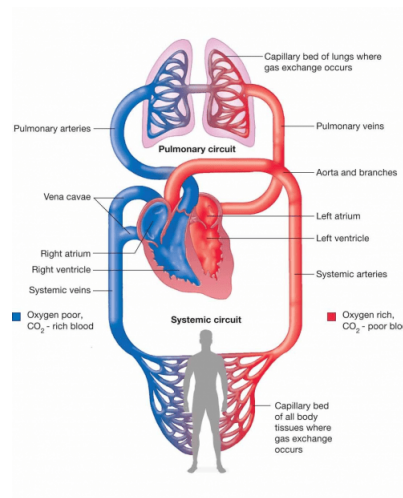


**Figure 2.1:** Pulmonary and Systemic circulation [3]

### 2.1.1 Heart's Electrical Conduction System

The heart's role in the cardiovascular system is to ensure blood circulation. To accomplish this, it is equipped with a closely interlinked electrical and mechanical mechanism. The electrical impulses propagate in every direction and the cells of the myocardium provide for an organized contraction that enable a rapid spread of the action potential. There are two syncytias: atrial and ventricular, connected by the atrioventricular (AV) node, located in the interatrial septum. The heart's electrical conduction system is depicted in Figure 2.2. The first impulse, that starts the flow of electric current through the heart, comes from the sinoatrial (SA) node, positioned in the right atrium of the heart. The electrical impulse generation is due to the automatism of the heart's electrical cells. By modifying the membrane, sodium enters in the cells while potassium exits from them; this creates a potential difference on the sides of the membrane, which results in the generation of an electrical current. From the SA node, the current travels through the atria along the internodal atrial pathway and reaches the AV node, causing the contraction of atria that pushes the blood into the ventricles. Once atria completed to pump blood, the electrical signal reaches the bundles of His in the ventricular septum and goes through the right and left bundles. Finally, the potential action arrives at the Purkinje fibers, which transmit it to the contractile fibers of each ventricle, resulting to their organized contraction. When the electrical charges are balanced and ready for discharge, we refer to polarization [37]. The depolarization insted, is the discharge of energy that follows the transfer of electrical charges through the cell membrane. Finally repolarization is the return of electrical charges to their original state. After each depolarization, a refractory periods occurs in which the action potential cannot be triggered [38].

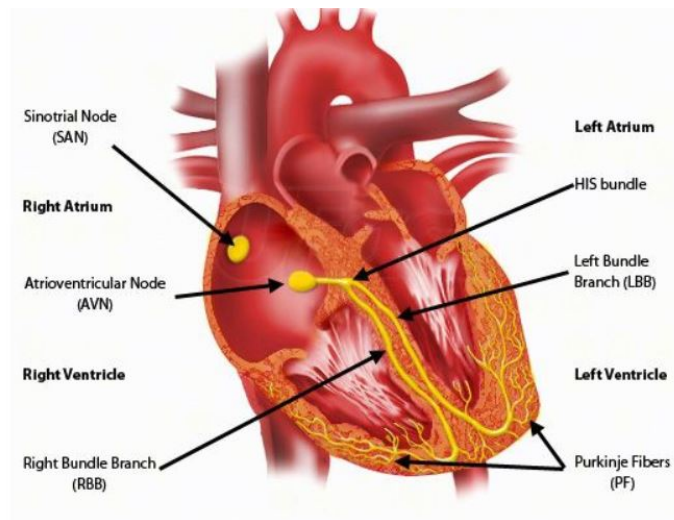


Figure 2.2: Cardiac conduction system [4]

The intrinsic frequency of the conduction system are listed below. The site who has the higher frequency (in an healthy heart is the SA node) acts as a pacemaker.

- SA node: 60-100 bpm (beats per minute)
- AV junction: 40-60 bpm
- Ventricles: 20-40 bpm

The most common way to obtain information about heart's electrical activity and function, is the electrocardiogram which requires the positioning of electrodes on the skin surface. A normal cardiac cycle registered by means of ECG (Figure 2.3) is characterized by the following element:

- **P wave:** it represents the atria depolarization
- **PR segment:** it indicates how much time the electrical pulse needs to travel from the SA node through the AV node
- **PR interval:** it comprises P-wave and PR segment and its duration is normally between 0,12 s -0,20 s
- **QRS complex:** it represents the rapid depolarization of the two ventricles and lasts less than 0,12 s.
- **ST segment:** it is the period when the ventricles are depolarized
- **T wave:** it is related to the repolarization of the ventricles
- **QT interval:** it is the interval between the beginning of the QRS complex to the end of the T wave

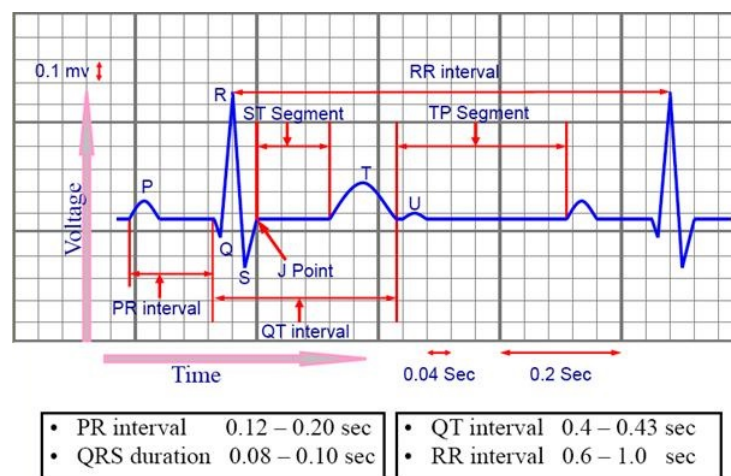


**Figure 2.3:** ECG signal with characteristic time durations [5]

The time interval between two R peaks of the QRS complex (RR interval) is used to determine the heart rate, which is measured in bpm. The HR, along with the above mentioned ECG signal characteristic, is used as a medical diagnostic parameter to indicate the heart's condition. The disturbance in the regular rhythm of the heartbeat is called arrhythmia and is generally caused by abnormalities in impulse formation or conduction. In the Section below, arrhythmia typologies along with their detection in clinic will be discussed.

## 2.1.2 Arrhythmia

In this Section, it is presented an overview of arrhythmia typology, following the work of *Gail Walraven [37]*. Arrhythmias can be classified into four groups, according to the pacemaker's location that controls the pace. The most common sites of the pacemaker and, consequently, the main categories of arrhythmias, are:

- Sinus Rhythms,
- Atrial Rhythms,
- Junctional Rhythms,
- Ventricular Rhythms.

### Sinus Rhythms

In this class, rhythms are generated by the SA node and for this reason, although the normal sinus rhythm (NSR) of the heart is not an arrhythmia, it will be described in this Section.

#### *Normal Sinus Rhythm*

The rhythm is regular and has the same frequency of the site from which it is generated (the SA intrinsic frequency is 60-100 bpm).

#### *Sinus Bradycardia*

The rhythm is regular but its frequency is lower than 60 bpm.

#### *Sinus Tachycardia*

The rhythm is regular but its frequency is higher than 100 bpm (at rest).

#### *Sinus Arrhythmia*

This arrhythmia is very easily confused with NSR. Its frequency varies with patient's breathing: it increases during inhalation but it slows down during exhalation. This results in an irregular rhythm, which, however, is physiological.

## **Atrial Rhythms**

Sometimes the SA node loses its pacemaker's role and the site having the next highest frequency, replaces it with its own intrinsic frequency. Usually this sites are located in the atria. Since the impulse is generated outside the SA node, it has difficulty in travelling through the atria and this is reflected in a wave called "Atrial P-wave" that appears toothed, flattened or biphasic.

### ***Migrant Pacemaker***

The rhythm is slightly irregular because it is composed of sinus beats interspersed with atrial beats, then characterized by abnormal P waves.

### ***Premature Atrial Beat***

It is not a rhythm but an ectopic beat. Ectopic beats can occur because of irritability or escapement. The first term is used when a site (in this case atria) accelerates and acts as a pacemaker while the second, when the normal pacemaker slows down or does not work, and the site of lower level, takes over as a pacemaker. Premature Atrial Beats are due to irritability and they come at an early stage of the heart cycle causing an irregular rhythm. They are characterized by an "atrial P-wave" and the PR interval is generally longer than 0.20 s.

### ***Atrial Tachycardia***

When the number of consecutive premature atrial beats increases, atrial tachycardia occurs. The irritable focus replaces the SA node and assumes the role of pacemaker for a long period. It is no more an ectopic beat but a regular rhythm in which the individual beats have the Premature Atrial Beat characteristics. The HR range between 150-250 bpm and the P atrial wave can be hidden by the T-wave of the previous beat.

### ***Atrial Flutter***

If the atria become even more irritable, up to a frequency of 250 - 350 bpm, it is referred to as atrial fluttering. With such a fast HR, the ventricles do not have time to fill up with blood between two beats and therefore, they continue to pump, without expelling high systolic volume. However, to avoid this, the AV node blocks certain impulses, preventing them from reaching the ventricles and not allowing them to be properly filled. In the ECG this results in a very rapid series of P-wave (flutter waves), not all followed by a QRS complex. Therefore, the ventricular rate is slower than the atrial rate.

### ***Atrial Fibrillation***

The atria are so irritable that they stop contracting and they experience an

ineffective tremor (called fibrillation). P-waves are not distinguishable on the ECG, and there are a number of undetectable oscillations along the isoelectric line. The atrial rhythm is therefore not measurable, the atrial activity is chaotic and the ventricular rate is slow because the AC node blocks most of the impulses.

## **Junctional Rhythms**

When the electrical impulses originate in the AV junction, the heart is depolarized in a unusual way because, being the pacemaker located in the center of the heart, the impulses travel simultaneously in two directions. When the atria are depolarized in an inverted way, the conduction is called 'retrograde' and, on the ECG signal, an inverted P-wave in the derivation II can be seen. The inverted P-wave may occur before or after the QRS complex or can be hidden by its. The PR interval, must be less than 0.12 s (otherwise it could be an atrial arrhythmia).

### ***Premature Junctional Complex***

It is an ectopic beat due to the irritability of the AV junction. The P-wave is reversed and may fall before or during the QRS; the PR interval is less than 0,12 s (if it is measurable).

### ***Junctional Tachycardia***

When the AV junction becomes more irritable, it can accelerate and overcome pacemakers at higher sites. The frequency varies from 100 to 180 bpm; if it is from 60 to 100, is called 'accelerated junctional rhythm'.

### ***Junctional Escapement Rhythm***

It is a lifesaving mechanism in which the AV junction, with its intrinsic frequency of 40-60 bpm assumes a pacemaker function.

The term 'supraventricular tachycardia' is often used. This does not refer to a particular type of arrhythmia but is used to describe a category of regular tachyarrhythmias, with a common frequency range (150-250 bpm), which cannot be identified accurately because they have indistinguishable P waves.

## **Ventricular Rhythms**

Ventricular arrhythmias are very serious for several reasons. The heart is made so that depolarization occurs from top to bottom and the atria contract before the ventricles but, when the pulse originates in the ventricles, this process is reversed and the efficiency of the heart is greatly reduced. Also, because the ventricles are the lowest site in the

conduction system, there is no life-saving mechanisms that can correct a ventricular arrhythmia.

### ***Premature Ventricular Beat***

Premature Ventricular Beats, also called ventricular extra-systoles or Premature Ventricular Contractions (PVCs), are ectopic beats produced by irritable ventricular foci, usually located in the bundle branches, Purkinje network or in the ventricular myocardium itself. In this situation, ventricles contract before they are completely filled, so the QRS-complex arrives earlier than expected in the heart cycle, interrupting the regularity of the underlying rhythm. The QRS-complex appears wider than normal ( $\geq 120$  ms) with an abnormal shape. Moreover, the ventricular ectopic beat usually is followed by a compensatory pause. The distance between the complex preceding the PVC and the complex following it, is exactly twice the distance of an RR interval. However, PVB can also not be followed by any pause (non-interpolated PVB). Retrograde capture of the atria may also occur: in this case, the ectopic impulse is conducted retrogradely through the AV node, producing atrial depolarization and therefore usually an inverted P-wave occurs after the QRS-complex.

- If the patient has only occasional PVB, this can be normal, but if he gets to 5-10 PVCs per minute, an increase in ventricular irritability should be suspected.
- PVBs may be either:
  - *Unifocal*: if all the PVCs arise from a single ectopic focus (they have the same morphology)
  - *Multifocal*: if PVCs arise from two or more ectopic foci (the QRS shapes are different). Since they come from more than one focus, they are more severe because they are associated with a general irritability of the myocardium and the possibility of even more dangerous arrhythmias.
- The most dangerous situation is called the R-on-T Phenomenon. It occurs when the PVC falls on the previous contraction T-wave. During the repolarization phase, the heart muscle is very sensitive to outside stimulus thus, a PVC can trigger a lethal arrhythmia called Ventricular Fibrillation (VF).
- PVCs may be single and isolated or they can form a regular scheme with the surrounding normal beats:
  - *Bigeminy*: if PVC is alternated with a regular sinus beat
  - *Trigeminy*: if PVC is alternated with two regular sinus beats
  - *Quadrigeminy*: if PVC is alternated with three regular sinus beats

- Another sign of increasing myocardial irritability is when PVCs occur in immediate succession, without interposition of normal beats: two successive PVCs are called "couplet" and three successive PVCs are called "triplet". When successive PVCs are equal or more than three, the situation is described as a "short burst of Ventricular Tachycardia (VT)", more commonly named "non sustained ventricular tachycardia".

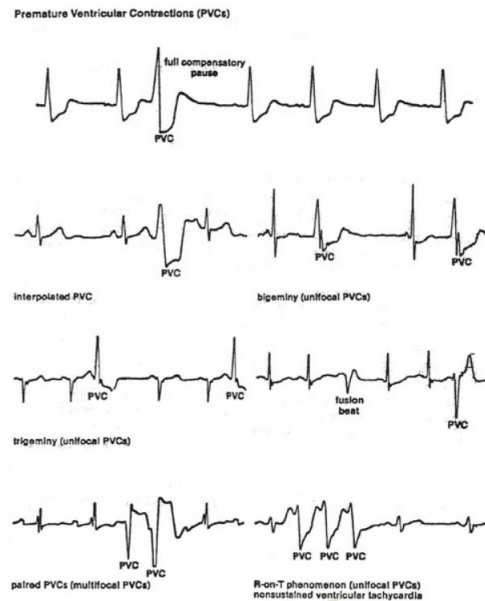


**Figure 2.4:** Different type of PVCs, detected through 12-lead ECG [6]

PVCs are usually benign and do not require treatment. They simply can occur because of too much caffeine intake, excess catecholamines, high level of stress, insomnia and electrolyte anomalies (low blood potassium, magnesium and high blood calcium). Also stimulants as alcohol, tobacco and illicit drugs are associated with PVCs [39]. Sometimes PVCs are also related to cardiac pathologies as severe left ventricular hypertrophy, myocardial infarction, hypertrophic cardiomyopathy and congestive cardiac failure or may also trigger more severe arrhythmia like VT, VF and AF. [40]. Patients with high frequency of PVCs have an high risk of heart failure and sudden death if a heart disease is suspected [41]. PVCs could also be used as a predictor of sudden cardiac death (even without recognized heart disease). Since PVCs usually cause inefficiency in blood circulation, notably in cases frequent PVCs, such condition may lead to a dizziness or a temporal loss of consciousness. Recent studies reveal also that PVCs that occurs during recovery phase of exercise, is connected with an higher long-term risk of mortality [42]. Non-cardiac diseases also could be involved in VPBs such as, for example, hyperthyroidism, anemia, and even hypertension.

The estimated prevalence of PVCs ranges from 1% to 4% on ECG and 40% to 75% on a 24 or 48-hour Holter monitor [43]. Young and healthy adults have shown a highly similar frequency rate of PVCs in contrast to the older parts of the population.

Patients usually complain heart palpitations and feel a skipped heartbeat followed by a fluttering sensation; some of them may have chest pain or discomfort, dyspnea, anxiety or dizziness. The great majority of them however, are asymptomatic and rarely require any treatment [39].

As PVCs are sporadic in most patients, the short duration of the standard 12-lead ECG may be fail in capturing ectopic beats. As alternatives, it is possible to use a 24 or 48 hours Holter Monitor or Event Monitor. In general it is also useful to perform laboratory testing (complete blood count, potassium, calcium, magnesium, thyroid stimulating hormone and thyroxine) in order to identify potential etiology of PVCs [44]. If there is clinical suspicion, it is also necessary doing echocardiography to exclude heart diseases. For a more detailed cardiac evaluation for those who have PVCs during exercise or in the recovery phase following it, stress testing is recommended [42].

In many cases patients with frequent or symptomatic PVCs can be treated through the minimization of stimulants and/or repletion of electrolyte or change of lifestyle. In some cases, antiarrhythmics (such as amiodarone and flecainide), beta-blockers, and calcium channel blockers are suggested [45]. But patients who have several thousand episodes per day or symptomatic PVCs refractory to pharmacologic treatment, may be candidates for radiofrequency catheter ablation which consists in the elimination of the heart tissue that cause the premature ventricular beat [46].

### ***Ventricular Tachycardia***

When three or more successive PVBs occur, at a rate of 100-250 bpm, the term used is Ventricular Tachycardia. If the HR is less than 100 bpm, the correct definition is instead "ventricular rhythm". It is possible to classify VT in non-sustained (if the condition lasts less than 30 seconds) and sustained (if VT lasts more than 30 seconds). When VT occurs, ventricles do not have sufficient time to fill and thus, the cardiac output is greatly reduced. This arrhythmia may also lead to ventricular fibrillation and death. The VT treatment consists in the administration of Lidocaine, Verapamil or Bretylium. If drug therapy fails or is contraindicated, cardio version or VT ablation may be used. It is important to act quickly as death can result rapidly.

### ***Ventricular Fibrillation***

It is one of the most common causes of cardiac arrest. It is lethal because of its chaotic and ineffective nature: many impulses are discharged from different ventricular foci and the heart muscle is not able to respond with an organized contraction. The appearance of the ECG is a chaotic fibrillatory pattern since there are no identifiable complexes or waveforms. As it has been mentioned before, VF can be initiated by the R on T phenomenon or by sustained VT, particularly when the heart has been altered by ischemia, acute myocardial infarction and coronary heart diseases. VF may also occur in cardiomyopathy, mitral valve prolapse, cardiac trauma and digitalis toxicity. Anaesthesia, surgery, cardiac catheterization, cardiac pacing, cardioversion or electrocution are other procedures that could lead to VF. The treatment is cardiopulmonary resuscitation until it is possible to perform defibrillation by DC shock: the electrical shock to the myocardium usually stops the fibrillation and allows the heart to restart its normal rhythm.

### ***Idioventricular Rhythm***

PVBs, VT and VF are all the result of ventricular irritability. Instead, idioventricular Rhythm is due to the heart's escape mechanism, which acts as a protective system. It allows the heart to keep beating at the intrinsic frequency of the ventricles (20-40 bpm) when higher pacemakers don't work.

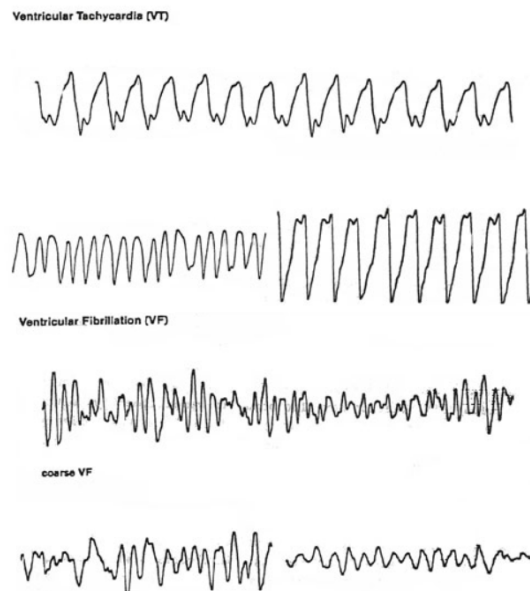


**Figure 2.5:** Different types of Ventricular Tachycardia and Ventricular Fibrillation, detected through 12-lead ECG [6]

### 2.1.3 Arrhythmia Diagnosis in Clinic

When an arrhythmia is suspected in a patient, several tests can be suggested by the doctor:

- **Electrocardiogram.** It is a non invasive and painless test, which can record the electrical activity of the heart and determines the cardiac rhythm, HRV and abnormalities in the cardiac conduction [47]. In Section 2.1.1, the ECG signal has already been illustrated. In the conventional standard 12-lead ECG, ten electrodes are required: as it possible to see in Figure 2.6 four electrodes are placed on the limbs and the other six on the chest. This test has to be done by an expert in an electro-physiology lab and usually is carried out twice: at rest and in motion state (e.g. running, cycling or walking). However, its ability in detecting arrhythmia is limited at the time of the test.

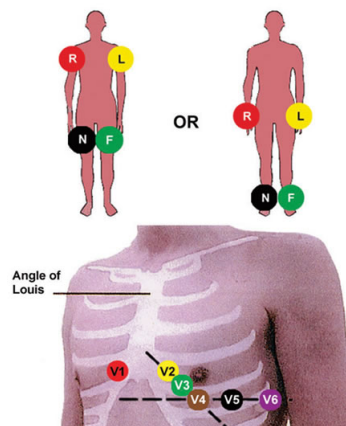


**Figure 2.6:** Electrode Placement in 12-lead ECG [7]

- **Holter Monitor.** The method was conceived in 1961 and takes its name from the American physicist Norman J. Holter, its inventor [48]. It consists in a small portable ECG, with 3-5 electrodes, that has to be taped on the patient chest skin. Thanks to this ambulatory ECG, the electrical activity of the heart can be monitored typically for 24-48 hours, in which the patient can carry out his/her daily routine, although with some limitations. The patient is also asked to write down a diary the activities carried out and the symptoms he has experienced. A 24-hour Holter monitor set up is shown in Figure 2.7.
- **Event Monitor.** When arrhythmia symptoms are occasional, doctor may propose the use of a small recording device, called cardiac event recorder. The instrument should be placed on the finger or chest through a belt and requires manual activation by the patient when he or she experiences symptoms of arrhythmia [48].



**Figure 2.7:** Holter Monitor Set-up [8]

- **Implantable loop recorder (ILR).** It is a small single-lead ECG monitoring device, which is implanted in patients who experience recurrent unexplained episodes of palpitation or syncope, or have a documented Atrial Fibrillation (AF), or have experienced myocardial infarction [49, 50]. It is capable of storing ECG automatically in response to a significant arrhythmia event or in response to patient activation. ILR also uses a loop recording that enables the registration of the cardiac rhythm that occurred just before the symptoms [51].

## 2.2 Photoplethysmography

Photoplethysmography is a very simple and low-cost technology which requires only a few opto-electronic components. A light source, usually a Light Emitting Diode (LED), illuminates the skin along with underlying blood vessels, and a suitable photodetector (commonly photodiodes, but photocells and phototransistors can also be used) measures the intensity changes of the reflected or transmitted light, associated with blood volume changes in the tissue micro-vascular bed.

PPG can potentially be acquired in any part of the body in a non-invasive way; this, makes the measurement particularly comfortable for the patient and therefore allows continuous and long-term monitoring.

The first report on the use of an optical device for measuring blood volume changes dates back to 1936. In this year, two research groups (*Molitor and Kniazuk of the Merck Institute of Therapeutic Research* and *Hanzlik et al. of Stanford University School of Medicine*) used similar instruments in order to detect changes in blood supply in the rabbit ear, under different conditions [52, 53]. But the pioneer of the PPG technique, who was also the first to use the term "photoplethysmography", was Alrick Hertzman from the *Department of Physiology at St. Louis University School of Medicine*. In his first paper, he described the use of a reflection mode system to measure blood volume changes in the fingers, induced by exercise, cold and Valsalva manoeuvre [54]. In 1938, Hertzman established the validity of the method for measuring blood flow and

blood volume changes and in the same year, Matthes and Hauss, reported preliminary observations on the PPG technique. Hertzman's early works [55–58] attempted to validate the method for measuring blood flow and blood volume changes. Later works of Hertzman [59–61] monitored vasomotor activity splitting the Alternating Current (AC) and Direct Current (DC) components with separated electronic amplifiers, assessed the completeness of sympathectomy and detected the onset of cutaneous vasodilatation in both forearm and digits. Recently, the desire for small, reliable, low-cost and simple-to-use cardiovascular assessment technology, along with the improvements in opto-electronics instrumentation and computer-based digital signal processing, have led to a considerable increase in clinical application of PPG-based technology [62].

### 2.2.1 Light Propagation Principles

The propagation of the light through a medium can be disturbed by three effects: reflection and refraction, absorption and scattering. The transmitted light is given by non-reflected and non-absorbed or forward scattered photons.

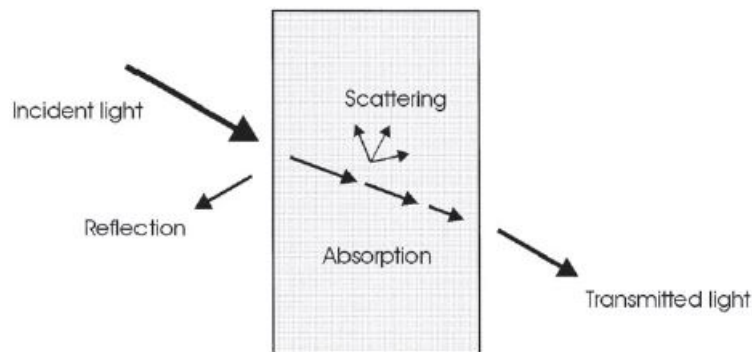


**Figure 2.8:** Light-Matter interactions [9]

#### Reflection and Refraction

Reflection is defined as the returning of electromagnetic radiation by surfaces on which it is incident. When a surface presents small irregularities compared to the wavelength of the radiation, the reflection angle  $\theta'$  (angle between the surface and the reflected beam) equals the angle of incidence  $\theta$  (angle between the surface and the incident beam) and the reflection is called 'specular'. In contrast, if the roughness is comparable or even larger than the wavelength of radiation, diffuse reflection occurs. Refraction originates from a change in speed of the light wave and is governed by Snell's law:

$$\frac{\sin\theta}{\sin\theta''} = \frac{v}{v'} \quad (2.1)$$

where  $\theta''$  is the angle of refraction and  $v$  and  $v'$  are the velocities of light in the media before and after the reflecting surfaces, respectively.

## Absorption

When the light travels the skin, it is absorbed by different biological tissues such as skin pigments, bone, arterial and venous blood, each one with its own length and light absorption coefficient. Assuming that the illuminated media indicates only an artery, it is possible to measure the amount of reflected or transmitted light, and trace the pulse changes inside the vessels during the cardiac cycle [12]. The attenuation of light from the light beam to the photodetector is typically modelled by the Lambert-Beer law:

$$I = I_0 e^{-\alpha l} \quad (2.2)$$

where  $I$  is the intensity of the transmitted light through the medium and  $I_0$  is the injected monochromatic light beam. This law states that in a homogeneous medium, light intensity decays exponentially as a function of path length ( $l$ ) and light absorption coefficient ( $\alpha$ ), corresponding to medium properties at a specific wavelength.

The Lambert-Beer law states that the incident light simply splits in transmitted and absorbed light; therefore, reflection at medium surface as well as light scattering are not contemplated by this model.

## Scattering

Depending on the relationship between the wavelength of the incident light and the dimensions of the scattering particles, there are different types of scattering. The most important ones are the Rayleigh's scattering and the Mie scattering. The former occurs when the scattering particles are much smaller than the wavelength, and a law related to it states that the scattering is inversely proportional to the fourth power of the wavelength [63]. If the spatial extent of scattering particles becomes comparable to the wavelength of incident radiation such as in blood cells, Rayleigh scattering no longer applies and Mie scattering occurs. Mie scattering takes place in the forward direction, whereas in Rayleigh scattering forward and backward scattered intensities are the same [64]. However, it is usually very convenient to define a probability function  $p(\theta)$  of a photon to be scattered by an angle  $\theta$ , which can be fitted to experimental data [9]. Several theoretical phase functions  $p(\theta)$  have been proposed and are known as Henyey-Greenstein, Rayleigh-Gans and Reynolds functions. The first one shows the best accordance with experimental observations. It was introduced by Henyey and

Greenstein [65] and is given by :

$$p(\theta) = \frac{1 - g^2}{(1 + g^2 - 2g\cos\theta)^{3/2}} \quad (2.3)$$

where  $g$  is the anisotropy coefficient that indicates a purely forward scattering when is equal to 1, a purely backward scattering when is -1 and isotropic scattering if it is 0.

## **Turbid Media**

The absorption and scattering processes are generally considered separately. However, human tissues can be considered to be ‘turbid media’, and therefore absorption and scattering phenomena have to be considered simultaneously [66]. In order to achieve a good mathematical description of this, it is possible to use the analytical theory or the transport theory. The first, that relies on Maxwell’s equations, represents the basic approach. However, due to the complexity of the analytical solutions, its applicability is limited; so, especially when dealing with laser-tissue interactions, the transport theory is preferred, that directly determines the transport of photons through absorbing and scattering media. Since scattered photons do not follow a determined path, and transport theory has to deal with the evaluation of the diffuse radiance, lot of approximations and statistical approaches must be chosen. Some of the most used ones are first-order scattering, Kubelka-Munk theory, diffusion approximation, Monte Carlo simulations, or inverse adding-doubling [67–69].

## **Optical properties of the skin**

Although without complete knowledge of the optical structure of tissues, lot of experiments and theoretical models have provided a general understanding of the skin optical behavior [70]. Direct or indirect methods can be used to measure the optical properties of tissues. Direct techniques (unscattered transmission, effective attenuation and gonioscopic measurements of the single scattering phase function) use very simple analytical expressions for data processing, but require that the experimental conditions dictated by the chosen model, are strictly fulfilled. Indirect methods involve solving the problem of reverse scattering by using a theoretical model of light propagation in a medium. They are in turn classified into iterative and non-iterative models. The former use equations in which the optical properties are defined by parameters directly related to the quantities to be assessed. The latter are based on the Kubelka-Munk model and multilayer models [71].

Since PPG sensing probes are placed on the skin surface, their anatomical and physiological characteristics play an important role on this technology. The basic anatomy

of the skin with the blood vessels is shown in Figure 2.9. Human skin can be divided into three layers: the epidermis, the dermis and the hypodermis. Some skin structural models, however, consider the outermost section of the epidermis, composed of dead cells and 0.01-0.02 mm thick, as an independent part named "stratum corneum" [72]. The epidermis (0.027-0.15 mm thick) has no blood supply and is nourished almost exclusively by diffused oxygen from the surrounding air. It is composed of four layers (stratum basale, stratum spinosum, stratum granulosum and stratum lucidum). The 90% of the cells in this layer are keratinocytes, which are continuously shed from the surface; less numerous cells, called melanocytes, located near the base of the epidermis, produce a dark-brown pigment called melanin, which is responsible for the protection of the skin against harmful radiation by means of absorption [73]. The dermis layer (0.6-3 mm thick) consists of two sub-layers: the papillary dermis which contains small blood vessels and the reticular dermis which contains the larger ones [74]. The hypodermis (1-6 mm thick) consists of a layer of fat and connective tissues that houses larger blood vessels and nerves [75].

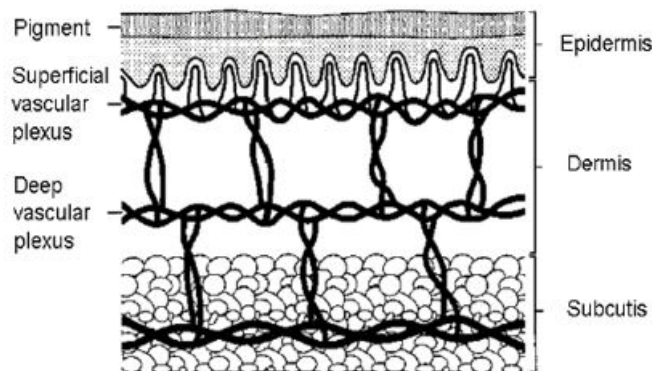


**Figure 2.9:** Basic anatomy structures of the skin [10]

Each tissue constituent has a specific optical behaviour when crossed by a precise wavelength. The absorption spectrum shown in Figure 2.10 represents the optical behaviour in terms of coefficient of absorption/extinction of the main skin absorber with respect to light wavelength [11].

- Water is the main constituent of tissues and enables an efficient transmission only for wavelengths shorter than 950 nm.
- Melanin concentration depends on skin pigmentation and it strongly absorbs light wavelengths shorter than 500 nm. Even if melanin absorption coefficients are, on average, much higher than those of haemoglobin, the total effect of melanin on

light propagation in thick tissues is generally less significant. Haemoglobin is in fact disposed all over the tissue whereas melanin is typically restricted to a thin, superficial skin layer.

- Hemoglobin is the principal constituent of blood and it can be divided in dysfunctional hemoglobin (molecules not able to bind reversibly with molecular oxygen) and functional hemoglobin that can be either fully saturated with oxygen (oxyhemoglobin  $HbO_2$ ) or not (reduced  $Hb$ ). The specific absorption spectra of  $HbO_2$  and  $Hb$ , differ particularly in the red and Near-InfraRed (NIR) region, except at the isobestic wavelengths (close to 800 nm). Using two wavelengths close to the cross-over point, it is possible to estimate oxygenation levels through absorption data [76].

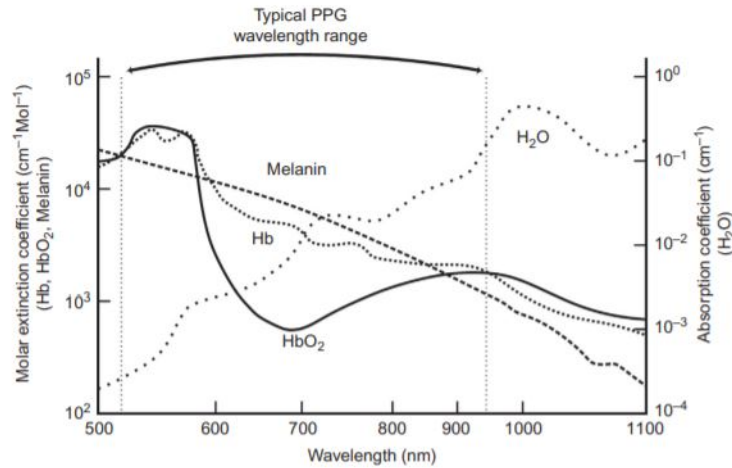


**Figure 2.10:** Absorption and molar extinction coefficients of main biological tissue constituents at 500 to 1100 nm window wavelengths [11]

The wavelength used in PPG, ranges from 510 to 920 nm, corresponding to green and infrared light, respectively. The choice of wavelength has a paramount importance and depends on the targeted application and on the PPG mode used.

## 2.2.2 PPG Modes and the Importance of Wavelength

PPG devices can be used in transmittance or in reflectance mode. In the former case, the photo-detector is placed at the opposite side of the LED source in order to measure the transmitted light components. This is the traditional use of PPG, but in order to be effective, it has to be used only in thin body sites such as fingertip, nasal septum or earlobe [12]. Recently, in the wearable PPG devices field, another transmission type, called reflectance mode, has obtained a lot of interest. It may be employed in wrist,

forearm, ankle and forehead and its set-up requires a photo-detector, located next to the LED, which measures the reflected or back-scattered light from tissue or blood vessels [17].

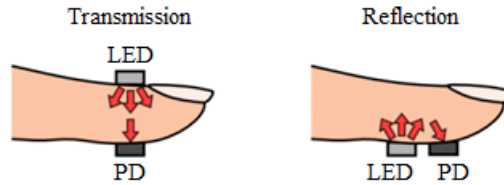


**Figure 2.11:** Placement of the LED and photo-detector in transmittance and reflectance mode [12]

As the Lambert-Beer law states, the penetration of optical radiation in the tissue is wavelength-dependent: as it can be seen in Figure 2.12 the longer the wavelength is, the deeper the light penetrates.

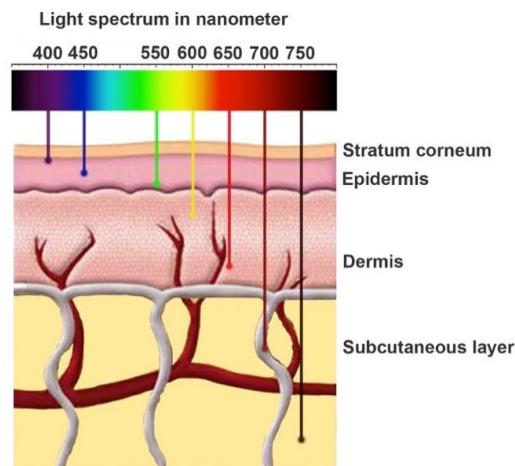


**Figure 2.12:** Propagation of light of different wavelength in the tissues [13]

Traditional pulse oximeters operate in transmission mode and usually employ red and NIR light (wavelength band 660 – 900 nm), able to penetrate relatively deeply (0.8 – 1.5 mm) into a living tissue [77]. On the other hand, wearable PPG devices tend to use reflectance mode, with shorter wavelengths (usually green light in the range 530 - 570 nm). This trend, beside the fact that the reflectance mode allows to take measurements in more comfortable body areas than the transmittance mode, is due to the much higher AC/DC ratio of the reflected green light and to its relative freedom from motion artifacts [78]. These characteristics make reflectance green mode particularly suitable for ambulatory monitoring applications [79]. However, in very cold environments, the microcirculation decreases and it is better to use infrared, capable of reaching deeper

tissues. Even for dark skin pigmentation, infrared light is advantageous. Therefore, selection of an optimal wavelength for ambulatory monitoring is a trade off between susceptibility to artifacts and sensitivity during poor skin perfusion [11].

Experimental observations reveal that the light measured at the photodetector is inversely proportional to the volume of blood in the tissue [55,80]. This is easy to understand in the case of transmission mode with NIR wavelengths: in fact, the tissue is less opaque than blood, and consequently, when the volume of blood increases, the light intensity measured at the output is lower and viceversa. Experimental tests, however, reveal an inverse ratio between the emitted light power and the volume of blood even in the PPG acquired in green reflectance mode [14]. This can hardly be due to pulse-pressure oscillations that occur in arteries because they are located deeper than 3 mm below the epidermis [81], while the depth of penetration of green light does not exceed 0.6 mm [77,82]. In [14] the authors propose a model in which the change in capillary density is responsible for the light modulation during the cardiac cycle. Capillaries are not affected by pulse-pressure oscillations but the transmural pulsatile pressure exerted by arteries on them, may cause variations.

- At the end of diastolic phase, there is a minimum compression that implies a lower density of capillaries reached by the light. In this situation, absorption and scattering phenomena are minimal and the green light re-emitted to the photo-receptor, reaches the maximum power.
- In the systolic phase, the transmural pressure compresses the dermis, the density of the capillaries reached by the light increases and the power of the remitted light is therefore minimal.

As a result, the inverted waveform of the remitted light power follows the changes of transmural blood pressure, not the arterial blood volume. However, the degree of dermis compression depends also on the boundary conditions of the skin (Figure 2.13): with no external contact an elastic skin results in small AC component amplitude, whereas for stiff skin or when an external contact is present, PPG signal is higher [14].

Obviously, any other variation in internal conditions, such as changes in venous pressure, muscle contractions or changes in lymphatic volume, can change the waveform of PPG. The origin of the PPG signal has been the subject of continuing debate [83]; nevertheless, it is generally accepted that both modes of PPG measure blood volume variations in the vascular bed.

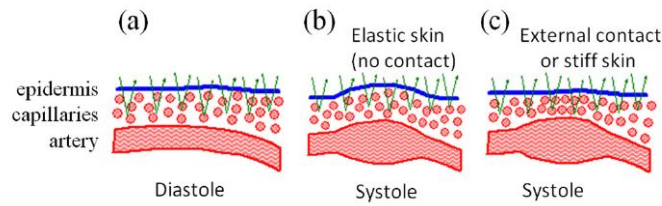


**Figure 2.13:** Origin of PPG waveform according to [14]. (a) Artery is in the diastole phase with the smallest compression of the capillary bed. (b) Systole phase with slightly compressed capillaries because of elastic external boundary. (c) Strongly compressed capillary bed in the case of external contact.

### 2.2.3 The PPG Signal

The PPG waveform encompasses a slow varying DC component, which depends on respiration, sympathetic nervous system activity and thermoregulation, and a pulsatile AC component, which is related to the cardiac synchronous variations in the blood volume with each heartbeat [15].

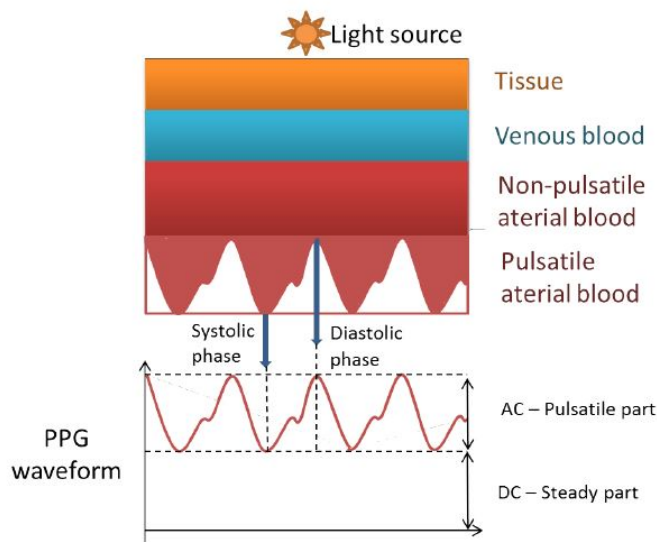


**Figure 2.14:** PPG Waveform [15]

It is essential to note that the PPG waveform is usually inverted (Figure 2.15) in order to vary in relation of blood volume [84]. In the AC pulse it is possible to distinguish two phases: the anacrotic phase, mainly related to systole and corresponding to the rising edge of the pulse, and the catacrotic phase, representing the falling edge of the pulse and identified with the diastole. The incident travelling wave from heart to periphery (anacrotic phase) is due to the left ventricular ejection and the arterial stiffness, whereas the reflected wave from the periphery to the heart (catacrotic phase) depends on the arterial stiffness and the potential sites of wave reflectance [85]. A dicrotic notch, related

to the reflection at bifurcations of the arterial tree, is usually observed in the catacrotic phase of young subject and tend to disappear with increasing age [86].

In general, the characteristic points of the PPG waveform are named as illustrated in Figure 2.15. The pulse wave begin (PWB) represents the start of the systolic phase, that ends at the pulse wave systolic peak (PWSP). The pulse wave end (PWE) indicates the end of the diastolic phase and the time between PWB and PWE is called pulse wave duration.

The time elapsing between two consecutive PWSP, usually expressed in ms, is called peak-to-peak interval (PPI) or interbeat interval (IBI) and has high correlation with the interbeat R-R interval of the ECG signal. The sequence of PPG IBI is called tachogram (as in the ECG case) and it is usually employed for HRV analysis [87].

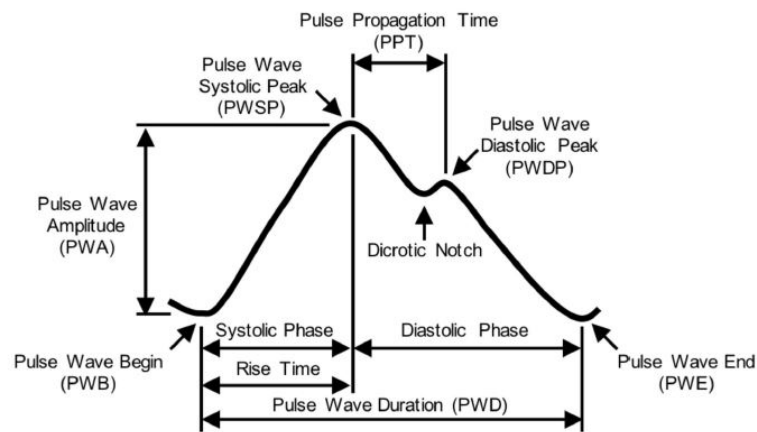


**Figure 2.15:** Pulse wave characteristic of the pulse wave AC component [16]

## 2.2.4 Factors affecting the Quality of the Signal

Phenomena that contribute to the formation of the PPG signal can be, in first approximation, divided into three classes, as shown in Figure 2.16.

In order to effectively extract useful information from the acquired signal, in addition to the wavelength choice, it is also important to properly define the acquisition set-up in such a way as to:

- manage the so-called optical shunting effect, which is the amount of direct light that travels from the light emitter to the photodetector without penetrating the biological tissue [11];
- minimise disturbances caused by ambient light;

- optimize the distance between the light source and the photo detector (empirical studies have shown that the optimal separation distances are between 6 and 10 mm for infrared light [88] and about 2 mm for green light [89]);
- optimize the sensor housing in terms of: adequate pressure of the sensor on the skin surface, mass of measurement system, friction force between the sensor and the skin surface.

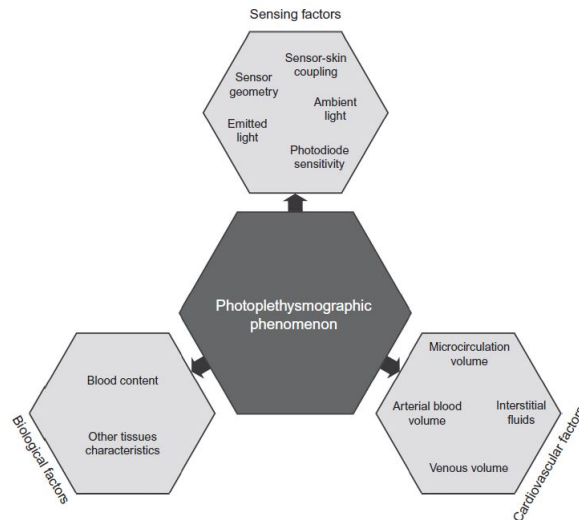


**Figure 2.16:** Families of factors that influence PPG signal [11]

## Motion Artifacts

One of the disturbances that most corrupts the PPG signal and that can be solved only through the opto-mechanical design is the motion artifact, which is due to: tissue modifications caused by movement, relative motion of the sensor-skin interface and changes in the pressure between the optical probe and the skin. Motion artifacts can be classified in three categories. The first is rhythmical motion, generated by activities such as walking, running and biking. The two others categories are non-rhythmical and are divided into intermittent and continuous motions. These latter, especially the continuous one, are generally more difficult to suppress [11]. The removal of motion artifacts from the PPG is mainly addressed through digital signal processing techniques. In order to do this, wearable devices generally acquire other signals as a motion reference. The simplest approach is to use the reference signal only to discard segments corrupted by noise on the other hand, more sophisticated approaches, use the benchmark for noise removal. Some works [90,91], in addition to the acquisition of PPG at the green wavelength, acquire PPG at red or NIR light since the latter two are more affected by movement [78] and, after doing some adaptation of the signal, subtract them from the

green PPG signal. Other works, integrate pressure sensors in the probe as a reference, but most include 3D accelerometers [92–94] although the correlation between the PPG signal and the accelerometer is not particularly accurate. The most commonly used technique is Adaptive Noise Cancellation (ANC); in Figure 2.17 a scheme of an adaptive noise cancellation utilizing an acceleration reference is shown. Other methods such as Moving Average filter [95], Fourier Analysis [96] and Passive Motion Cancellation [97] have been employed.

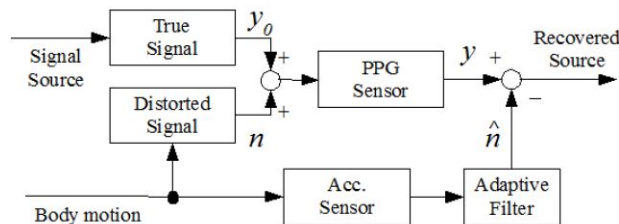


**Figure 2.17:** Block diagram of an adaptive filter with an accelerometer [17]

Adaptive filters exhibit a frequency response that varies depending on the characteristics of the input signal. The adaptive process is carried out in such a way that the filter uses the input signal to adapt its own parameters in order to optimize a predetermined performance index. Therefore, adaptive filters only require little or no prior knowledge of the characteristics of the input signal and noise. ANC filters used in PPG processing include or are integrated with: Least Mean Square (LMS) adaptive algorithm [98], Kalman Filter [99], Time-Frequency Methods and Wavelet Transformation [100,101], Principal Component Analysis (PCA), Independent Component Analysis (ICA), Widrow’s ANC and others [17].

## 2.2.5 Photoplethysmography Applications

PPG has been employed in a variety of clinical contexts for decades and its principal application is the Pulse Oximetry that, in the early 1990s, became a mandated international standard for clinical physiological monitoring during anaesthesia [102]. It measures heart rate and peripheral blood oxygen saturation (SpO<sub>2</sub>) in the course of patient transport [103], fetal monitoring [104], neonatal and pediatric care [105], dentistry and oral surgery [106] and sleep studies [107]. Through PPG it is possible to measure other parameters in physiological monitoring (e.g. blood pressure, cardiac output and respiration) and it can also be used in vascular assessment (e.g. arterial disease/compliance and ageing, endothelial function, venous assessment, vasospastic conditions) and autonomic function assessment (vasomotor function and thermoregulation, blood pressure and heart rate variability, orthostatic intolerance, neurology

and other cardiovascular variability assessments) [108]. Some of these applications are briefly discussed below.

### **Blood Oxygen Saturation**

In Pulse Oximetry, red and NIR lights are used to illuminate the vascular tissue, with rapid switching between the two wavelength. HbO<sub>2</sub> and Hb exhibit differences in the light absorption at these two wavelengths, and this makes possible to estimate the SpO<sub>2</sub> level. For more detailed information on the basic principle of operation, measurement technology and clinical applications, refer to the work of Kyriacou [109].

### **Heart Rate**

Measuring heart rate is important in many clinical settings, including hospital-based and ambulatory patient monitoring. Using the PPG signal, it is possible to provide a HR estimation because its AC component is synchronous with the beating heart. In pulse oximetry systems, this information is often displayed along with the SpO<sub>2</sub> level. In addition, HR estimation is increasingly being used in non-medical areas, for example by sports-people who prefer fitness trackers or smartwatch to annoying ECG chest strap. Even in smartphones, simply putting the finger on the camera with the flash on, it is possible to measure HR along with HRV and other parameters.

The main problem of HR estimation is that movement artifacts and arrhythmias can heavily impair the reliability of the assessment. In order to improve the evaluation accuracy, numerous computer algorithms have been designed. These methods are divided into frequency- and time-domain approaches. The former estimates the spectral density of the signal with a non-parametric (fast Fourier, discrete cosine, or wavelet transforms) or parametric method (autoregressive model), and are usually coupled with the entropy value of the spectrum as a reliability index [11]. Approaches in the time-domain can be based on the detection of the temporal interval between two events related to the heartbeat such as maxima, minima or zero-crossing; the dispersion of the values of these intervals is usually employed as a reliability index [110]. Adaptive frequency tracking approaches have also been proposed. They track the PPG dominant frequency by adjusting the parameters of a model. As for the accuracy assessment, the energy at the dominant frequency over the energy of whole signal is used [111]. The final HR estimation can be obtained through different elaborations such as Bayesian estimation [112], autoregressive estimation using reliability [113], outlier rejection [114].

## **Cardiac Output**

Cardiac output is the stroke volume multiplied by HR. An accurate assessment via reliable and non-invasive measurements is very important. However, among researchers, there is a debate about the real accuracy of the PPG-based cardiac output evaluation [115]. The stroke volume (the quantity of blood pumped out of a ventricle during one ventricular contraction) can be estimated from PPG-derived pulse contour analysis on a beat by beat basis, and methods for doing this include Pressure Recording Analytical Method (PRAM) [116] and the ModelFlow™ method [117].

## **Respiration**

Through a PPG sensor it is possible to monitor breathing, because respiration induces changes in the peripheral circulation. Monitoring the respiratory rate is important in many clinical environments, for example in critical and neonatal care, in anaesthetics and for sleep study. The low frequency Respiratory Induced Intensity Variations (RIIV) in the PPG signal are well known [118, 119]. The RIIV mechanism is not totally understood, but many researchers state that is due to the return of the venous blood to the heart induced by respiratory changes in intra-thoracic pressure and also variations in the sympathetic tone control of blood vessels of the skin [12].

## **Blood Pressure**

Arterial blood pressure is very important in clinical measurement, in particular in autonomic function and vascular disease studies. Since 1980s, the PPG signal has been used for measure arterial blood pressure non-invasively, and different approaches has been described in the literature [120, 121]. In order to measure the dynamic pulsatile vascular unloading of the finger arterial wall, it is necessary to use an inflatable cuff integrated with a PPG sensor [12]. Since cuff-less blood pressure measurement methods are highly-desirable, many researchers [122] have focused on the relationship between blood pressure and Pulse Transit Time (PTT), which can be estimated using both PPG and ECG signals, by measuring the distance between the ECG's R peak and the PPG's peak. PTT is the time that a pressure pulse spends to propagate through a length of the arterial tree. Others similar parameters such as Pulse Wave Velocity (PWV) and Pulse Arterial Time (PAT) have been used for this purpose [123, 124]. Recent studies have also been focused on the blood pressure estimation with the solely usage of the PPG signal. In order to do this, PPG pulse features were extracted and analysed using neural networks [125].

## **Vascular Assessment**

In case of arterial disease, the peripheral pulse is usually lower and delayed. In order to establish the severity of vascular disease, numerous features have been explored such as risetime, frequency parameters, width/height ratio, amplitude and shape. Particular in literature, attention devoted the lower limb arterial disease detection [126].

Another factor that can be controlled through PPG is the vascular ageing. It is known that the stiffer the artery is, the faster the pulse reaches to the periphery; hence, the PWV increases. The arteries compliance have also been determined by means of the PTT, which is inversely related to the PWV [127]. The determination of arterial stiffness is significant since it is associated to hypertension, a risk factor for stroke and heart diseases. Furthermore, arterial ageing could be accelerated by other diseases such as diabetes mellitus [128].

Along with other assessment such as endothelial function and vasospastic conditions, the PPG waveform can be used to determine venous conditions [12]. In particular, lower limb chronic venous insufficiency (CVI), due to damaged valves, often causes the blood reflux in the legs on standing position. The PPG-based exam to investigate CVI, also referred as Light Reflection Rheography, consists in measuring the time for the PPG signal to recover to baseline, while the patient is doing tip-toe exercise [129].

## **Autonomic Function**

The variability of PPG components such as the low-frequency ones related to respiration, blood pressure and thermoregulation as well as the high frequency ones, related to the heartbeat, has been used to study the autonomic function [12]. It is well known that HRV obtained from ECG is an important parameter to determine the autonomic activity [130]. Therefore, since HR and its variability can easily be extracted from PPG pulse signals, Pulse Rate Variability (PRV) has been investigated. Another example is the use of beat-to-beat peripheral arterial blood pressure waveforms, measured using PPG technology with pressure on the finger, in order to measure Baroreflex Sensitivity, associated with cardiovascular disease. Using bilateral PPG at the forehead, it is possible to determine the autonomic function in patients having migraine, by detecting the trigemino-parasympathetic reflex to vasodilator response [12].

# Chapter 3

## State of the Art

As discussed in Section 2.1.3 the ECG, considered the standard in the detection of arrhythmias, does not allow continuous monitoring over a long period of time, and this could imply a misdiagnosis. Current standard of care include also Holter and Event Monitor, but the electrodes used to record the signals often result in discomfort, limited freedom of movement and sense of unhealthiness, especially after wearing the device for several days [131]. For these reasons, they are usually not worn for more than 72 hours (Holter Monitor) and 30 days (Event Monitor). Moreover, they are costly and not accessible to all. For these reasons, many wearable PPG-based devices have been designed in recent years, and researchers have shown interest in detecting arrhythmias through them. Of all the PPG-based wearables (earphones, rings, gloves, glasses, ear-clips), wristwatch-type ones are the most common and are traded by several companies as pulse oximeter, blood pressure sensors or heart rate detector.

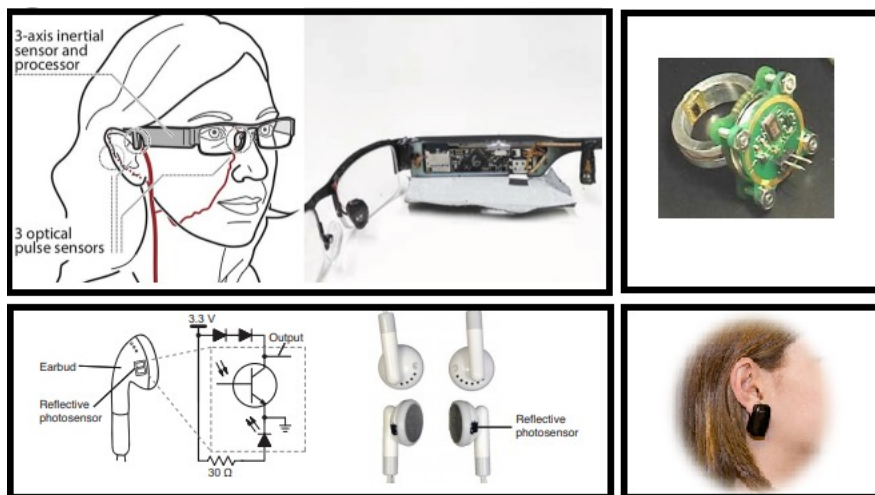


**Figure 3.1:** Wearable PPG-based devices [17–19]

The HR-detector wearables are mostly used in sport and fitness area and the biggest challenge from the algorithmic point of view, as it has been explained in Section 2.2.5, is to correctly remove movement artifacts, in order to provide a reliable HR estimation. It is important to underline that these smartwatches are not usually employed in clinical settings, because obtaining a "medical device certification" is not trivial [17]. Among all the arrhythmias, researchers have been particularly interested in detecting atrial fibrillation through PPG-based wearables. AF is very common and can cause thrombosis, it may also be asymptomatic and it is not always possible to detect it during ECG test. Holter Monitor test or more accurated exams are often required therefore, a device capable of continuously and non-invasively monitoring could be very useful not only in detecting AF but also in supporting patients (with AF already diagnosed) for the management of their therapy [132]. The most striking example of a PPG-based device, capable of detecting AF, is the Apple Watch (Series 1-4 with watchOS 5.2 or later) paired with iPhone 5s or later (with at least iOS 12.2). The AF detection it is not exactly continuous but it is performed on PPG-tachograms which are recorded every 2 to 4 hours. If an irregular tachogram is registered, the algorithm starts to acquire more tachograms (with a minimum distance of 15 minutes) and, when 5/6 successive tachograms are irregular in 48 hours, a notification of possible AF is sent [133]. Many other researchers have designed AF detection algorithms: some have implemented it on the Physionet databases's signals (acquired in a clinic environment from the finger), others have used signals acquired from the phone, placing a finger on the flash [134], while others, like Apple, have tested it on a wearable device [135–139]. From the algorithmic point of view, most of the developed methods for AF detection rely on the extraction of IBI from PPG signals, and investigate the possibility of decision making based on IBI series (tachogram) statistics. Some authors have preferred simple methods such as a set of decision rules, while others selected more complex machine learning classifiers.

As described in Section 2.1.2, although premature ventricular contraction can be generally considered benign, it is important to monitor their frequency, their pattern, the presence of multifocal PVCs and the R-on-T phenomenon occurrence, since they may be associated with underlying heart disease or may trigger more severe arrhythmia. PVCs research can also be useful in determining whether the patient's symptoms can be linked to more critical conditions, and therefore, if further investigations are needed. Although it can be convenient to screen PVCs on large scale, by means of a more comfortable device which allows a continue and long-term monitoring, to date the amount of PPG-based algorithms for detecting PVC, is very scarce.

*Solensko et al.* yielded the major contribution in this field. In their first work [20] they

extracted 7 simple features from the signal time domain: amplitudes of the rising and falling fronts, peak-to-peak intervals, pulse durations and pulse widths. These features, which describe every single beat, are then normalized and processed for the heartbeat categorization through a Naive Bayes Classifier (NBC). Results show high sensitivity (96.40%), specificity (99.92%) and accuracy (99.89%).

In another research project [20] the authors extracted 6 features (3 temporal-derived and 3 power-derived), obtained from a 12-s analysis frame. Three successive Peak-to-Peak Intervals (normalized using the fundamental frequency calculated over the 12-s frame) and 3 successive Variance Ratios are extracted and pre-processed, in order to be classified using an Artificial Neural Network (ANN) with one hidden layer. Severely corrupted segments are removed from the analysis. Not only the algorithm is able to divide normal beats from PVCs, but it is also capable to distinguish between two different PVC morphologies (Figure 3.2). Sensitivity and specificity for the two main PVC types are 96.05/95.37% and 99.85/99.80% respectively.

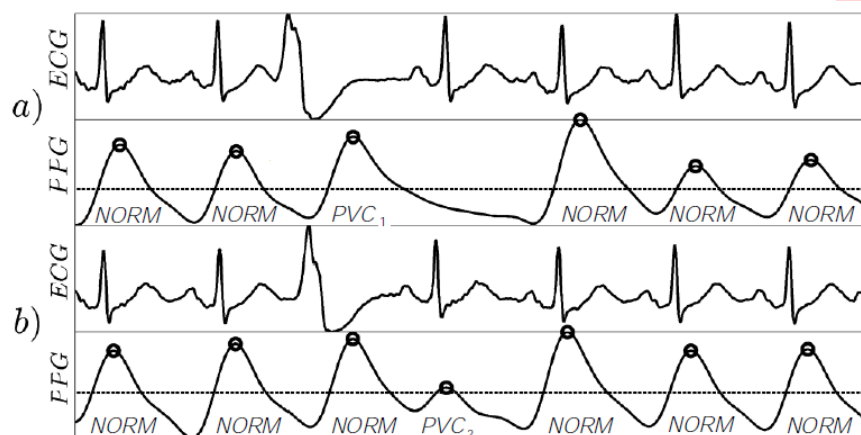


**Figure 3.2:** Types of PVCs in the PPG signals: a) with premature pulse  $PVC_2$  b) without premature pulse  $PVC_1$  [20]

Finally, in their most recent work [140], the authors aim to improve the previous algorithm performance. Features are still extracted on a 12 s frame, but the 3 PPI features are normalized with an estimated normal sinus rhythm's frequency (in order to reduce noise influence) and the 3 Variance Ratios features are replaced with 3 different Power Ratios features. To reduce the number of false alarms, an artifact detector has been included. The classification of the features has been performed using a feed-forward ANN with 40 hidden layers. PPG pulse classification has been done into 10 classes and 3 super-classes (normal beat, PVC with premature pulse  $P_1$  and PVC without premature pulse  $P_2$ ) but only super-class results have been reported. Sensitivity for normal beats,  $P_1$  and  $P_2$  turned out to be 99.8%, 93.2%, 92.4% respectively. Specificity

values 93.3%, 99.9%, 99.9% respectively.

All the Solensko's algorithms are evaluated on data from the Physionet MIMIC and MIMIC II databases [141], as well as one signal obtained from a clinical study.

*Yousefi et al.* have also used MIMIC and MIMIC II databases in order to extract features from PPG signal. Among different statistical and chaotic features, they have selected (using PCA) kurtosis, skewness, entropy, fuzzy entropy, power spectral entropy and maximal Lyapunov exponent, in order to evaluate the performance of different classifiers (k-nearest neighbors (kNN), support vector machine (SVM) and neural network) in recognizing PVCs from normal beats [142]. The best results has been obtained using a kNN classifier with accuracy of 95%, specificity of 90.4% and 89.9% sensitivity.

In [143] the authors present a method for classifying PVC and VT from NSR and supraventricular premature contraction recorded in patients subjected to ablation therapy for arrhythmia. Different discriminative features have been extracted: they are based on time-domain signal processing, Fourier Analysis and non-linear dynamics of the HRV. The classification has been performed through a SVM and for all the cases, classification accuracy above 90% has been obtained. However the results cannot be generalized since in this work the arrhythmias were induced during electrophysiology laboratory for arrhythmia ablation.

## **Part II**

# **Materials and Methods**



The real-time implemented algorithm will be embedded into the *Bio2Bit Move* (a STMicroelectronics prototype) for an arrhythmia telescreening application. However, as a preliminary stage, it is necessary to design, test and optimize the algorithm using off-line signals in a PC environment. The algorithm development was done by the analysis of the off-line *Bio2Bit Move* signals, using the software Matlab<sup>®</sup>.

The algorithm structure is shown in Figure 3.3 and it is composed of six main blocks:

- **PPG Signals Preprocessing:** the red and green PPG signals are imported and processed in order to remove high-frequency noise and baseline wandering.
- **Features Extraction:** features in both time and frequency domain, as well as morphological parameters, are extracted to be analysed and used in further steps.
- **Motion Analysis:** accelerometer signals are filtered and used to calculate movement indices, which are employed to establish whether the PPG signal segment under analysis is usable or not (because too noisy).
- **Heart Rate Estimation:** through the extraction of the time position peaks and frequency features calculated over a 10-seconds sliding window (with 50% of overlap), it is possible to provide an estimation of the HR every 5 seconds.
- **Arrhythmia Detection:** morphological features of the single pulse are used in order to detect PVCs, but also other temporal, statistical and frequency features are investigated. An alarm is setted in case of more than 7 PVCs per minute.
- **Reliability Level Computation:** the HR estimation is always coupled with a measure of reliability. This is based on the parameters evaluated from the accelerometer signal or from the PPG signal itself and establish if the level of the reliability is low, medium or high.

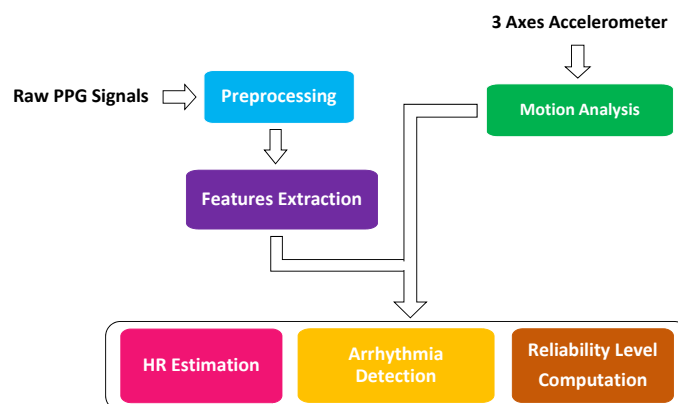


**Figure 3.3:** Algorithm's Block Diagram

# Chapter 4

## Data and Acquisition

### 4.1 Subjects and Databases

The algorithm was developed using off-line signals acquired by the *Bio2Bit Move*, except for the PVC detection. For this part, in fact, since no patients with previously diagnosed PVCs were available, 15 signals taken from the openly available MIMIC [144] and MIMIC II/III Waveform Database [141, 145, 146] were used. MIMIC Databases contains recordings of multiple physiological signals (almost always ECG and often finger PPG in transmission mode, continuous ABP together with others) and time series of vital signs (called "*numerics*") collected from bedside patient monitors in adult and neonatal intensive care units (ICUs). In order to implement the algorithm, only PPG and ECG signals were downloaded. ECG signals, along with the respective annotation signals (named "*PVC Count*"), that indicates how many PVCs occur in one minute, were used as a reference. However, the annotations are not always reliable, so a double visual check was made on the ECG signal. Signals sampling frequency is 125 Hz and their duration is about 1 hour.

In order to gather off-line signals through the *Bio2Bit Move*, 8 volunteers were recruited. In addition to the *Bio2Bit Move*, patients were asked to wear the *BioToBit HI* which served as a reference for the HR Estimation. Recorded subjects were in healthy state, their age ranged from 21 to 33 and as for the gender, 4 were male and 4 were female. The acquisitions duration ranges from 10 to 20 minutes, but the record *S#1*, that was used for building the algorithm, has a duration of 45 minutes. Acquisitions were done in a daily-life environments: this meets the non-invasivity requirement for a screening device used 24/7 in a non hospital contest and exploits the spreading of smart devices able to embed such systems. Recorded reflectance PPG and accelerometer signals were used in order to extract features, estimate the HR and calculate the reliability of the measure.

From now, for the sake of clarity, the signals acquired from the *Bio2Bit Move* will be called  $S\#N$  where N indicates the number corresponding to the subject, while the signals downloaded from the MIMIC Database, will be indicated with  $D\#N$ .

## 4.2 Acquisition System

The signal acquisition process was carried out by placing the *Bio2Bit Move*, inserted in a suitable housing with an adaptable strap, on the left wrist of the volunteers (2 cm from the ulnar styloid process). The subjects were also asked to wear the *BioToBit HI* device, a 3-Lead ECG patch designed by STMicroelectronics, as a reference. The positioning of the devices is shown in Figure 4.1.

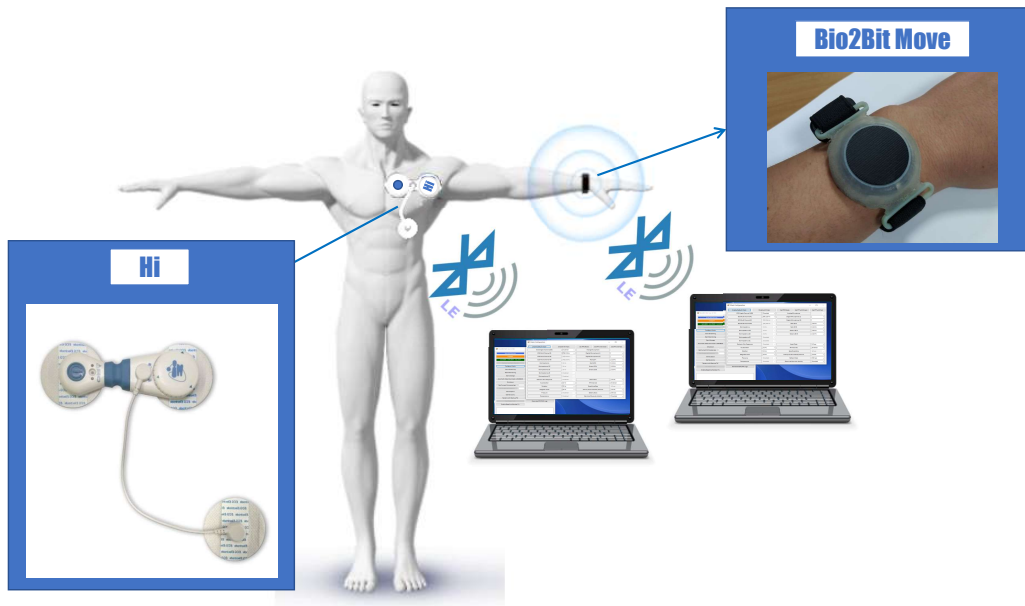


**Figure 4.1:** Signals Acquisition System

Since the application *Bio2Bit BLE (rev. 0.130)* for the signal acquisition is capable of handling only one device at a time, two computers were used in order to record PPG and ECG at the same time. Both the PCs must support BLE.

In order to acquire the signals, after positioning and turning on the devices, the following steps are necessary:

1. Start the *Scan BLE Devices* from the main application screen (Figure 4.2).
2. Select the device from the drop-down menu.

3. Connect the device by clicking on *"Connect and Sync the Device"*.
4. Open the section *"Configure Vitals"* (Figure 4.2). For the *Bio2Bit Move* enable *Acceleration, Red LED A* and *Green LED A*, selecting for all a sampling frequency of 128 Hz. For the *BioToBit HI* enable only *Multi Channel #3 ECG* with a sampling frequency of 128 Hz on the other computer. To exit and save, click on *"Configure Vitals"* again.

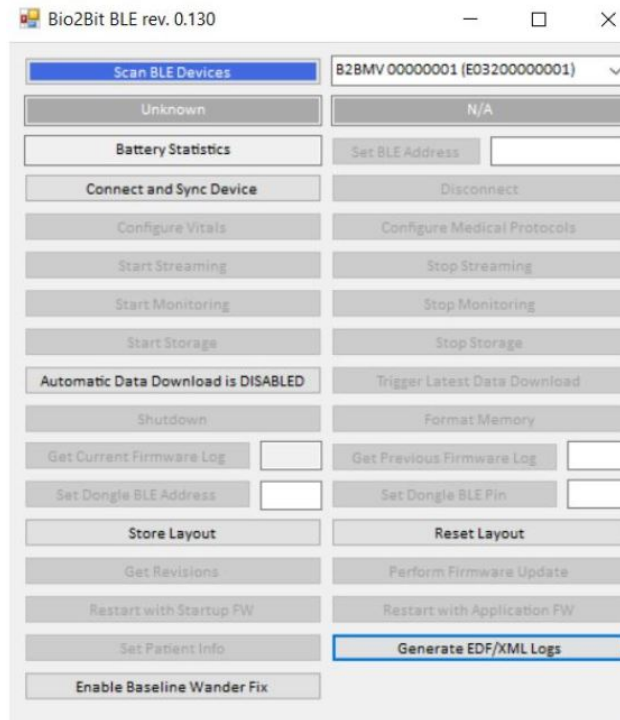


**Figure 4.2:** Main Bio2Bit BLE Application screen

5. To standardize the off-line synchronization of the signals, start first the recording with the *HI* device, clicking on *"Start Monitoring"*.
6. Start then the acquisition with the *Bio2Bit Move* clicking on *"Start Streaming"*.
7. To stop the recording, press first *"Stop Streaming"* for the *Bio2Bit Move*. In this case, the recorded signals are stored directly in binary format, in the log folder.
8. Stop then the *HI* acquisition clicking on *"Stop Monitoring"*. In this case it is necessary to download the binary files by clicking on *"Trigger Latest Data Download"*.
9. At the end, shut down the devices by means of the application.

After the acquisition, the signal binary files are parsed through a Matlab script and are ready to be analysed through the software.

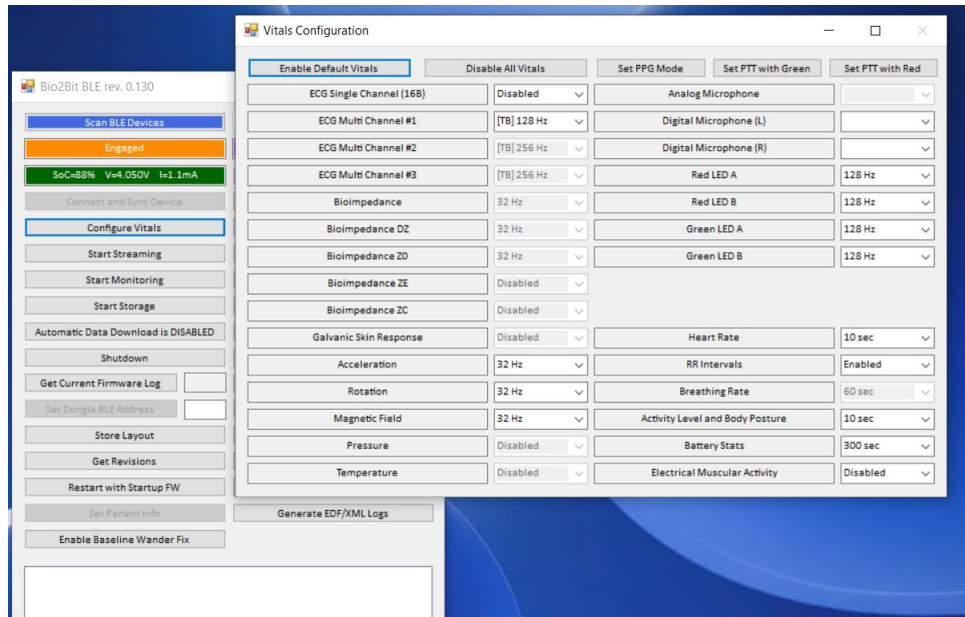


**Figure 4.3:** Bio2Bit BLE Application - Vital Configuration section

### 4.2.1 Bio2Bit Move

In order to acquire the signals, the *Bio2Bit Move* (3.5 cm in diameter) is placed in a custom-designed 3D-printed ABS (Acrylonitrile Butadiene Styrene) case, which is 1.5 cm thick and has an external diameter of 3.8 cm. As illustrated in Figure 4.4, it is suitably drilled in correspondence of the LEDs, the photodiode, the on/off button, the Debug/Extender Connector and the Micro-USB exit. This case can be placed in a more flexible 3D-printed rubber-like photopolimeric support (4.5 cm of external diameter) on which is possible to insert an elastic strap with velcro patches, so as to adjust the positioning of the instrument on the wrist.

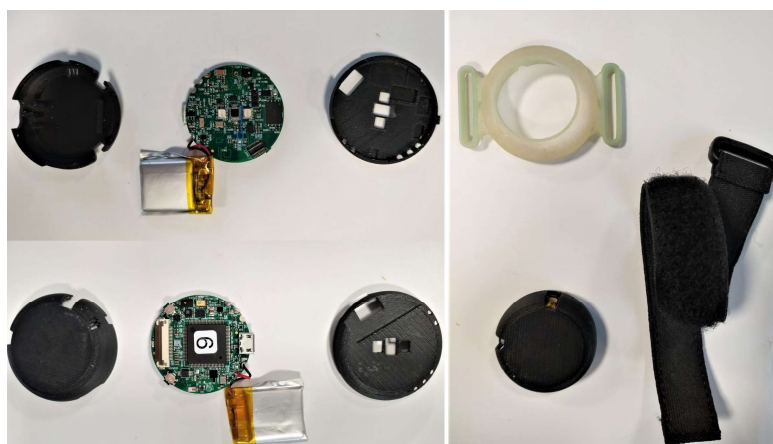


**Figure 4.4:** *Bio2Bit Move* and accessories for board housing and for its positioning on the wrist

*Bio2Bit Move* is a wearable electronic, battery operated device for the acquisition and transmission of physiological parameters to external devices which can analyse or forward the data to additional storage elements or systems. Applications for which it was designed include: chronic disease monitoring, elderly people home monitoring, event monitoring, measure of HR, RRV,  $SpO_2$  and PTT, through PPG and/or ECG (1 lead) recording.

In Figure 4.5, it is possible to see that the board houses a certain number of sensors, managed by a Microcontroller Unit (MCU) which belongs to the ultra-low power microcontrollers family (STM32L4+ Series) based on a 32 bit Arm Cortex<sup>®</sup> -M4 RISC (Reduced Instruction Set Computer) core. The devices of the STM32 series are low-power and low-voltage with dynamic voltage scaling (from 1.7 to 3.6 V). They includes comparator, ADC/DAC (with 12-bit native resolution and built-in calibration and typical Signal to Noise Ratio (SNR) about 71 dB) and hardware encryption. The CPU working frequency is up to 120 MHz. The Cortex-M4 core features a single-precision floating-point unit (FPU) and it also implements a full set of digital signal processing instructions. The integrated memories are a 2 MB Flash memory and a 640 kB SRAM (Static Random Access Memory). These devices embed an extensive range of enhanced I/Os and peripherals connected to two APB (Advanced Peripheral Bus), two AHB (Advanced High-performance Bus) and a 32-bit multi-AHB bus matrix.

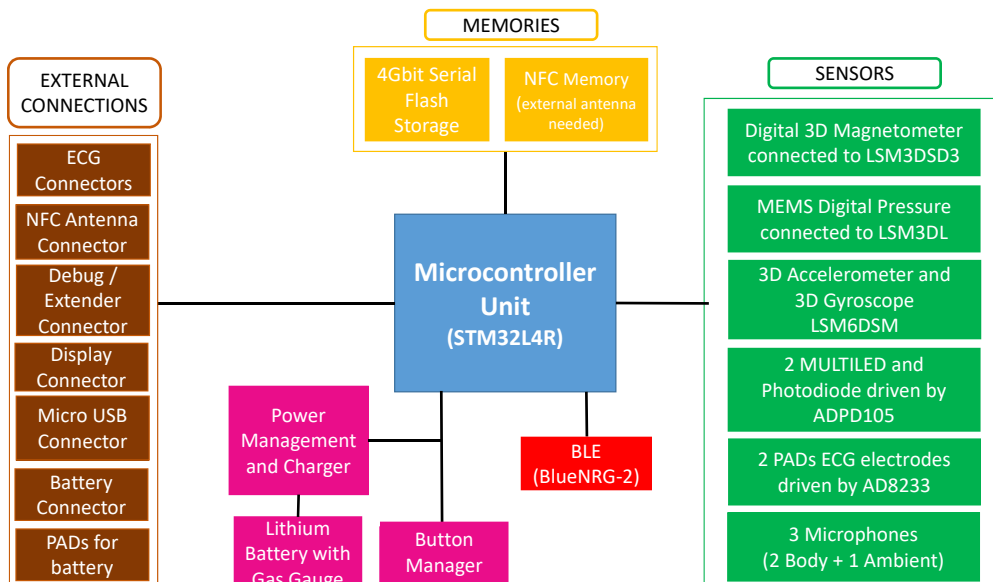


**Figure 4.5:** *Bio2Bit Move* Hardware block diagram

Among all the sensors embedded into the board, only the 3D digital Accelerometer (present in the LSM6DSM system along with a 3D digital Gyroscope) and the PPG sensor system were used in this work. Their position on the board, along with that one of the main components, are highlighted in Figure 4.6.

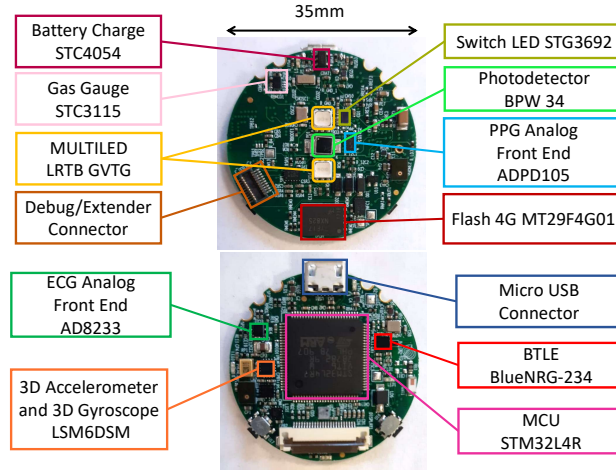


**Figure 4.6:** Position of the sensors used and the main components on the *Bio2Bit Move* board

The main characteristics of the **3D Accelerometer** are:

- *Dimensions:* 2.5x3x0.83 mm (they are referred to the entire LSM6DSM module);
- *Full Scale:*  $\pm 2/\pm 4/\pm 8/\pm 16$  g ( $\pm 2$  g was used);
- *Sensitivity:* 0.061 mg/LSB (using  $\pm 2$  g as full scale);
- *Noise Density:*  $75 \mu\text{g}/\sqrt{\text{Hz}}$  (using  $\pm 2$  g as full scale);
- *Supply Voltage:* 1.7 - 3.6 V;
- *Bandwidth:* 128 - 636 Hz

The **PPG Sensor** consists of 2 *MultiLED* (*LRTB GVTG*), a *Silicon PIN Photodiode* (*BPW34*) and a *Photometric Front End* (*ADPD105*).

Each *MultiLED* has a red, green and blue LED but the blue one is disabled on the board. *MultiLED* and *Photodiode BPW34* main features are listed in Tables 4.1 and 4.2, respectively.

*ADPD105* is an highly efficient front end, with an integrated 14-bit ADC: considering a transimpedance amplifier feedback resistor of 25 k $\Omega$  and a photodiode capacitance of 70 pF, the saturation SNR per pulse per channel is 78.3 dB. It also has a 20-bit burst accumulator that stimulate a LED and measures the corresponding optical return

signal. The data output and functional configuration occur over a 1.8 V  $I^2C$  interface. The analog device operates in two independent time slots (Time Slot A and Time Slot B), which are carried out sequentially for every sampling period, as illustrated in Figure 4.7. The entire signal path from LED stimulation to data capture and processing is executed during each time slot in a separate datapath that uses independent settings. Each Time Slot ( $t_A$  and  $t_B$ ) can be calculated as:

$$t_S = Slot_{OFFSET} + n_S \times Slot_{PERIOD} \quad (4.1)$$

where  $n_S$  is the number of pulses for Time Slot (Register 0x31, Bits [15:8]),  $Slot_{OFFSET}$  is the delay from power-up to LED rising edge and  $Slot_{PERIOD}$  is the time between LED pulses in the Time Slot. The minimum  $Slot_{PERIOD}$  can be obtained from:

$$Slot_{PERIOD, minimum} = 2 \times 4 \mu s + 11 \quad (4.2)$$

where  $4\mu s$  is the Slot Analog Front End Width.  $Slot_{PERIOD}$  can range between 19 -  $63\mu s$  whereas  $Slot_{OFFSET}$  varies between 23 -  $63\mu s$ . After each Time Slot there are also two fixed times ( $t_1 = 68\mu s$  after  $t_A$  and  $t_2 = 20\mu s$  after  $t_B$ ) that depend on the computation time for each slot. The sleep time between sample periods is minimum  $222 \mu s$ .

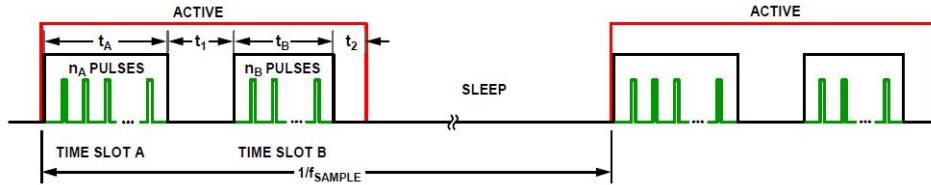


**Figure 4.7:** Time Slot Timing Diagram.

In order to perform streaming of signal acquisition or data download, a Bluetooth low energy single mode system-on-chip (*BlueNRG-2*) is integrated in the board, along with an antenna and a Balun chips. Bluetooth Low Energy protocols, only transmits small packets as compared to Bluetooth Classic. *BlueNRG-2* improves the *BlueNRG* sleep mode current consumption (down to  $1 \mu A$ ) allowing a further increase in the battery lifetime of the applications. The *BlueNRG-2* includes 256 kB of programming Flash memory, 24 kB of static RAM memory with retention (two 12 kB banks) and SPI, UART,  $I^2C$  standard communication interface peripherals. It also features multifunction timers, watchdog, real-time clock and Direct Memory Access controller. An ADC (10-bit) is available to interface with analog sensors, and to read the measurement of the integrated battery voltage sensor (the operating supply voltage ranges from 1.7 to 3.6 V).

<b>MultiLED LRBT GVTG</b>			
	<i>Red</i>	<i>Green</i>	<i>Blue</i>
Surgent Current ( <i>mA</i> )	100	300	300
Reverse Voltage ( <i>V</i> )	12	5	5
Wavelength at peak emission ( <i>nm</i> )	632	523	465
Dominant wavelength ( <i>nm</i> )	619-631	519-546	459-476
Spectral Bandwidth at 50% $I_{rel,max}$ ( <i>nm</i> )	18	33	25
Viewing Angle at 50% $I_V$ ( $^\circ$ )	120	120	120
Forward Voltage ( <i>V</i> )	1.8-2.4	2.9-3.7	2.9-3.7
Reverse Current ( $\mu A$ )	0.02-10	0.01-10	0.01-10

**Table 4.1:** Main MultiLED LRTB GVTG Characteristics for a *Forward Current* of 20 *mA*

<b>Photodiode BPW34</b>	
Reverse Voltage ( <i>V</i> )	32
Total Power Dissipation ( <i>mW</i> )	150
Spectral Sensitivity ( <i>nA/lx</i> )	80
Wavelength of max Sensitivity ( <i>nm</i> )	850
Spectral range of Sensitivity $S= 10\%$ of $S_{max}$ ( <i>nm</i> )	400 ... 1100
Dimensions of Radiant Sensitive Area ( $mm^2$ )	2.65x2.65
Noise equivalent power ( $W/\sqrt{Hz}$ )	$4.1 \times 10^{-14}$
Rise and fall time of the photocurrent ( <i>ns</i> )	20
Forward Voltage ( <i>V</i> )	1.3
Capacitance ( <i>pF</i> )	72

**Table 4.2:** Main Photodiode BPW34 Characteristics

## 4.2.2 BioToBit HI

The *BioToBit HI* device is a wearable electronic, coin battery operated device that is worn on the chest with standard patches. It allows to acquire and transmit physiological parameters to external devices which can analyze or forward the data to additional storage elements or system. Its applications include:

- Chronic cardiac disease monitoring
- Elderly people home monitoring
- Event monitoring
- Cardiac rhythm disturbances detection

Thanks to BLE 4.1, *HI* is characterized by a low power consumption during data transfer and sleep mode. Moreover, it allows to transfer the acquired signals to an external device in real-time (streaming mode) or simply download the data previously recorded (monitoring mode) and stored in the internal Flash Memory. The board is able to register 3-leads ECG and 3-axis accelerometer and to process the HR, HRV, RR intervals, Activity Level and Body Posture. In Figure 4.8 channels and signal polarity setting are shown. In this work only the Channel II of the ECG was used as a reference.

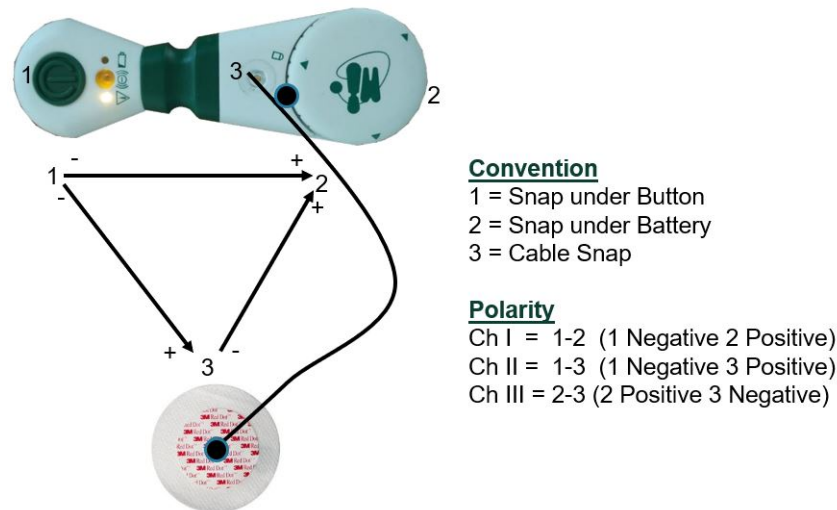


**Figure 4.8:** HI Hardware Signal Polarity

# Chapter 5

## Implemented Algorithm

### 5.1 PPG Signals Pre-Processing

The pre-processing phase was implemented using a real-time setting and all the steps performed for the PPG green signal were also implemented for the PPG red one. Block diagram of the pre-processing phase is shown in Figure 5.1. In Figure 5.2, signals obtained at each step are illustrated.

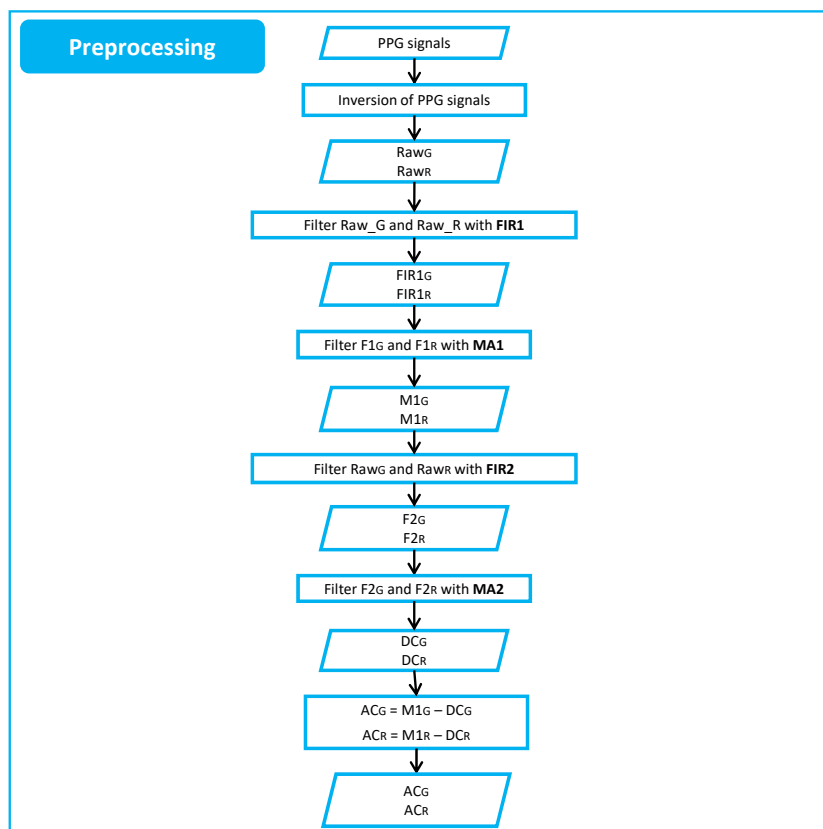
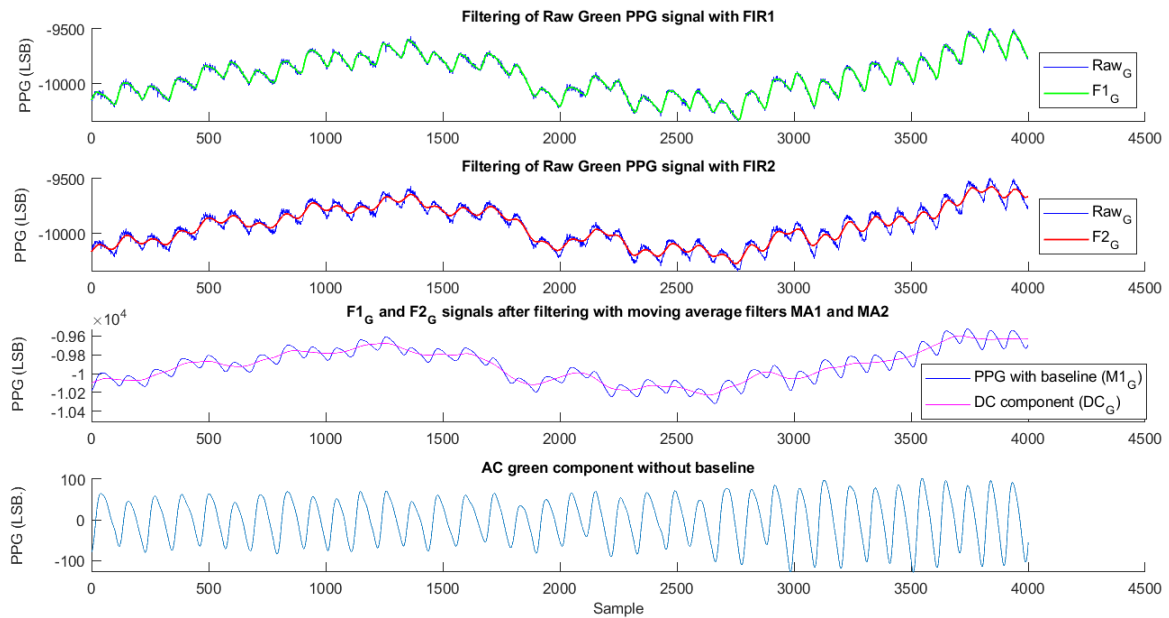


Figure 5.1: Pre-Processing Block Diagram

PPG signals were initially inverted: in this way their amplitude varies in a proportional relation with blood volume. Usually PPG signals are filtered with high-order passband filter in the range of [0.5 - 5] Hz. IIR (Infinite Impulsive Response) filters have non-linear phase so FIR (Finite Impulsive Response) filters were employed but since after a simple bandpass filter, the PPG signal was still corrupted by noises, a different approach was used. The inverted raw PPG green and red signals (called respectively  $Raw_G$  and  $Raw_R$ ), were filtered through a Low-Pass Finite Impulse Response (FIR) 100-order filter, with a cut-off frequency of 6 Hz (called  $FIR1$ ). In order to smooth the signal, the filtered data ( $F1_G$  and  $F1_R$ , respectively) were processed with a moving average filter using a sliding window 21 samples long, named  $MA1$ . The output signals are called  $M1_G$  and  $M1_R$ .

$Raw_G$  and  $Raw_R$  were also filtered with  $FIR2$ , a different Low-Pass FIR 100 order filter with a cut-off frequency of 0.001 Hz, in order to isolate the DC component of the raw signals. Since the output waveforms ( $F2_G$  and  $F2_R$ ) still contained the pulsatile component, a moving average filter, with a sliding window 101 samples long, was used (named  $MA2$ ). The obtained  $DC_G$  and  $DC_R$  components are respectively subtracted from  $M1_G$  and  $M1_R$  signal, in order to remove the baseline wandering from them. The obtained signals  $AC_G$  and  $AC_R$ , are the pulsatile components, which were used in further steps in order to estimate the HR. FIR filters ( $FIR1$  and  $FIR2$ ) were designed in MATLAB and are represented in module and phase in Figure 5.4.



**Figure 5.2:** Signals obtained at each pre-processing phase

In Figure 5.3 the signal spectral estimation along with the SNR, before and after pre-processing is reported. The SNR in dB is calculated as the ratio between the power in the signal AC frequency band [0.5-5] Hz and the power of the noises frequency band (that also includes the DC component frequencies):

$$SNR = \frac{\sum_{f=0.5Hz}^{5Hz} PSD(f)}{\sum_{f=0Hz}^{0.5Hz} PSD(f) + \sum_{f=5Hz}^{64Hz} PSD(f)} \quad (5.1)$$

PSD was estimated through a Periodogram using an apparent resolution of 125 mHz.

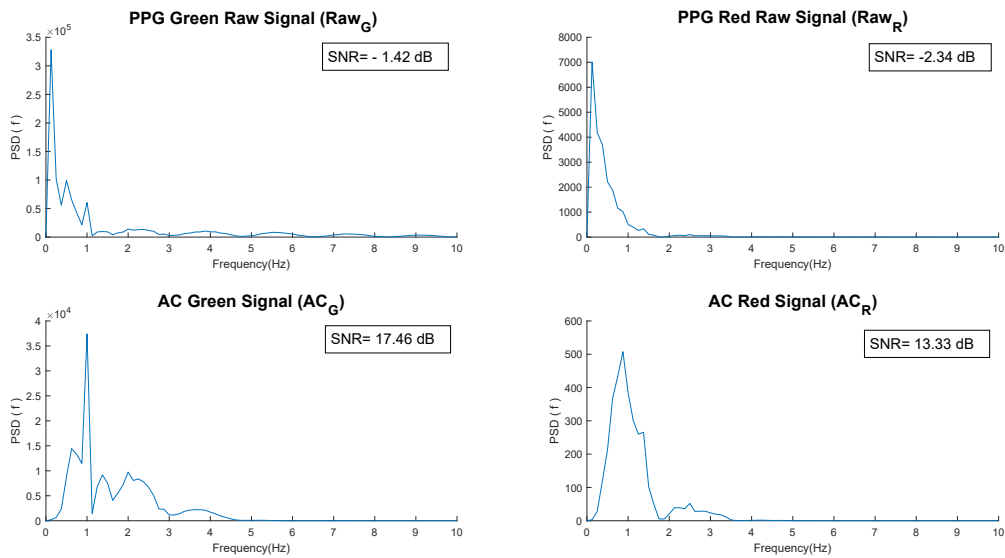
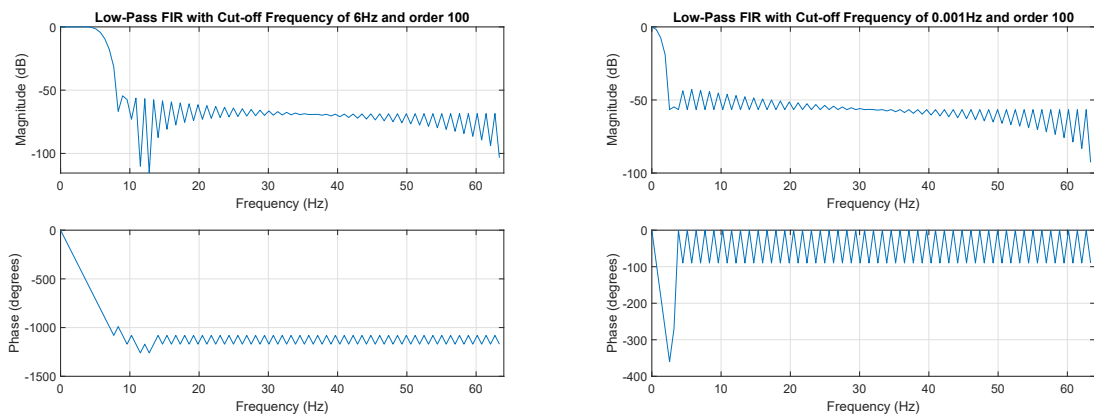


**Figure 5.3:** Spectral Estimation of the PPG signals, before and after the pre-processing phase.



(a) FIR1: Order=100 and Cut-off Frequency=6Hz

(b) FIR2: Order=100 and Cut-off Frequency=0.001Hz

**Figure 5.4:** Low-Pass FIR Filter Design

## 5.2 Feature Extraction

The Feature Extraction can be divided in a "Morphological Feature Extraction", performed on the single pulses and in a "Segment Feature Extraction", executed over a 10 seconds time segment with a 50% of overlap.

### 5.2.1 Morphological Feature Extraction

In order to perform the Morphological Feature Extraction, it was necessary at first to detect peaks and valleys from the preprocessed  $AC_G$  signal. The selection of morphological parameters and their extraction process will be described later.

All the algorithm steps performed in Figure 5.5 were also executed on the preprocessed  $AC_R$  signal but for illustrative purposes, only operations on the  $AC_G$  signal are represented.

When five samples of the pre-processed signal are acquired, the derivative of the  $AC_G$  signal ( $dG$ ) is computed. The sign of the derived sample  $dG(i)$  is analysed and, if there is a positive zero-crossing (the sign goes from minus to plus), the  $i$ -th index is stored as the hypothetical position of a valley ( $CROSSv(c) = i$ ). If instead, there is a negative zero-crossing (the sign goes from plus to minus) the  $i$ -th index is stored as the hypothetical position of a peak ( $CROSSp(c) = i$ ). When no zero-crossing occurs, the algorithm continues to derive and to analyse the sign.

When at least two peaks and two valleys are found, controls are made to determine if the identified points are really peaks and valleys:

- The first threshold is the minimum distance between two peaks: in literature values over 180 bpm are often chosen and, since our final purpose is to find arrhythmias, we selected  $Threshold1=200$  bpm, corresponding to 300 ms. If the distance is greater than the threshold, the algorithm continues with  $Threshold2$ . If it is less than 200 bpm, the peaks are too close and one of the two peaks is not a real peak. The algorithm therefore calculates the amplitude of the peak in the  $AC_G$  signal and chooses the peak with the higher amplitude as the real one. The real valley is that one that precedes the real peak. Morphological features related to the real pulse are calculated and the search of a new peak and a new valley, proceeds.
- $Threshold2$  is the minimum distance between a valley and a peak and was setted equal to 10 samples (corresponding to about 80 ms). If the condition of minimum is not satisfied, the peak and the valley are eliminated because they are too close to each other and so they are identifiable as noise. Otherwise, the algorithm proceeds with the calculation of the features.

- Among the morphological parameters extracted, an approximated *Pulse\_Area* is present. To determine further if the candidate peak and valley are real, two tests using the *Pulse\_Area* are made. The first check is aimed at excluding big areas (related to the movement) from the next test: if the actual  $Pulse\_Area(c)$  is twice the area of the previous pulse ( $Pulse\_Area(c-1)$ ) then  $Pulse\_Area(c)=Pulse\_Area(c-1)$ .
- The successive test establishes that if the  $Pulse\_Area(c)$  is less than 40% of the  $Pulse\_Area(c-1)$ , the current peak and valley, along with their related features, are removed and the algorithm proceeds with the search for a new peak and valley pair. If instead, the condition is not satisfied, the current peak, valley and their relative morphological features are confirmed, before going forward with a new search.

The result of peak and valley detection algorithm is shown in Figure 5.6. Features extracted from the pulse morphology are described below and are illustrated in Figure 5.7. Some of the waveform's characteristic points have already been defined in Section 2.2.3.

- **Systolic Phase Duration**

$$SPD(c-1) = xP(c-1) - xV(c-1) \quad (5.2)$$

- **Diastolic Phase Duration**

$$DPD(c-1) = xV(c) - xP(c-1) \quad (5.3)$$

- **Pulse Wave Duration**

$$PWD(c-1) = xV(c) - xV(c-1) \quad (5.4)$$

- **Distance between c-th valley and (c-2)th valley**

$$Dist2Val(c-1) = xV(c) - xV(c-2) \quad (5.5)$$

- **Pulse Wave Amplitude of the Rising front**

$$PWAR(c-1) = yP(c-1) - yV(c-1) \quad (5.6)$$

- **Pulse Wave Amplitude of the Falling front**

$$PWAF(c-1) = yP(c-1) - yV(c) \quad (5.7)$$

- **Pulse Wave Amplitude**

$$Pulse\_Amp(c-1) = \frac{PWAR(c-1) + PWAF(c-1)}{2} \quad (5.8)$$

- **Peak-to-Peak Interval**

$$PPI(c-1) = \frac{(xP(c) - xP(c-1)) \cdot 1000}{f_s} \quad (5.9)$$

- **Systolic Approximated Area**

$$A1(c-1) = \frac{(SPD(c-1)) \cdot (PWAR(c-1))}{2} \quad (5.10)$$

- **Diastolic Approximated Area**

$$A2(c-1) = \frac{(DPD(c-1)) \cdot (PWAF(c-1))}{2} \quad (5.11)$$

- **Pulse Approximated Area**

$$Pulse\_Area(c-1) = A1 + A2 \quad (5.12)$$

- **Rising front's Angle**

$$\alpha1 = \arctan\left(\frac{PWAR(c-1)}{SP(c-1)}\right) \cdot \frac{180}{\pi} \quad (5.13)$$

- **Falling front's Angle**

$$\alpha2 = \arctan\left(\frac{PWAF(c-1)}{DP(c-1)}\right) \cdot \frac{180}{\pi} \quad (5.14)$$

- **Instantaneous HR**

From  $PPI(c-1)$ , expressed in ms (Expression 5.9), it is also possible to deduce the instantaneous HR expressed in bpm:

$$IHR(c-1) = \frac{60 \cdot 1000}{PPI(c-1)} \quad (5.15)$$

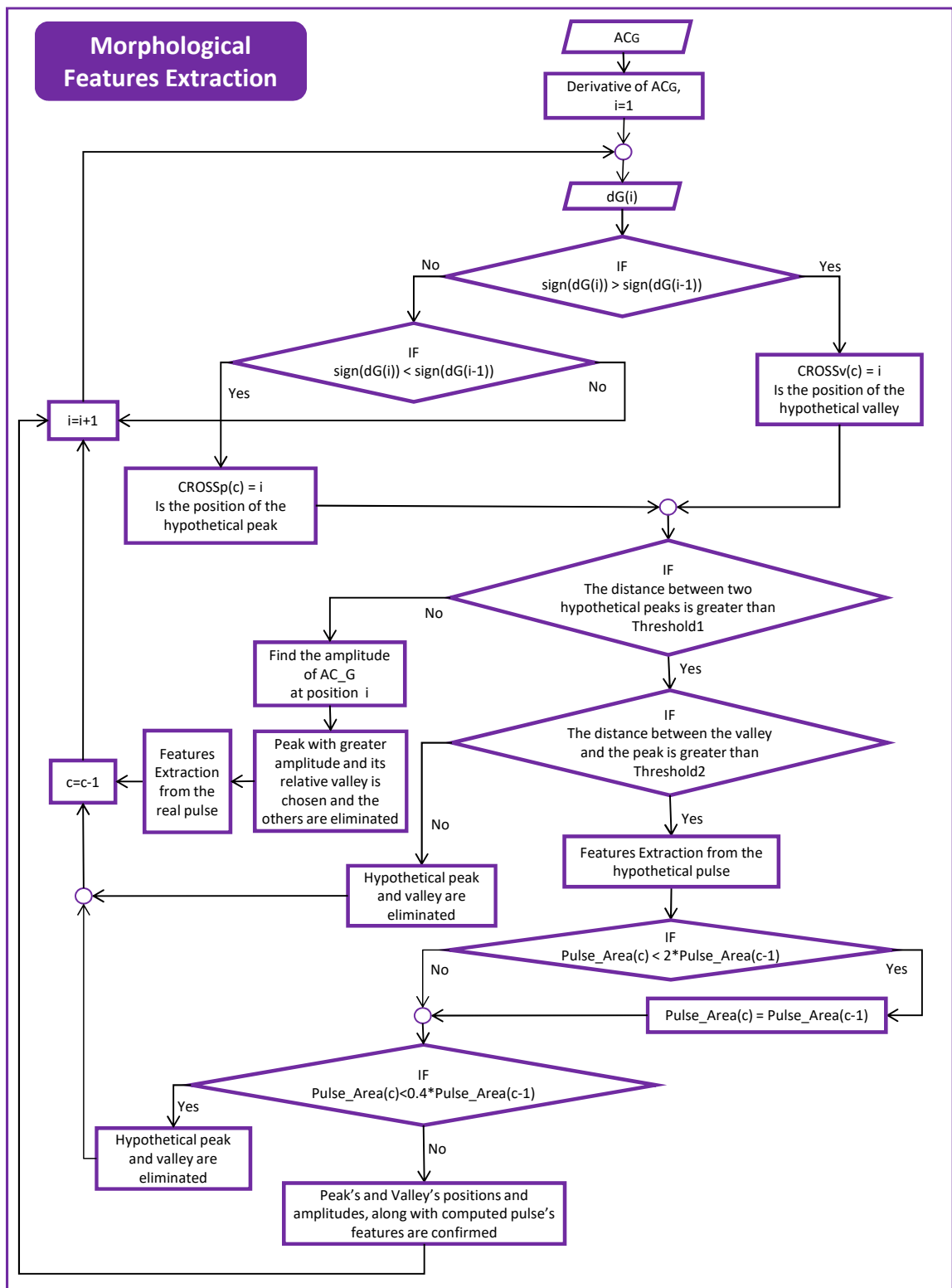


**Figure 5.5:** Morphological Feature Extraction's Block Diagram

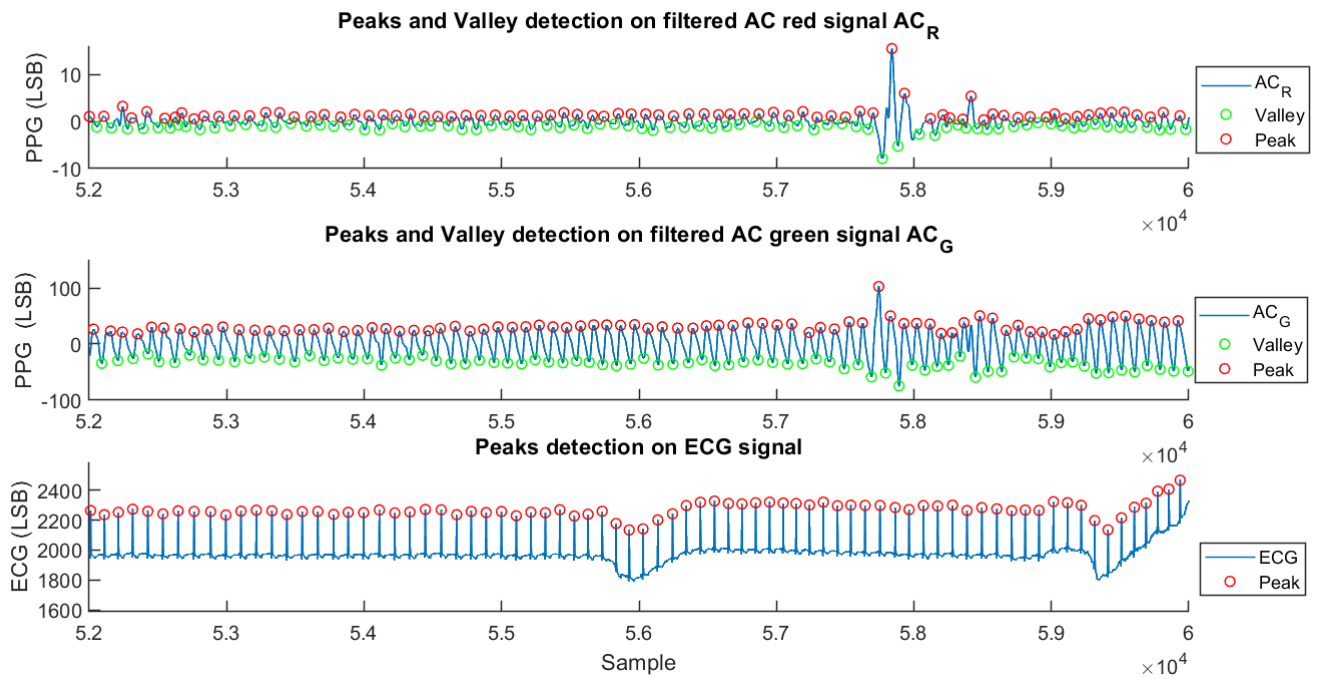


**Figure 5.6:** Peak and valley detection. The detection of the peaks in the ECG reference signal has been performed through the *peakdetection* function of MATLAB

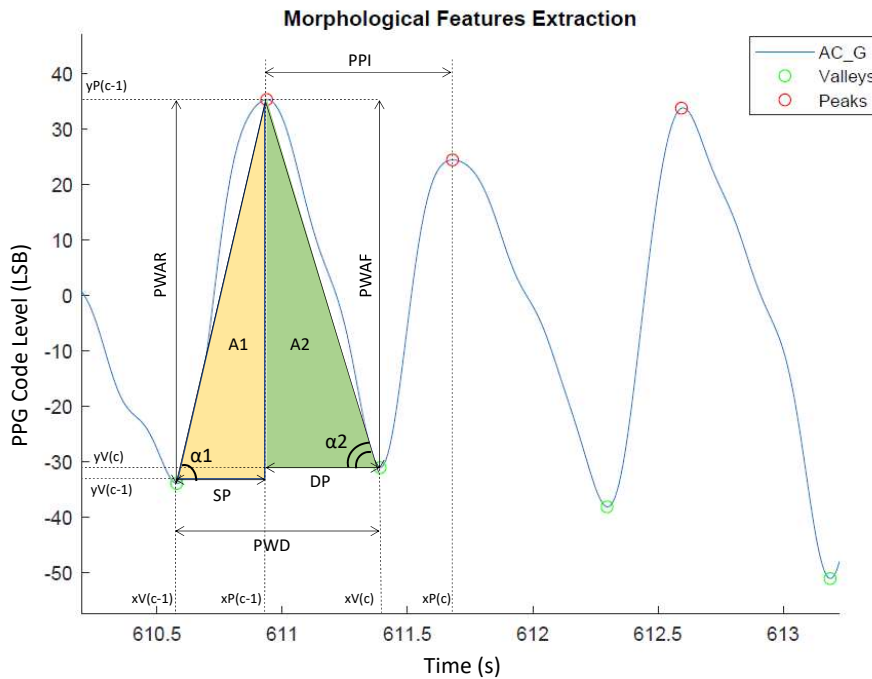


**Figure 5.7:** Morphological Feature Extracted from the pulse

## 5.2.2 Segment Feature Extraction

Statistical, temporal and frequency features were also calculated in order to study how the signal varies during motion and arrhythmia events. The features were extracted using a 10-seconds time sliding window with a 50% overlap, which gives a value each 5 seconds. With the letter  $y$  we intend the filtered PPG signals ( $AC_G$  and  $AC_R$ ), whereas with  $x$ , we mean the raw PPG signals ( $Raw_G$  and  $Raw_R$ ). Unless otherwise specified, the features were calculated for both the red and green PPG signals.

- **Zero Crossing Rate:** it is the rate of sign-changes from positive to negative or back and it is defined as:

$$ZC(j) = \frac{1}{N} \sum_{n=1}^N \mathbb{1}\{y(n) < 0\} \quad (5.16)$$

where  $N$  is the number of samples contained in the 10 seconds segment. The  $j$  index indicate that the value refers to the  $j$ -th segment. The indicator function  $\mathbb{1}\{A\}$ , is 1 if the argument  $A$  is true and 0 otherwise.

- **Perfusion:** it is the gold standard for assessing PPG signal quality [147]. The perfusion index is the ratio of the pulsatile blood flow to the static blood in peripheral tissue and it is defined as:

$$Per(j) = \frac{y_{max} - y_{min}}{|\bar{x}|} \cdot 100 \quad (5.17)$$

where  $\{\bar{x}\}$  is the mean of the raw PPG signal over the  $j$ -th segment and  $y_{max}$  and  $y_{min}$  are its maximum and its minimum respectively.

- **Skewness:** it is a statistic measure and indicates the asymmetry of the data around the sample mean. It may be positive or negative depending on whether the asymmetry is shifted to the right or to the left. It is defined as:

$$Sk(j) = \frac{1}{N} \sum_{n=1}^N \left[ x(n) - \frac{\hat{\mu}}{\sigma} \right]^3 \quad (5.18)$$

where  $\hat{\mu}$  and  $\sigma$  are the empirical estimate of the mean and standard deviation of  $x$  respectively. For our purpose, the absolute value of the skewness will be considered.

- **Kurtosis:** this statistic quantity indicates whether the distribution of sample

values is flattened or sharpened and it is defined as:

$$Kur(j) = \frac{1}{N} \sum_{n=1}^N \left[ x(n) - \frac{\hat{\mu}}{\sigma} \right]^4 \quad (5.19)$$

- **Green DC/AC Amplitude Ratio:** it is the ratio between the DC and the AC component of the PPG green signal and it is calculated as:

$$GAR(j) = \frac{\frac{1}{N} \sum_{n=1}^N DC_G(n)}{\frac{1}{C} \sum_{c=1}^C \left[ \frac{PWAR_G(c) + PWAFF_G(c)}{2} \right]} \quad (5.20)$$

where C is the total number of the peak detected in the *j*-th segment.

- **Red DC/AC Amplitude Ratio:** it is the ratio between the DC and the AC component of the PPG red signal and it is calculated as:

$$RAR(j) = \frac{\frac{1}{N} \sum_{n=1}^N DC_R(n)}{\frac{1}{C} \sum_{c=1}^C \left[ \frac{PWAR_R(c) + PWAFF_R(c)}{2} \right]} \quad (5.21)$$

- **Green/Red Amplitude Ratio:** it is the ratio between the two aforementioned parameters:

$$GRAR(j) = \frac{GAR(j)}{RAR(j)} \quad (5.22)$$

The following frequency domain features were calculated using the PPG signal PSD, which was estimated through the *pwelch* Matlab function over a the 10 seconds sliding segment. For the estimation it was set a simple periodogram (rectangular window 10-seconds long with no overlap). The Number of the points of the Fast Fourier Transform (NFFT) employed to calculate the PSD was imposed equal to 1024, in order to have an apparent resolution of 125 mHz.

- **Spectral Entropy:** it is an adaption of the Shannon Entropy definiton and indicates the deviation of the probability density function of the signal from a uniform distribution and therefore, it provides a measure of the uncertainty present in the signal [148]. The following definition was used:

$$En(j) = \sum_f \left[ p_{xx}(f) \cdot \log\left(\frac{1}{p_{xx}(f)}\right) \right] \quad (5.23)$$

$$\text{where } p_{xx}(f) = \frac{PSD(f)}{\sum_f PSD(f)} \quad (5.24)$$

Spectral Entropy was calculated for both raw and filtered signals:

– Raw Signal's Entropy:

$$En_{Raw}(j) = |En_{RawG} - En_{RawR}|; \quad (5.25)$$

where  $En_{RawG}$  is the spectral entropy calculated for the  $Raw_G$  signal and  $En_{RawR}$  is the spectral entropy calculated for the  $Raw_R$  signal.

– AC Signal's Entropy:

$$En_{AC}(j) = |En_{ACG} - En_{ACR}|; \quad (5.26)$$

where  $En_{ACG}$  is the spectral entropy calculated for the  $AC_G$  signal and  $En_{ACR}$  is the spectral entropy calculated for the  $AC_R$  signal.

- **Relative Power:** since most of the energy of the systolic and diastolic waves is concentrated within the [1-2.25] Hz frequency band [147], the relative power is calculated as the ratio of the PSD in this band, over to the PSD in the overall signal [0-8] Hz:

$$RP(j) = \frac{\sum_{f=1Hz}^{2.25Hz} PSD(f)}{\sum_{f=0Hz}^{8Hz} PSD(f)} \quad (5.27)$$

- **Green DC/AC Power Ratio:** it is the ratio between the total power in the DC component band [0-0.5] Hz, extracted from the  $DC_G$  signal and the total power in the AC component band [0.5-4] Hz, extracted from the  $AC_G$  green filtered signal:

$$GPR(j) = \frac{\sum_{f=0Hz}^{0.5Hz} PSD_{DC}(f)}{\sum_{f=0.5Hz}^{4Hz} PSD_{AC}(f)} \quad (5.28)$$

where  $PSD_{DC}$  is the PSD of the  $DC_G$  signal and  $PSD_{AC}$  is the PSD of the  $AC_G$  signal.

- **Red DC/AC Power Ratio:** it is the ratio between the total power in DC component band [0-0.5]Hz, extracted from the  $DC_R$  signal and the total power in

the AC component band [0.5-4]Hz, extracted from the  $AC_R$  red filtered signal:

$$RPR(j) = \frac{\sum_{f=0Hz}^{0.5Hz} PSD_{DC}(f)}{\sum_{f=0.5Hz}^{4Hz} PSD_{AC}(f)} \quad (5.29)$$

where  $PSD_{DC}(f)$  is the PSD of the  $DC_R$  signal and  $PSD_{AC}(f)$  is the PSD of the  $AC_R$  signal.

- **Green/Red Power Ratio:** it is the ratio between the two aforementioned parameters:

$$GRPR(j) = \frac{GPR(j)}{RPR(j)} \quad (5.30)$$

### 5.3 Motion Analysis

The accelerometer signals were filtered with the above mentioned  $FIR1$  filter, which had also been used to remove high frequency components from the PPG signals. After filtering the accelerometric signals were processed, in order to obtain three different movement indices. These were calculated on 10 a seconds sliding segment with a 50% overlap. These indicators were also clipped and normalized considering the 99-th percentile of the movement distribution of all patients. How the indices were calculated is explained below, and in Figure 5.8, it is possible to see how they vary respect to the accelerometric signal amplitude and to the PPG signal.

- **Movement Intensity**

$$MI(j) = \sum_{ax=1}^3 \left[ \frac{1}{l_{acc}} \sum_{i=1}^{l_{acc}} (acc(i)_{ax} - m_{ax})^2 \right] \quad (5.31)$$

where  $j$  is the segment number,  $ax$  is the accelerometer axis,  $l_{acc}$  is the samples contained in the 10-seconds segment and  $m_{ax}$  is the mean acceleration over the sequence on that axis [149].

- **Mean of the Acceleration Index:** ( $Mean_{Acc}(j)$ ) is the average value of the accelerometer's magnitude ACC [135] within each 10-seconds window; ACC is computed as:

$$ACC = \sqrt{ax_x^2 + ax_y^2 + ax_z^2} \quad (5.32)$$

- **Standard Deviation of the Acceleration Index:** ( $Dev_{Acc}(j)$ ) is the standard deviation of ACC within each 10-seconds window.

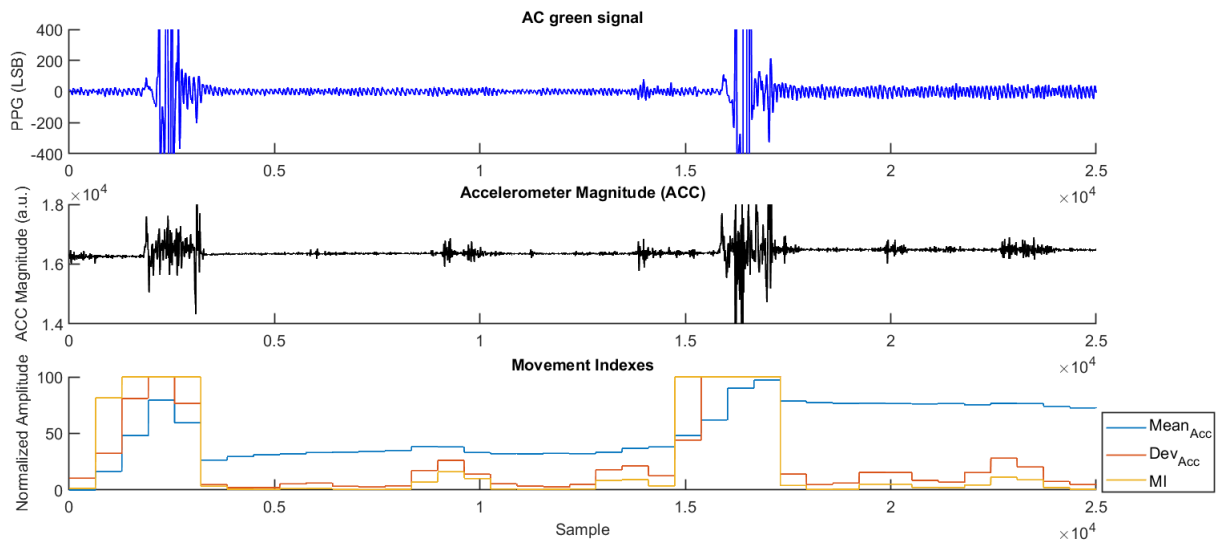


**Figure 5.8:** Movement Indices trend respect to  $ACC$  and AC green signal

Since  $MI$  and  $Dev_{ACC}$  indices consistently follow the intensity of the noise detected by the accelerometer, they are used to determine whether the segment is to be discarded or whether it can be used for HR estimation. When one of the two indices exceeds the value of 70 (indices were normalized between 0 and 100, considering the maximum value equal to the 99-th percentile of the movement indices distribution of all patients), the segment under analysis is considered too noisy to be used. An example of motion analysis result is shown in Figure 5.9 and the movement decision block diagram is illustrated in Figure 5.10.

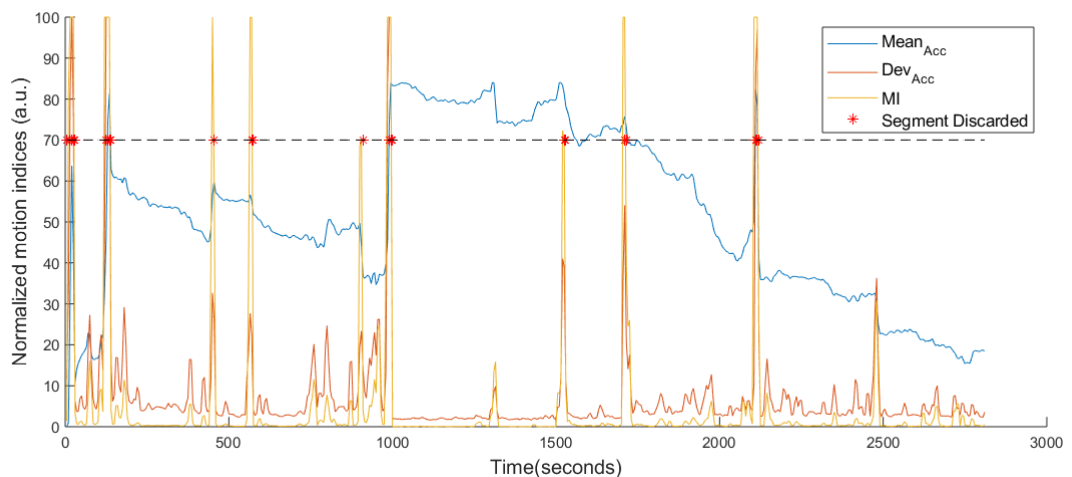


**Figure 5.9:** Motion analysis process over the signal  $S\#1$ . Segment considered too noisy to be used are marked with a red asterisk.

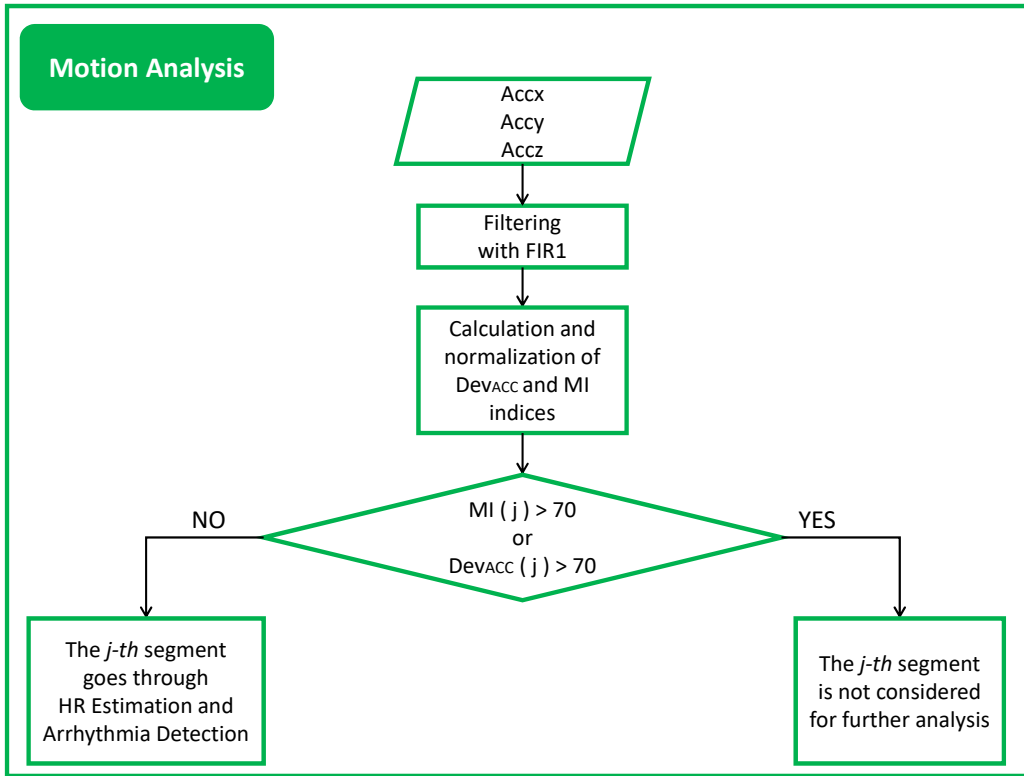


**Figure 5.10:** Motion analysis phase block diagram

## 5.4 HR Estimation

Before the final estimation, HR is calculated in two different ways:

- $HR_T$  is calculated in the time-domain for each segment  $j$ , averaging the vector ( $IHR_{10s}$ ) of the instantaneous HR (Equation 5.15) found in 10 seconds;
- $HR_F$  is calculated in the frequency-domain, performing the PSD of the  $AC_G$  over each  $j$ -th segment and extrapolating the frequency  $fmax_{AC}$  corresponding to the max PSD. To have  $HR_F$  expressed in bpm,  $fmax_{AC}$  must be multiplied by 60.

Both the estimations are done over a 10 seconds segment, which slide on the signal with a 50% of overlap, giving an HR output each 5 seconds. A decision making process, illustrated in Figure 5.11, was elaborated in order to choose the best HR estimation. The frequency  $fmax_{Raw}$ , corresponding to max PSD of the  $Raw_G$  signal in the [0-5] Hz band, is multiplied by 60 and is used for the final HR choice. When the absolute difference between  $HR_T$  and  $fmax_{Raw}$  is smaller than that between  $HR_F$  and  $fmax_{Raw}$ , the final HR ( $HR_{FINAL}$ ) is equal to  $HR_T$ , otherwise another verification occurs: if the  $HR_F$  differs more than 15 bpm from the  $HR_{FINAL}$  of the previous segment,  $HR_{FINAL}$  is equal to  $HR_F$ , otherwise it is left equal to  $HR_T$ .

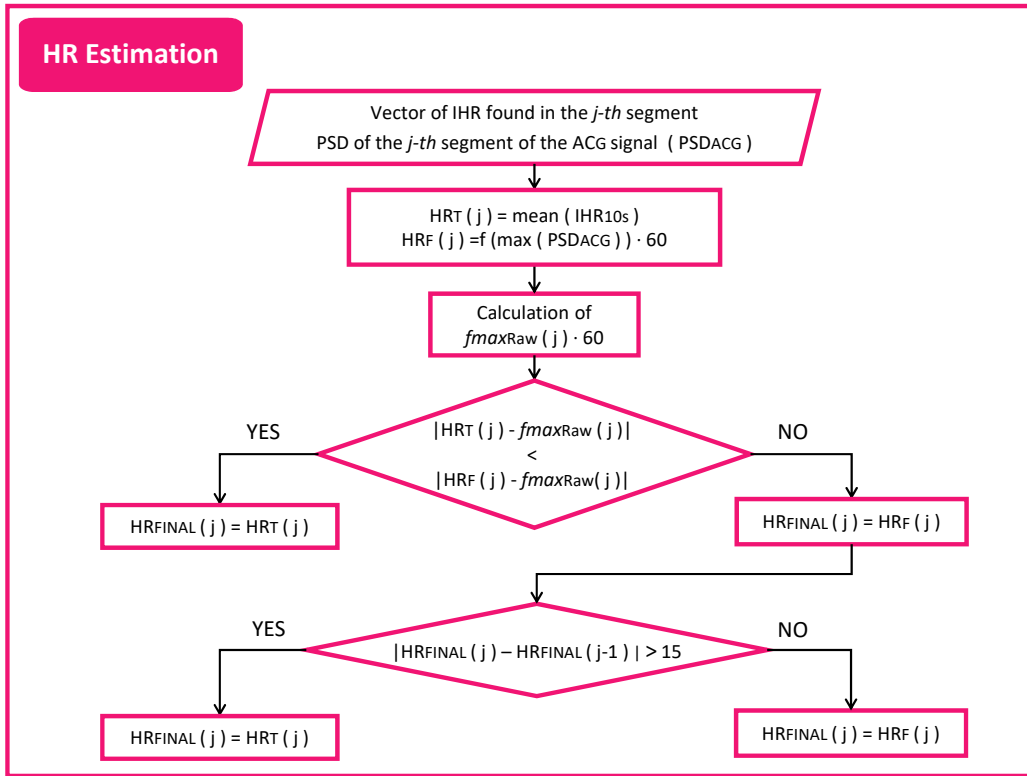


Figure 5.11: HR estimation block diagram

## 5.5 Arrhythmia Detection

ECG and PPG signals downloaded from the database have a sampling frequency of 125 Hz and are represented in Figure 5.12 along with the "*PVC Count*" annotations that reports the number of PVC in one minute.

PPG signals are filtered using an High Pass FIR with cut-off frequency of 0.5 Hz (order 2000) and a Low Pass FIR in cascade with cut-off frequency of 5 Hz (order 400). The filtering introduce an SNR enhancement of about 12 dB. Here the pre-processing phase is not performed using a real-time setting as done in Section 5.1 because the signals of the database are only employed for the preliminary creation of the Arrhythmia Detection algorithm and not for a real-time implementation.

Based on the finding of the Peak Detection algorithm (an example is reported in Figure 5.12), it is possible to divide the PVCs into two types:

- $P_1$ : the PVC peak is too low to be detected from the peak detection algorithm.
- $P_2$ : the PVC or one of the its successive low-amplitude peak is detected.

Feature Extraction is performed with the algorithm explained in Section 5.2. However, for the Segment Feature Extraction only PPG acquired from the finger in transmittance

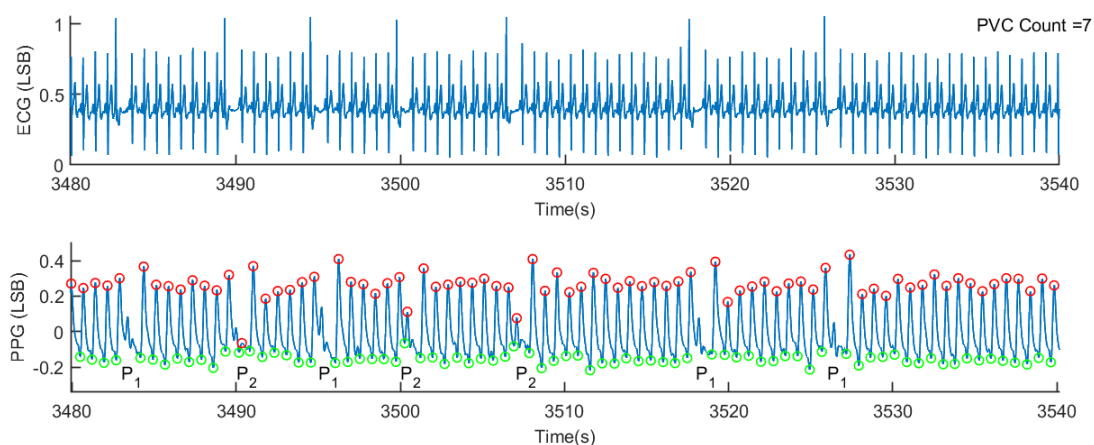


**Figure 5.12:** ECG and filtered PPG signal with correspondent PVC Count annotation (reported as a text for illustrative scope). Detected peaks and valleys are marked and the PVC's typology is indicated below the corresponding pulse.

mode (the wavelength employed is not specified in the database description) was considered, since acceleration and PPG signals acquired from the wrist in reflectance mode, were not available on Physionet Databases.

Among all the Morphological and Segment Features extracted, the pulse wave duration  $PWD$  was chosen in order to detect the  $P_1$  beat and the rising front's angle  $\alpha_1$  for the  $P_2$  one. The Arrhythmia Detection block diagram is represented in Figure 5.13. A beat is recognised as a  $P_1$  when examining three consecutive PWDs, the central one differs from the lateral ones by at least 200 ms. On the other hand, there is an ectopic  $P_2$  beat when examining three consecutive  $\alpha_1$ , the central one is at least 10 degrees away from the previous one and the next one is greater than the previous one.

## 5.6 Reliability Level Computation

In Section 5.3 it was illustrated how the motion analysis process works in order to discard too noisy segments. However, lower movements detected by the accelerometer should also be considered since they affect the signal PPG quality and therefore, the HR estimation. Furthermore, there are situations in which the accelerometer magnitude indicates that no movement occurs, but PPG signal quality is very low. This could happen for example in case of finger tapping or loss of adherence of the device from the wrist. In these conditions it is advisable to have a reliability index calculated directly on the signal. In order to match these two needs, the segment features calculated in Section 5.2.2 were analysed with respect to the quality of the PPG  $AC_G$  signal (Figure 5.14) and three level of reliability based on  $Per_G$  and  $Dev_{ACC}$  were set. Reliability Levels

are:

- **High Reliability:** when  $Per_G$  is less or equal than 4, we expect the maximum difference (in absolute value) between the estimated BPM and the real one, to be less than 4 BPM
- **Medium Reliability:** when  $Per_G$  is between 4 and 10 or when  $Dev_{ACC}$  is greater than 10, we expect the maximum difference (in absolute value) between the estimated BPM and the real one, to be greater than 6 BPM but less than 10 BPM;
- **Low Reliability:** when  $Per_G$  is larger than or equal to 10, we expect the maximum difference (in absolute value) between the estimated BPM and the real one, to be greater or equal than 10 BPM;

Since the final purpose is to use the *Bio2Bit Move* also for the arrhythmia detection, reliability index regarding the quality of the signals taken from the database, was not computed. The database also lacks the accelerometer signals, and the PPG signal was taken in transmission mode from the patient's finger, while our aim is to evaluate the quality of the green PPG in reflective mode, taken from the wrist.

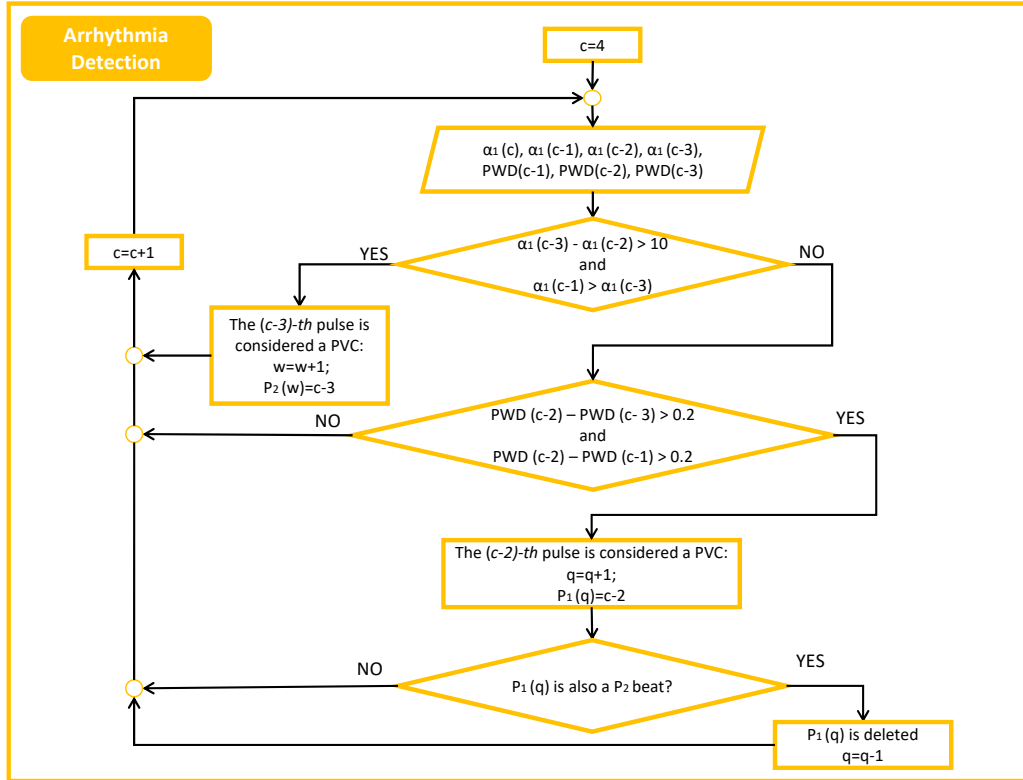
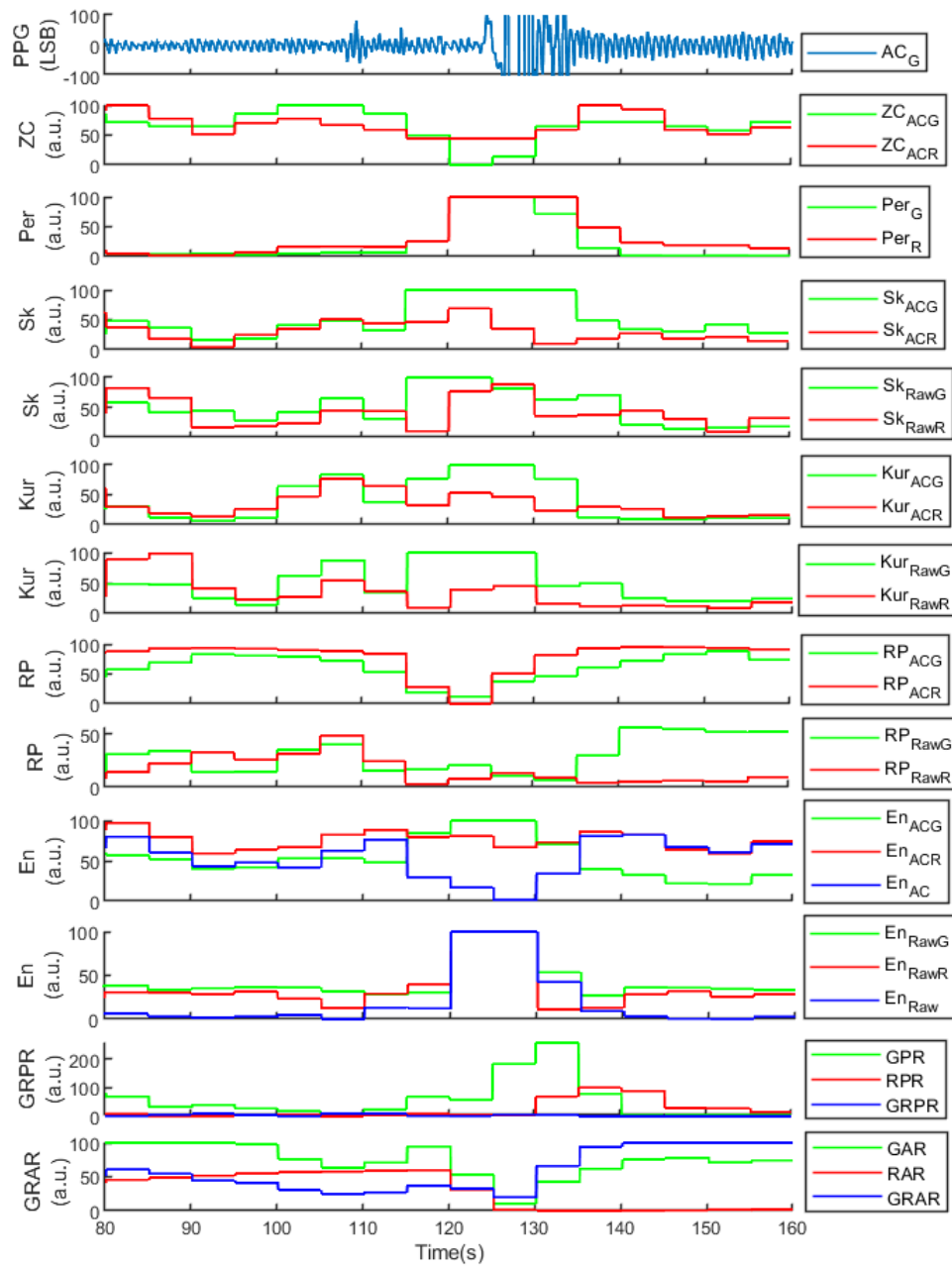


Figure 5.13: Arrhythmia Detection block diagram

Summarizing, after a pre-processing phase necessary to extrapolate the AC component of the signal, the algorithm identifies the points too affected by noise and excludes them. In time segments that can be used for further analysis, peaks and valleys are detected, and a series of morphological characteristics on the signal can be calculated. Using a 10-seconds time window that runs over the signal with a 50% of overlap, two HR measurements (one in the time domain and one in the frequency domain) are extrapolated and compared. A final HR estimation is then produced, and on the basis of two indices (one extrapolated from the accelerometer signal and one obtained from the PPG signal itself), a level of reliability is attributed to the HR estimation. The algorithm then continues with the detection of PVCs; this part has been implemented and tested on the MIMIC Database. All the algorithm steps are characterized by the calculation of certain indices and thresholds that govern different decision-making processes. The employed parameters, along with the threshold applied to them, are summarized in Table 5.1.



**Figure 5.14:** Segment Features behaviour respect to the  $AC_G$  signal

Step	Parameter	Equation / Algorithm	Normalization	Threshold	Notes
Peak and Valley Detection	PP Interval	Eq. [5.9]	-	PPI > 300ms <i>Minimum distance between two peaks</i>	PPI and SPD thresholds were established according to physiological time of the PP and SP interval. PA thresholds were set experimentally.
	Systolic Phase Duration	Eq. [5.2]	-	SPD > 80ms <i>Minimum distance between a valley and a peak</i>	
	Pulse Approximated Area	Eq. [5.12]	-	PA (c) < 2 * PA (c-1) PA (c) > 0.4 * PA (c-1) <i>Area limit for PPG pulse</i>	
Motion Analysis	Movement Intensity	Eq. [5.31]	1.0566e+06	MI < 70	Motion Indices are normalized in relation to the 99-th percentile of the corresponding index calculated over all the subjects. Thresholds were set experimentally.
	Standard Deviation of ACC	Eq. [5.32]	400	Dev <sub>ACC</sub> < 70	
HR Estimation	HR <sub>FINAL</sub>	Fig. [5.11]	-	HR <sub>FINAL</sub> (c) – HR <sub>FINAL</sub> (c-1) > 15 BPM <i>Difference between two consecutive HR values</i>	When motion occurs, the HR estimation in frequency tends to be much higher than the previous one so, when this occurs, the HR estimated in time domain is chosen.
Arrhythmia Detection	Pulse Wave Duration	Eq. [5.4]	-	$PWD(c-1) - PWD(c) > 0.2$ $PWD(c-1) - PWD(c-2) > 0.2$	Thresholds were set experimentally.
	Rising Front's Angle	Eq. [5.13]	-	$\alpha_1(c-2) - \alpha_1(c-1) > 10$ $\alpha_1(c) > \alpha_1(c-2)$	
Reliability Level Calculation	Standard Deviation of ACC	Eq. [5.32]	400	Dev <sub>ACC</sub> > 10 (MRL)	Thresholds were set experimentally.
	Perfusion of PPG green signal	Eq. [5.17]	-	$Per_G \leq 4$ (HRL) $4 < Per_G < 10$ (MRL) $Per_G \geq 10$ (LRL)	Thresholds were set experimentally.

**Table 5.1:** Parameters and Threshold employed in the different algorithm step.

# Part III

## Results



# Chapter 6

## HR Estimation and Reliability Level Classification

### 6.1 Performance Metrics

The ground-truth HR was calculated using the ECG *Channel III* signal (sampled at 128 Hz) acquired by the *BioToBit HI* device by using the *"findpeak"* Matlab function and then visually checking that all the R-peaks were identified, in order to avoid any possible detection errors. Instantaneous HR was calculated using the Equation 5.15 replacing PPI with the RR interval. As it was done for the PPG signal, the IHR values are then averaged using a 10 seconds window that slides on the signal with a 50% of overlap. In this way, an HR value each 5 seconds is given as output. To evaluate the HR Estimation's algorithm performance, the measurement indexes used in [92–94, 150, 151] were used. These are:

- **Average Absolute Error in BPM:**

$$AAE = \frac{1}{S} \sum_{j=1}^S |BPM_{est}(j) - BPM_{true}(j)| \quad (6.1)$$

where  $BPM_{true}$  is the HR measured in the  $j$ -th ECG time window,  $BPM_{est}$  denotes the estimated HR ( $HR_{FINAL}$ ) in the  $j$ -th PPG time window, and  $S$  is the total number of time segments.

- **Relative Percentage Error:**

$$RPE = \frac{1}{S} \sum_{j=1}^S \frac{|BPM_{est}(j) - BPM_{true}(j)|}{BPM_{true}} \quad (6.2)$$

- **Scatter plot and Pearson coefficient:** scatter plot shows the strength, direction and form of the relationship between two quantitative variables [152]. The values of one variable appear on the horizontal axis, and the values of the other variable appear on the vertical axis. If the relationship between the two variables is linear, it is possible to calculate the Pearson coefficient that measures the strength of the relationship. Pearson coefficient is computed as:

$$r = \frac{Cov(BPM_{est}, BPM_{true})}{\sigma_{BPM_{est}} \cdot \sigma_{BPM_{true}}} \quad (6.3)$$

where  $Cov$  is the covariance between  $BPM_{true}$  and  $BPM_{est}$  and  $\sigma_{BPM_{est}}$  and  $\sigma_{BPM_{true}}$  are the standard deviations of the two variables.

- **Bland-Altman plot:** it is a dispersion diagram that examines the agreement between the results of an approach and ground-truth. The difference between the two measurements is shown on the y-axis and the arithmetic mean of the two measurements on the x-axis [153]. The Limit of Agreement (LOA) used was  $\mu \pm 1.96\sigma$ , where  $\mu$  is the average difference between each estimate and the associated ground-truth against their average, and  $\sigma$  is its standard deviation.

Both the Scatter and the Bland-Altman plot were created in *Microsoft® Office Excel*. Shapiro-Wilk and QQ Plot tests, to check the normality assumption, were performed.

The performances of the Reliability levels classification were calculated for each subject by checking that Low Reliability Level (LLR) corresponds to error greater or equal to 10 BPM, Medium Reliability Level (MRL) to error between 4 and 10 BPM and High Reliability Level (HRL) to error smaller or equal than 4 BPM. The following parameters were calculated for each subject:

- **Class Percentage over the total (%):** it is the number of the segments in the LRL class over the total segments present in the signal.
- **Correct Level of Reliability (%):** it is the segments' number of the class under consideration that actually belong to that class, over the segments' total number in the class.
- **AAE in the Class (BPM):** it is the AAE (Equation 6.1) of the segments in the class.

In addition, to better analyse global misclassification errors, confusion matrix all over the 8 datasets was calculated, along with its associated parameters. In Table 6.1 is represented how the parameters were extrapolated from the matrix. The performance parameters considered are:

- **Positive Predictive Value (or Precision):**

$$PPV (\%) = \frac{TP}{TP + FP} \quad (6.4)$$

where TP are True Positive values (the observation is positive and is predicted to be positive) and FP are False Positive values (the observation is negative but is predictive is positive).

- **Negative Predictive Value:**

$$NPV (\%) = \frac{TN}{TN + FN} \quad (6.5)$$

where TN are True Negative values (the observation is negative and is predicted to be negative) and FN are False negative values (the observation is positive, but is predicted negative).

- **Sensitivity (or Recall):**

$$Sensitivity (\%) = \frac{TP}{TP + FN} \quad (6.6)$$

- **Specificity (or Selectivity):**

$$Specificity (\%) = \frac{TN}{FP + TN} \quad (6.7)$$

- **Overall Accuracy:**

$$Accuracy (\%) = \frac{TP + TN}{TP + TN + FP + FN} \quad (6.8)$$

Total Segment $N$		Actual Class			False Positive	PPV (%)	Specificity (%)
		HRL	MRL	LRL			
Predicted Class	HRL	A	B	C	B+C	$\frac{A}{A+B+C}$	$\frac{E+F+H+I}{B+C+E+F+H+I}$
	MRL	D	E	F	D+F	$\frac{E}{D+E+F}$	$\frac{A+C+G+I}{A+C+G+I+D+F}$
	LRL	G	H	I	G+H	$\frac{I}{G+H+I}$	$\frac{A+B+D+E}{A+B+D+E+G+H}$
<i>False Negative</i>		D+G	B+H	C+F	<i>Overall Accuracy (%)</i> $\frac{A+E+I}{N}$		
<i>NPV (%)</i>		$\frac{E+F+H+I}{E+F+H+I+D+G}$	$\frac{A+C+G+I}{A+C+G+I+B+H}$	$\frac{A+B+D+E}{A+B+D+E+C+F}$			
<i>Sensitivity (%)</i>		$\frac{A}{A+D+G}$	$\frac{E}{B+E+H}$	$\frac{I}{C+F+I}$			

**Table 6.1:** 3x3 Confusion Matrix for classification problem

## 6.2 Performance Assessment

How SNR was calculated was explained in Section 5.1. Table 6.2 shows SNR value for each subject, before and after the pre-processing phase for both the red and green PPG signals. On average, the pre-processing phase introduces an enhancement of 24.02 dB for the PPG green signals and 17.87 dB for the red ones.

	S#1	S#2	S#3	S#4	S#5	S#6	S#7	S#8	Average Enhancement (dB)
$SNR_{Raw,G} (dB)$	-1.42	-18.71	2.66	6.81	-10.03	-11.02	-7,55	-1.22	24.02
$SNR_G (dB)$	17.47	10.67	22.06	33.53	18.7	11.20	14.03	23.92	
$SNR_{Raw,R} (dB)$	-2,34	-13.84	-9.58	-5.26	-4.36	-2.99	-0.1	-0.34	17.87
$SNR_R (dB)$	13.33	12.58	8.00	15.85	13.05	11.96	12.77	16.57	

**Table 6.2:** SNR before and after the preprocessing phase for both the red and green PPG signals.

In Figure 6.1 Motion Analysis and the HR algorithm results for Subject 1 are shown. It can be observed that the HR calculated on the PPG signal produced estimations close to the ground-truth. It is possible to see that too noisy segments often correspond to a large error in establish the HR value. However, the HR estimation algorithm is

sometimes able to well estimate the cardiac frequency also under motion. Table 6.3 lists the AAE and PRE calculated over the all 8 datasets, without performing the Motion Analysis step. Averaged across the 8 Subjects, the absolute estimation error was  $2.50 \pm 0.51$  BPM (mean  $\pm$  standard deviation), and the relative percentage error was  $3.68 \pm 0.84$ . Table 6.4 instead, lists the AAE and PRE after the Motion Analysis step. The automatic segments rejection operation was not so selective in fact only the 4.59% of the total segments were discarded. In this case, the average AAE and PRE across all the Subjects was  $2.25 \pm 0.68$  BPM and  $3.36 \pm 1.06$ , respectively. The Scatter Plot between the ground-truth HR values and the estimated ones over the 8 trials is represented in Figure 6.2. It shows a strong relationship between the two variables, except for some outliers in the upper part of the plot. The Pearson correlation coefficient was 0.909 and the probability value  $p$  is less than 0.05 ( $\alpha$  level), which indicates that the results are significant. Bland-Altman plot was used to analyse the agreement between the estimations and the ground-truth. As shown in Figure 6.3, 95% of the differences were located in the Limit Of Agreement  $[-11.76, 5.90]$  BPM. The mean of the difference ( $-2.93$  BPM) indicates that the algorithm tends to over-estimate the real HR value of about 3 BPM.

Errors calculation without applying Motion Detection step									
	S#1	S#2	S#3	S#4	S#5	S#6	S#7	S#8	Average
<b>AAE (BPM)</b>	2.67	1.96	1.97	1.91	2.57	2.62	3.13	3.16	2.50 (SD=0.51)
<b>PRE (%)</b>	3.67	2.61	3.23	3.21	3.21	3.44	5.26	4.84	3.68 (SD=0.84)

**Table 6.3:** Average Absolute Errors and Relative Percentage Errors on the 8 Subjects' signal without apply the Motion Analysis algorithm. This means that there are not discarded segment. SD denotes the standard deviation.

Errors calculation applying Motion Detection step									
	S#1	S#2	S#3	S#4	S#5	S#6	S#7	S#8	Average
<b>AAE (BPM)</b>	2.54	1.33	1.66	1.44	2.57	2.46	3.14	2.82	2.25 (SD=0.68)
<b>PRE (%)</b>	3.50	1.81	2.87	2.63	3.21	3.26	5.28	4.35	3.36 (SD=1.06)
<b>Discarded Segments (%)</b>	3.91	9.03	9.19	5.7	0	2.47	4.03	3.76	

**Table 6.4:** Average Absolute Errors and Relative Percentage Errors on the 8 Subjects' signal applying the Motion Analysis algorithm. The total percentage of discarded segments is 4.59%. SD denotes standard deviation

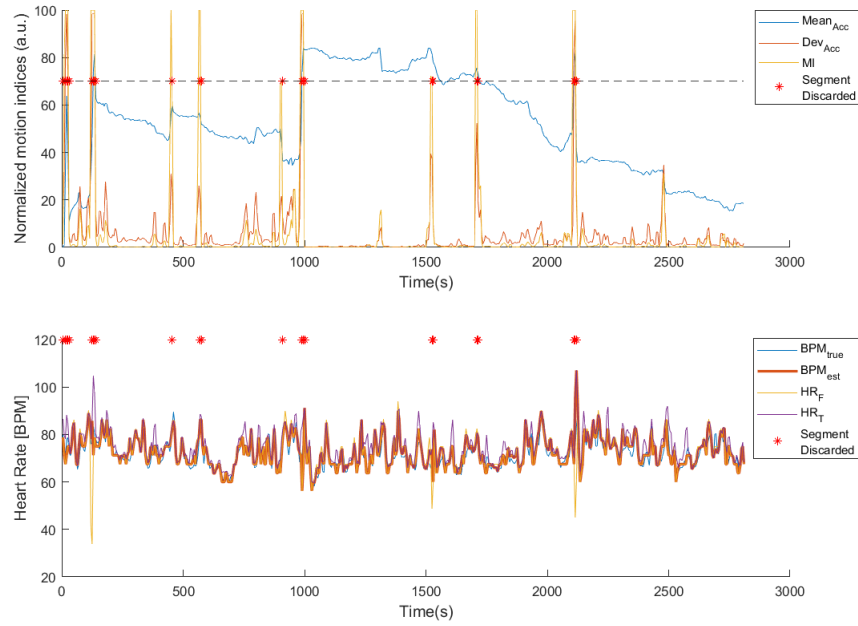


**Figure 6.1:** Motion Analysis and  $HR_{FINAL}$  ( $BPM_{est}$ ) Estimation process over signal  $S\#1$ .

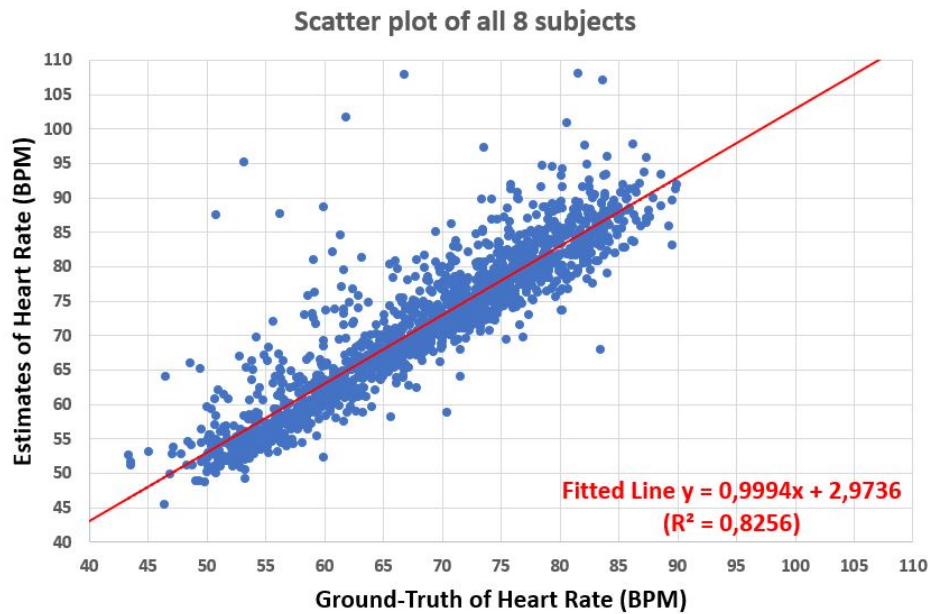


**Figure 6.2:** Scatter plot between  $BPM_{true}$  (the ground-truth HR values) and  $BPM_{est}$  (the associated estimates over the 8 signal of the Subjects). The fitted line was  $y = 0,9994x + 2,9736$ , where  $x$  indicates the ground-truth heart rate value, and  $y$  indicates the associated estimate. The  $R^2$  value measure the goodness of fit and was 0.8256. The Pearson correlation coefficient was 0.909.

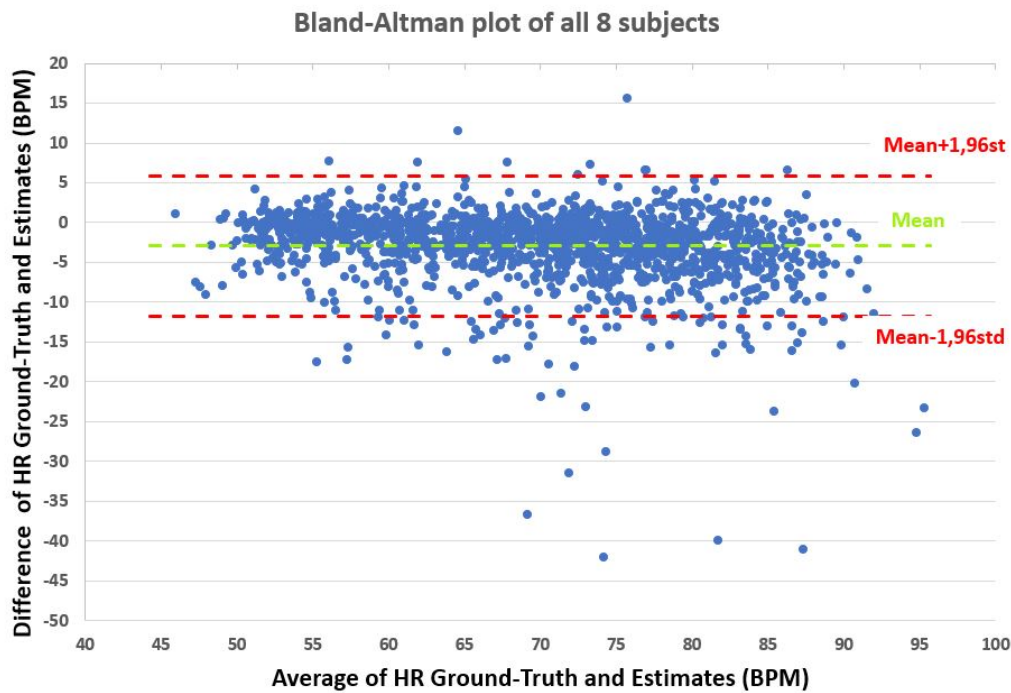


**Figure 6.3:** The Bland-Altman plot of the estimation results on the 8 Subjects' signal. The LOA was  $[-11.76, 5.90]$  BPM and the mean of the difference was  $-2.93$ .

On Figure 6.4 results of the Reliability Level classification are shown. Green and yellow lines are the estimated HR and the ground-truth HR, respectively, and in blue line the absolute difference error in BPM is represented. Dot lines are the indices employed to assess the level of Reliability (represented in black). In the case of Subject 6, it can be seen that LRL corresponds to an high HR estimation error (above 10 BPM) only twice out of three and many HRL are detected as MRL. Table 6.5 provides a complete individual analysis of the performance achieved in the Reliability calculation. For each subject, the percentage of the class over the total, the percentage of true positives and the AAE within the class are reported. It is possible to see that usually the HRL class is much larger than the other two moreover, LRL class is usually empty and it is associated with a low correct level of reliability. In Table 6.6, the confusion matrix calculated considering all the subjects' segments, shows a Sensitivity of 84.85% (HRL), 17.71% (MRL), 26.67% (LRL) and a Specificity of 21.05% (HRL), 85.36% (MRL) and 99% (LRL). The overall Accuracy is 68.4%. These results partly confirm what was seen in Figure 6.4 because many HRL are classified such as MRL however, a low number of LRL and MRL are classified such as HRL. The high specificity of LRL indicates that with there is an high probability for a LRL to be classified correctly however, the prevalence of LRL class is very low, also because a big part of it was rejected through the Motion Analysis algorithm. Figure 6.5 shows a case in which the reliability was

identified as low (because the Perfusion Index was about 25) but the error in BPM respect to the reference was less than 4 BPM and therefore it was supposed to be classified as an "high reliability" measure. However it is possible to see that even though the HR Estimation was near to the reference value, the quality of the signal was low.

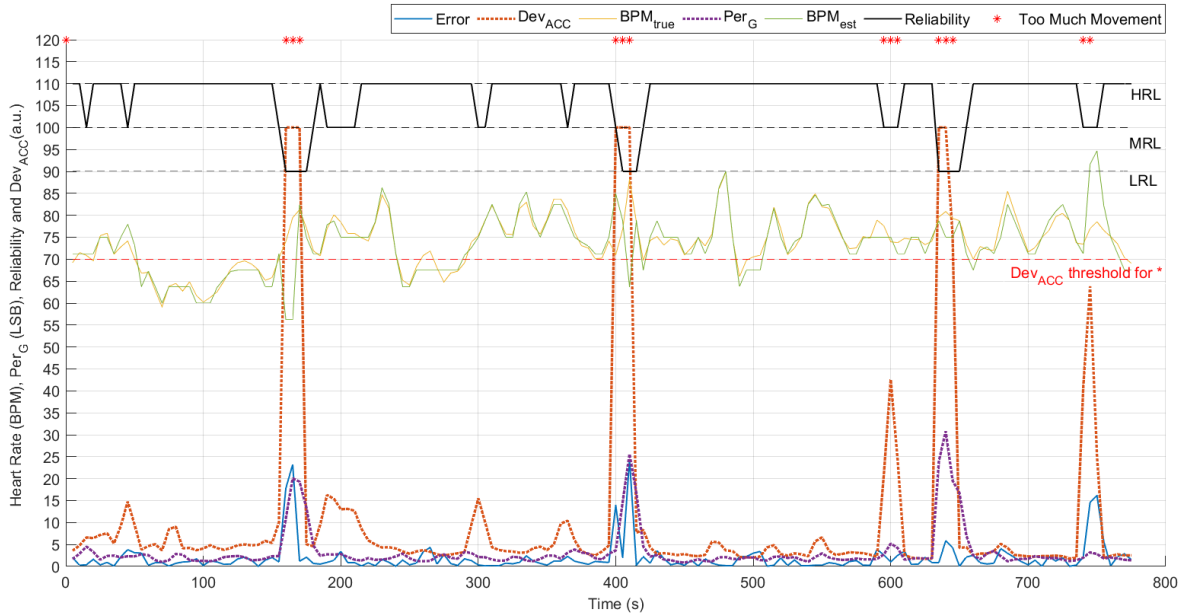


**Figure 6.4:** Reliability results on the Subject 6 (randomly chosen) respect to the HR Error in BPM performed. Discarded Segment are also shown, along with the threshold and the  $Dev_{ACC}$  used to determine if the movement's amount was too big.

<i>Total Segment</i> 1620		<b>Actual Class</b>			<i>False Positive</i>	<i>PPV (%)</i>	<i>Specificity (%)</i>
		HRL	MRL	LRL			
<b>Predicted Class</b>	HRL	1036	307	8	315	76.67	21.05
	MRL	178	68	3	181	27.31	85.36
	LRL	7	9	4	16	20	99
<i>False Negative</i>		185	316	11	<b>Overall Accuracy (%)</b> 68.4		
<i>NPV (%)</i>		31.23	76.95	99.31			
<i>Sensitivity (%)</i>		84.85	17.71	26.67			

**Table 6.6:** 3x3 Confusion Matrix of Reliability Level classification performance

		<i>Class Percentage over the total (%)</i>	<i>Correct Level of Reliability (%)</i>	<i>AAE in the Class (BPM)</i>
<b>Subject 1</b>	HRL	71.11	81.51	2.3 (SD=1.94)
	MRL	27.04	24.66	2.78 (SD=2.13)
	LRL	1.85	30	7.07 (SD=7.24)
<b>Subject 2</b>	HRL	87.23	97.56	1.21 (SD=1.08)
	MRL	10.64	0	2.45 (SD=3.95)
	LRL	2.18	0	2.11 (SD=1.13)
<b>Subject 3</b>	HRL	73.21	94.31	1.59 (SD=1.28)
	MRL	26.19	9.09	1.88 (SD=1.46)
	LRL	0.6	0	1.37 (SD=0)
<b>Subject 4</b>	HRL	70.88	97.67	1.25 (SD=1.11)
	MRL	28.6	13.46	1.89 (SD=2.19)
	LRL	0.55	0	2.46 (SD=0)
<b>Subject 5</b>	HRL	87.5	77.02	1.59 (SD=1.28)
	MRL	12.5	31.74	1.88 (SD=1.46)
	LRL	0	-	-
<b>Subject 6</b>	HRL	34.81	83.33	2.22 (SD=1.89)
	MRL	65.19	20.39	2.59 (SD=2.30)
	LRL	0	-	-
<b>Subject 7</b>	HRL	82.35	71.04	3.16 (SD=2.68)
	MRL	17.65	31.43	3.13 (SD=2.58)
	LRL	0	-	-
<b>Subject 8</b>	HRL	53.9	89.86	2.11 (SD=2.01)
	MRL	44.53	7.02	3.11 (SD=4.07)
	LRL	1.56	50	23.37 (SD=25)

**Table 6.5:** Reliability Level results for the 8 subjects. SD denotes standard deviation.

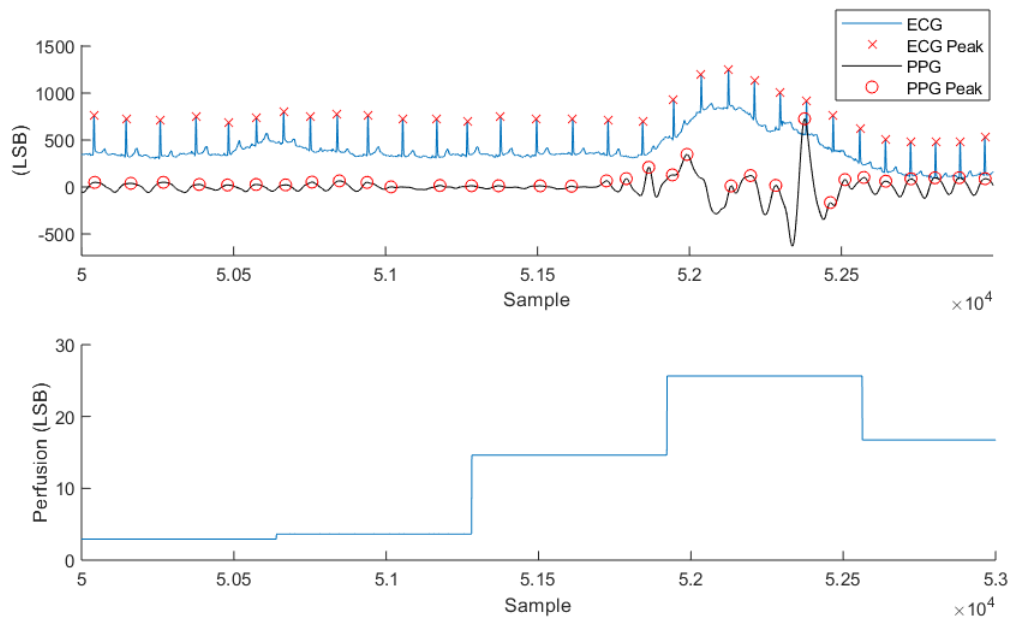


**Figure 6.5:** Perfusion Index changes respect to the quality of the PPG signal.

# Chapter 7

## Arrhythmia Detection

### 7.1 Performance Metrics

In order to evaluate Arrhythmia Detection performance, the 1-hour signals of the MIMIC Database were divided in 1-minute segments. A Matlab figure, such as the one represented in Figure 7.1, was generated per each 1-minute segment. Since the annotation file often makes mistakes in counting PVCs (as it happens in Figure 7.1), it is necessary to visually check arrhythmias directly on the ECG trace. When the PPG and/or the ECG signal is too noisy or absent for more than 30 seconds (as shown in Figure 7.2), the corresponding segment is discarded. All the detected TP, TN, FP and FN, were then used for the construction of a 2x2 Confusion Matrix, similar to the one computed in Section 6.1. Also in this case, the parameters of performance evaluation, associated to the confusion matrix, were calculated.

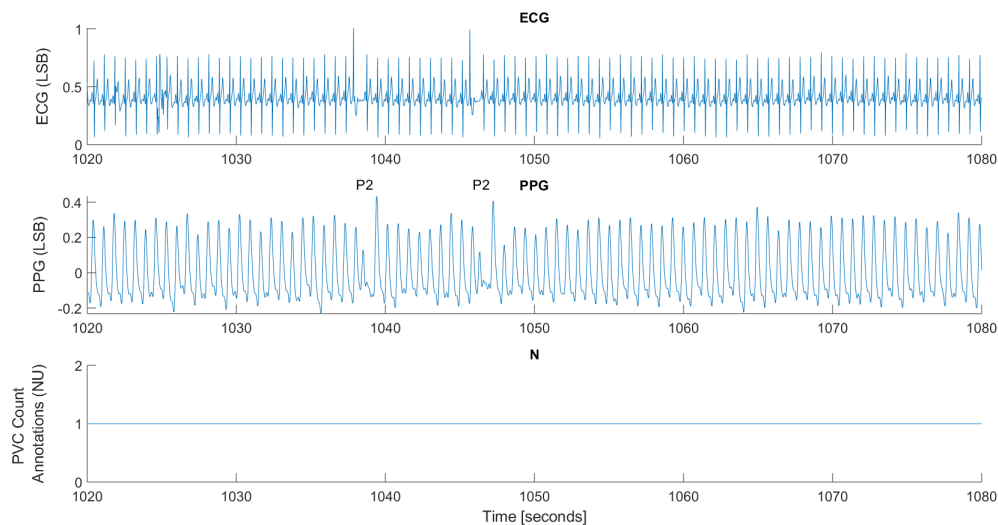


**Figure 7.1:** Screen employed for the arrhythmia detection evaluation.

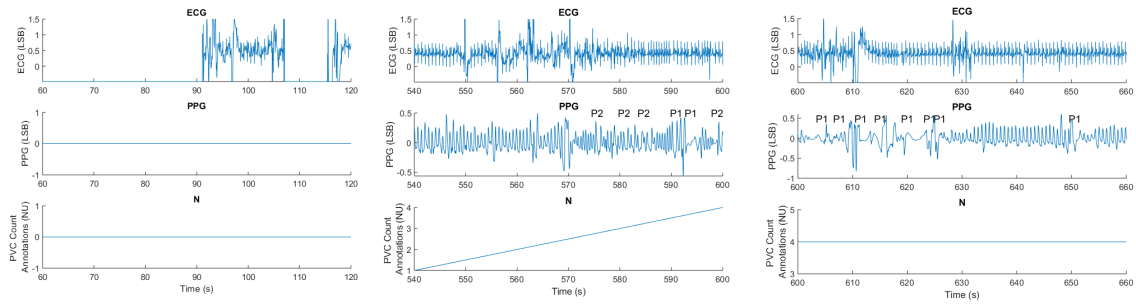


**Figure 7.2:** Screen employed for the arrhythmia detection evaluation.

## 7.2 Performance Assessment

Pulse Wave Duration and Rising Front's Angle were employed in order to detect PVC. But others morphological indices as well as some of the computed features over the sliding time window were investigated. Figure 7.3 and 7.4 shows the trend of the investigated parameters respect to the PPG signal and PVC events. All the morphological features show more or less significant changes when P1 and P2 events occur. As regards the trend of the segment features, the correspondence between P1 and P2 events and significant changes in the parameters, is less evident and does not always occur.

In Table 7.1 the Confusion Matrix computed over the 15 signals of the database is shown. Values of Sensitivity and Specificity are 90.10% and 99.34%, respectively and Accuracy is 98.83%. The percentage of the segments not taken into account because their poor quality, amounts to 8.25% of the total ones.

Total Pulses 55635		True Condition		PPV (%)	Specificity (%)
		PVC	NO PVC		
Predicted Condition	PVC	2730	349	88.67	99.34
	NO PVC	300	52256		
NPV (%)		99.43		Accuracy (%) 98.83	
Sensitivity (%)		90.10			

**Table 7.1:** 2x2 Confusion Matrix for the evaluation of PVCs detection

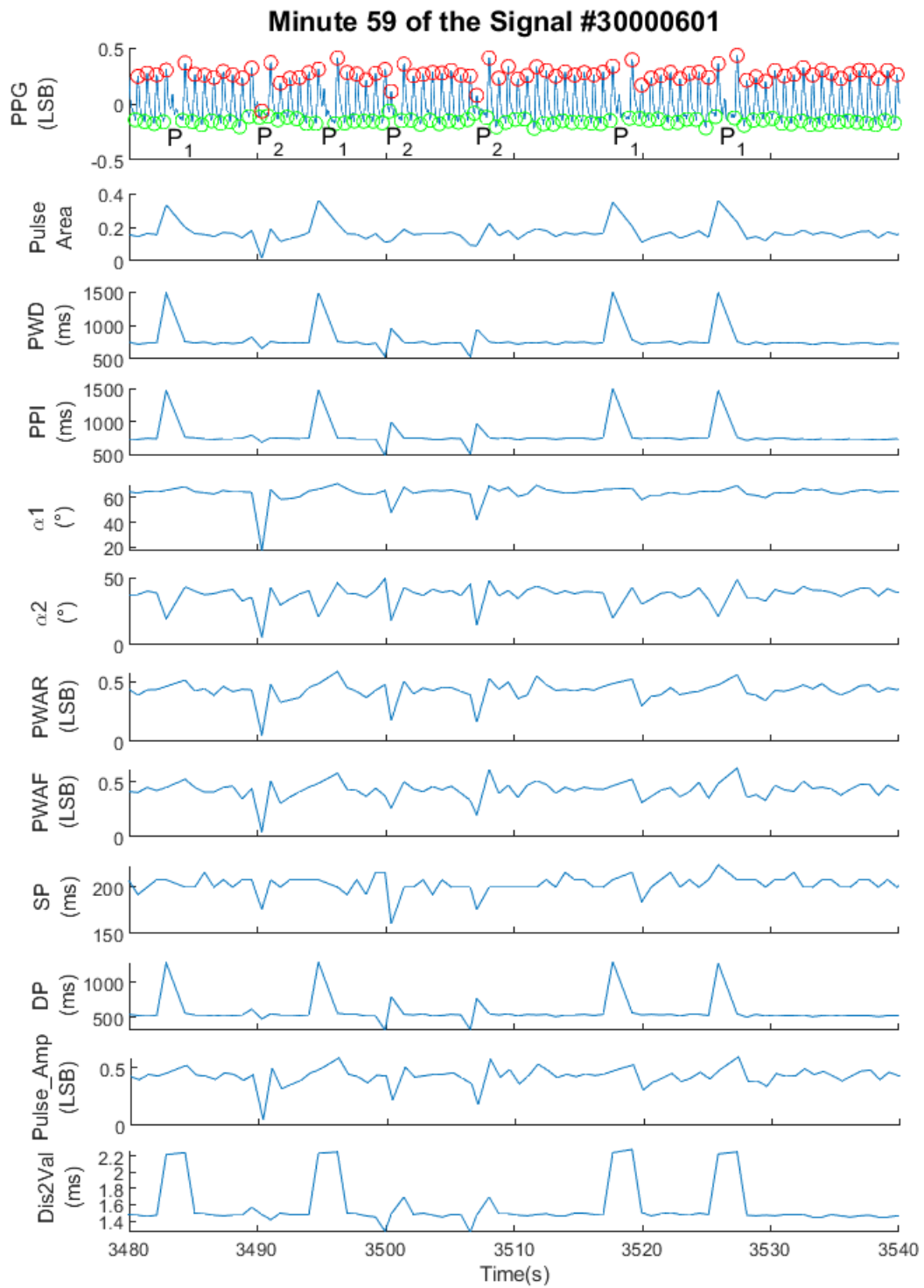


**Figure 7.3:** Trend of the Morphological Features with respect to the PPG signal

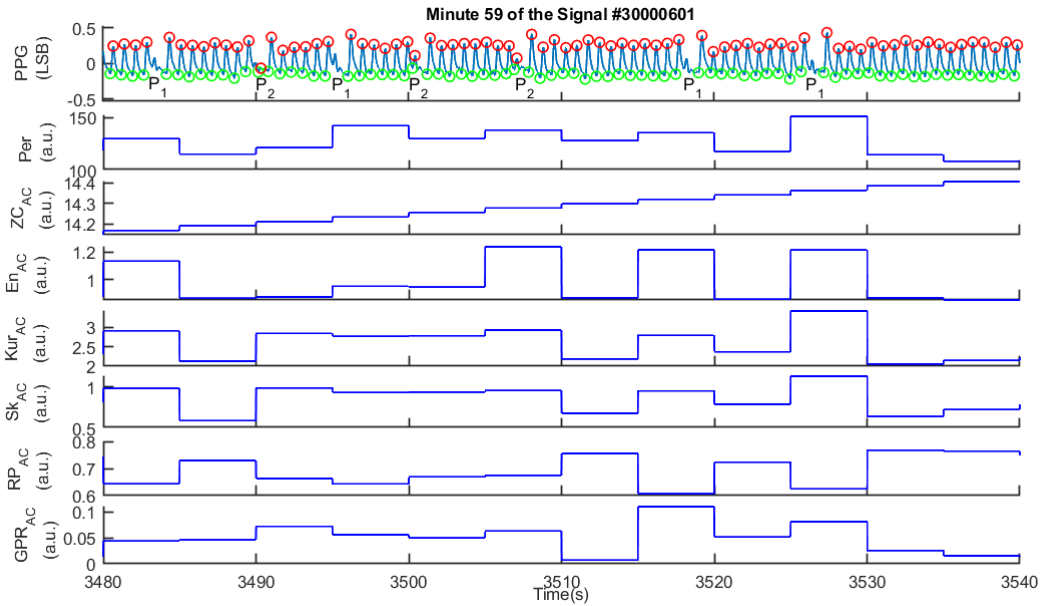


**Figure 7.4:** Trend of the Segment Features with respect to the PPG signal

Since the segments were only discarded when the artefact was present for more than half of the window considered for the evaluation, most of the FN PVCs, as can be seen in Figure 7.5, were due to the low quality of the PPG signal in that points.

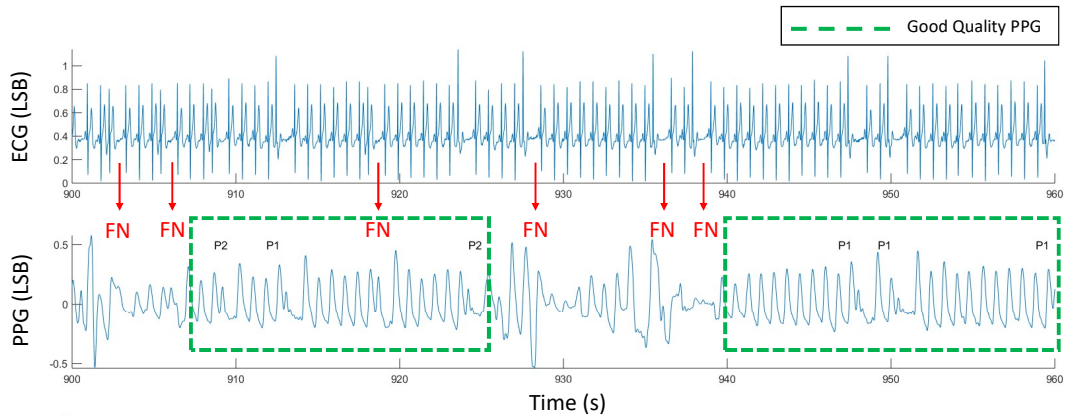


**Figure 7.5:** Low quality PPG signal often leads to FN and PVCs detection. Five out of six FN detections are due to the artefacts present in the PPG signal.

Many FP PVCs were also due to the poor PPG signal quality, but sometimes they also occur because a PVC can produce many lower intensity PPG peaks, and the algorithm detects a P2 after the P1, which is actually referred to the previous P1 PVC. Both the situations are present in the segment represented in Figure 7.6. Even if many errors are due to the poor quality of the PPG signal, the algorithm is often able to detect and locate correctly the PVCs surrounded by artefacts, as can be seen in Figure 7.7.

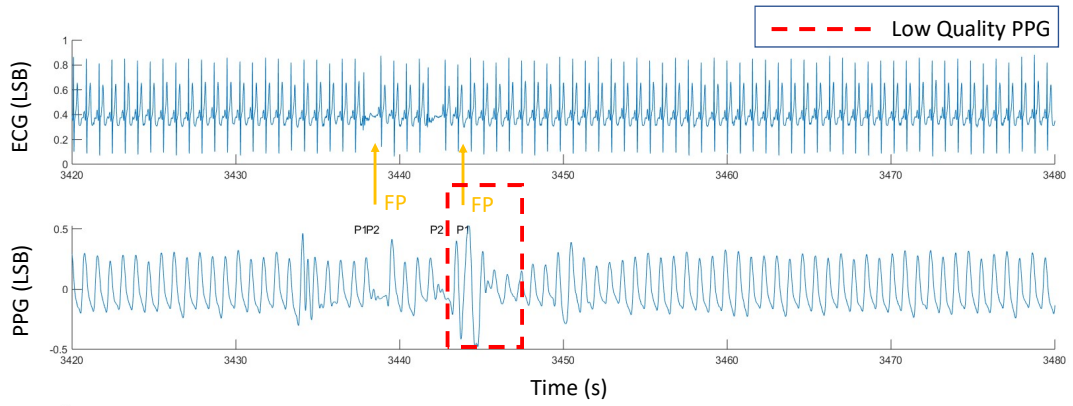


**Figure 7.6:** Typical cases in which a FP PVC is detected.

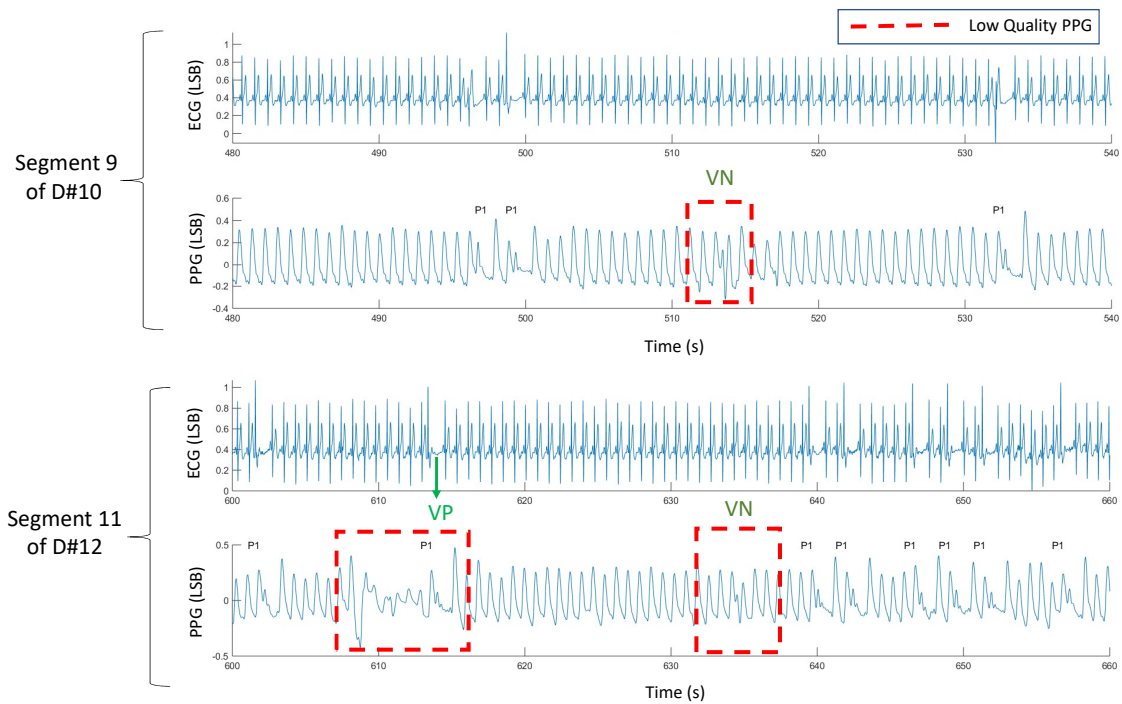


**Figure 7.7:** Algorithm behaviour in segment 9 of signal D#10 and segment 11 of signal D#11.

Furthermore, it was observed that P1 and P2 often corresponds to different form of PVC not only in the PPG signal, but also in the ECG (Figure 7.8).

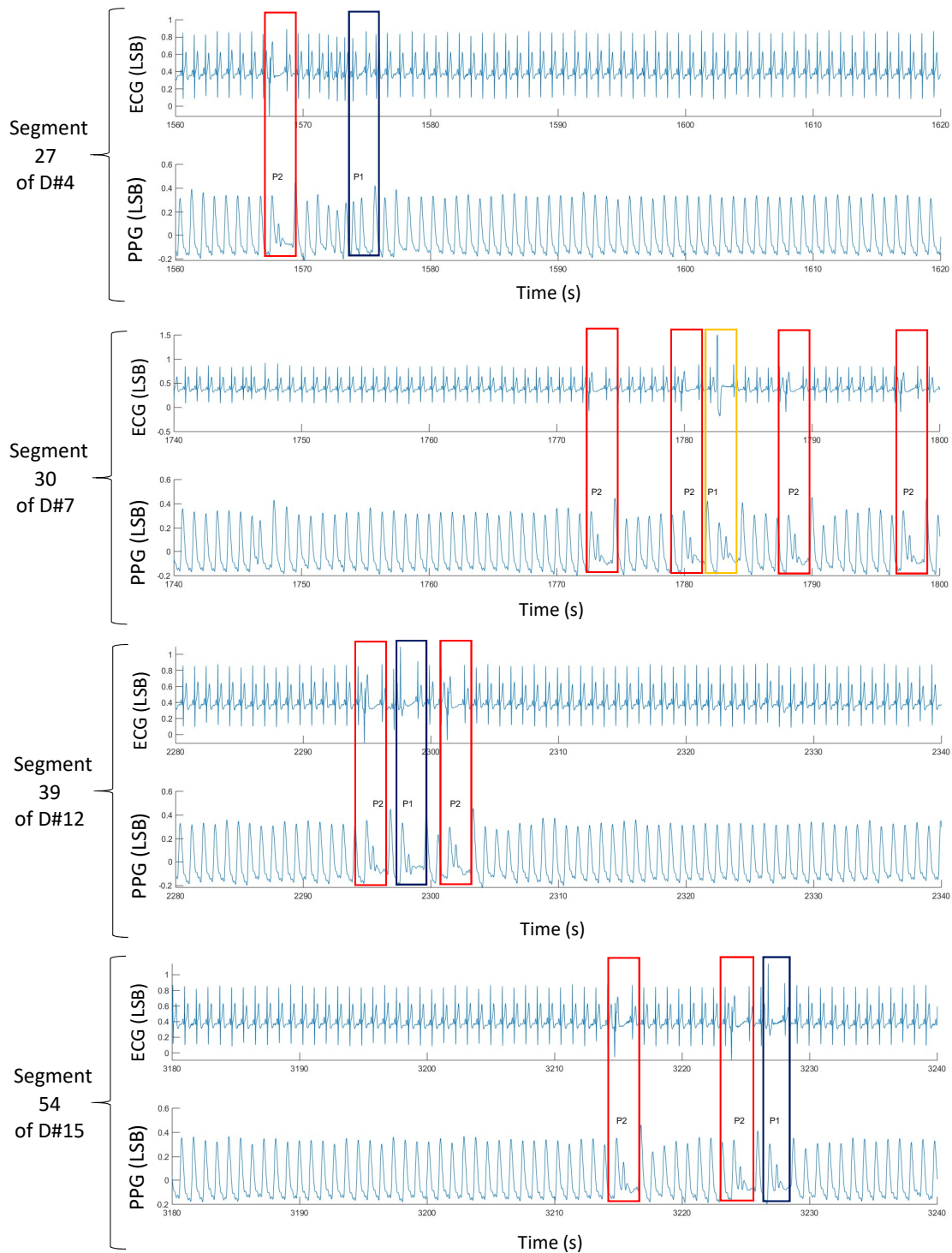


**Figure 7.8:** Multiform PVCs in ECG signal, along with the correspondent detected PVC type in the PPG signal, are highlighted in different colours for different database signals.

## **Part IV**

# **Conclusions and Future Works**



The carried out work is related to Telemedicine, a field in strong growth that aims to promote distance communication between patient and doctor, and to enhance the provision of health services from the diagnosis to the treatment. Thanks to Telemedicine, the patient actively takes part in the management of their own health and this allows them to do prevention and rationalize medical interventions and examinations.

Wearable devices play a central role in this context. In particular, the *Bio2Bit Move* STMicroelectronics prototype, housed in a suitable wrist band, acquires among other signals the PPG signal, taken under reflectance mode at a wavelength of 523 nm (green). PPG signal is inversely proportional to the volume of blood in the tissue and therefore allows continue monitoring of heart conditions over long periods. Moreover, PPG reflectance mode enables a non invasive monitoring, which can be performed in comfortable body sites. The device embed a BLE chip, capable of sending streaming data to other devices, or downloading data previous stored in the internal memory.

These properties allowed to design an algorithm, which was able to provide a real-time HR estimation and to detect and analyse arrhythmia, with the ultimate aim of establishing whether they can be considered harmless or if they need further investigation.

Among all the arrhythmias, Premature Ventricular Contraction detection was performed. PVCs can result from a variety of factors and conditions, including consumption of alcohol, caffeine, tobacco or drugs, certain medications (e.g. antihistamines), physical exercise and stress (anything that increases adrenaline levels), certain electrolyte deficiencies and damaged cardiac tissue caused by heart diseases (coronary artery disease, congenital heart disease, high blood pressure and heart failure). In order to assess the PVCs severity, it is necessary to monitor their occurrence, if they appeared in couplets or triplets, if they come from different ventricular foci and if they are present in an alloarrhythmia form.

The first step of the algorithm, the pre-processing phase, allows to enhance the PPG signals SNR (on average, 24.02 dB and 17.87 dB for the green and red PPG signal, respectively) and correctly extract the AC pulsatile component. To obtain an higher initial SNR and simplify the pre-processing phase, different PPG wavelength should be tested, and the board's housing and wrist holding system should be optimized to reduce the impact of ambient light, minimize the board's movement relative to the wrist and maximize the skin contact.

A motion detection system, based on two indices derived from the 3D Accelerometer signal (embedded in the board) decides if the time window under investigation has to be discarded because too noisy to be further analysed. Thresholds for segments

rejection were not so restrictive, so as to also test the algorithm behaviour against the movement artefact. HR Estimation errors are lower when applying the motion analysis system (AAE=2.25 BPM and PRE=3.36%) but small AAE (2.50 BPM) and PRE (3.68%) occur also without it. This happens because in several cases the HR estimator, based on both time and frequency data, is able to correctly estimate the HR. One could think that the motion analysis system is useless, but the low difference in errors with or without applying the motion analysis phase, it may have been due to the fact that the acquisitions were made in a work-office context, where movements are limited. It will be necessary therefore, to test motion analysis system under situations in which more movement occurs.

In order to provide an indicator of the HR measurement reliability, three level of reliability were defined. Since it was noticed that artefact in PPG signal can happen also when accelerometer do not detect any movement, it was decided to use an index based on the accelerometer ( $Dev_{ACC}$ ) and one based on the PPG signal itself. Many features were extracted from PPG red and green signals but, after the observation of the features trend respect to the PPG signal quality, only Perfusion green index ( $Per_G$ ) was considered. Performances of the level classification is not good enough (the overall Accuracy is 68.4%). Solutions for the performance enhancements could be: a more accurate definition of level boundaries, make acquisition with more movement to increase the prevalence of low level reliability class elements, better analyse all the computed features (feature selection, crosses and normalization should be considered) and employ a machine learning classifier. However, it was also noted that when a PPG segment was classified as having a "low-reliability", the HR estimation was often close to the real HR value and therefore, according to the evaluation method, it should have been classified as an "high-reliability" segment. But looking at the corresponding PPG segment in time-domain, it was possible to see that the quality of that PPG segment, was truly low. So in some cases it turns out that the established Reliability Level is correct, even if the method for assess its accuracy says that is not. This is because the movements and artifacts that contaminate the PPG signal, often have a waveform similar to that of the PPG pulse, and their frequency bands are close to each other. So it happens that the HR estimation is close to the real one, even if it comes from wrong informations that do not derive from the PPG signal, but from the artifacts one. Since the method used to assess the reliability level classification accuracy tends to underestimate the performance, others evaluation methods should be considered.

By introducing more movement into the acquisitions, a lower algorithm performance and an higher number of discarded segments are expected. Therefore, it would be

appropriate to design a movement cancellation algorithm. Since the accelerometer is not always related to the quality of the signal, and the board also integrates the red PPG signal, the algorithm should allow the red PPG to be used to remove motion artefact.

Performance of PVCs detection are high (Sensitivity of 90.10% and Specificity of 99.34%) and main errors in classification are due to the low quality of the PPG signal in that points. The detection algorithm is also able to differentiate some of the multiform PVC present in the ECG trace and, it is expected that the analysis of the other computed Morphology and Segment Features, could be effective in discriminating other multiform PVCs and in turning down FP and FN rates. After optimizing multiform PVCs detection, Alloarrhythmia events along with Ventricular Tachycardia should be investigated.

The arrhythmia detection algorithm should be finally adapted and tested on the signals taken from the *Bio2Bit Move* as we expect differences from those taken from the database. MIMIC database signals are in fact acquired in transmittance mode from the finger, using NIR wavelengths, while the device acquire signals from the wrist, in reflectance mode, using green wavelengths.



# Acknowledgements

Vorrei ringraziare anzitutto la Professoressa Gabriella Olmo per avermi dato l'opportunità di lavorare in un'azienda importante come la *STMicroelectronics*, per la sua disponibilità e per tutti i suoi preziosi suggerimenti.

Vorrei poi ringraziare tutte le persone che ho avuto il piacere di conoscere all'interno della *STMicroelectronics* e che mi hanno guidato in questo percorso: grazie a Luigi, Marco, Alessandro, Stefano, Valeria e Giorgio per la loro disponibilità, per i consigli e tutta l'esperienza che hanno messo a mia disposizione. Grazie anche al gruppo stagisti "*ST Confident*" con cui ho condiviso preziosi pareri, problemi, ansie ma anche gioie e momenti di svago e divertimento milanesi.

Grazie ad Angela per tutti i suoi consigli e le sue sessioni serali informative sulle aritmie. Ma soprattutto grazie per aver creato con me un bel clima di convivenza in casa, che nonostante tutto, ha contribuito a ristabilire la serenità di cui necessitavo.

Ringrazio poi tutti gli amici di Torino: Giulia per il suo essere sempre solare e disponibile, Elia per aver riempito la mia playlist di canzoni ad alta frequenza, Luca con cui ho condiviso un'amicizia basata su: discorsi circa il senso della vita e la società, litigate per la gestione dei progetti e innumerevoli cene di sushi. Grazie a tutto il gruppo di "*Sola Acqua Naturale*" per tutti i pranzi, le cene e le feste. Indimenticabile il limoncino di Simone, e il mare e i taralli di Graziano. Grazie a Sofia per avermi introdotta nel mondo del gossip, della moda, delle canzoni Indie e della popolarità sui social. E un grazie infinito a Bea che è venuta a Milano per salvarmi dal grigio Nord a suon di apericena, karaoke, lavori di bricolage e pigiama party pieni di confessioni. Un grazie dal profondo del cuore va a Simo, la prima persona con cui ho fortemente legato a Torino, collega, coinquilino, amico. Senza il suo sostegno mi sarei sentita totalmente persa. Grazie per gli esami superati insieme, per la tua pazienza nei miei confronti, per la tua disponibilità, per le serate, per la tua solarità insomma... grazie per essere quello che sei.

Vivere lontano da casa a volte può farti sentire sola e senza punti di riferimento, ma non se vivi con la Frejus Squad, la mia seconda famiglia. Grazie a loro, stare giornate intere rinchiusa a casa a studiare, non è stato poi così pesante. Sempre pronti a viziarmi, a strapparmi un sorriso, ad obbligarmi a sentire musica trap, a rompere la mia pentola a pressione, a venirmi a prendere al pronto soccorso. Onorata di aver vissuto con il plurilaureato Abbo, con il grande economista Rocco, con il giramondo spaziale Paolo Pino e con il già menzionato professor Borrelli.

Grazie agli amici di sempre, quelli che ci sono sempre stati e sempre ci saranno: Marta, Marco e Pierca, che è stato sempre presente e mi ha sempre supportato in tutti i miei momenti di difficoltà. Grazie ad Agnese, Mariachiara e Silvia, esempi viventi del fatto che quando un'amicizia è vera, mai scomparirà a causa della lontananza.

Un semplice grazie non è poi sufficiente per dire tutto quello che la mia famiglia ha fatto per me, ciò che essa rappresenta nella mia vita e quanto io sia legata a loro. Grazie a mia sorella Marta e a ciò che ha creato con Giorgio, il mio adorato nipotino Cesare. Grazie a mio fratello Tommaso, che mi capisce sempre al volo e con il quale ho da sempre un legame molto profondo che non si affievolisce nè con il passare del tempo nè a causa di barriere geografiche. Grazie a Nonno Mario, che ogni volta aspetta con ansia il mio ritorno per condividere con me le sue storie e il suo bicchiere di vino. Grazie a Babbo Francesco, che sempre mi tranquillizza e ogni volta che me ne vado, riesce a trasmettermi in quell'abbraccio, tutto l'amore del mondo. Mi devo poi scusare con Mamma Annarella per le chiamate intrise di ansia che l'hanno contagiata e fatta stressare. Lei è la mia roccia, la roccia della mia famiglia, so che farebbe di tutto per noi ed effettivamente lo fa, senza rancore e senza rimpianti. Spero di rendervi tutti orgogliosi di questo traguardo e sappiate che se l'ho raggiunto è anche merito vostro perchè siete voi che mi avete formato nella perseveranza, nella pazienza, nel rispetto, nella correttezza e nell'altruismo.

In ultimo ringrazio Lorenzo, che aspettava questo momento tanto quanto me. Abbiamo condiviso tutto questo percorso insieme: ogni singola emozione, ogni singola preoccupazione. Lui per primo mi ha spinto ad inseguire i miei sogni, ha supportato (e sopportato) la mia scelta di non accontentarmi e di mettermi alla prova. La sua presenza e il suo aiuto sono stati per me fondamentali e con il tempo abbiamo imparato cosa significa esserci veramente per l'altro, nonostante la lontananza. Lontananza che cambia le persone, innesca ansie, dubbi e paure. Ma se nonostante questo, la nostra stima reciproca e il nostro amore ha perseverato negli anni, arricchendosi di nuove consapevolezze, allora credo che tutto ciò sia davvero profondo, autentico e meriti davvero di continuare, più forte di prima. Grazie amore, ce l'abbiamo fatta!



# Bibliography

- [1] S. Hiremath, G. Yang, and K. Mankodiya, “Wearable internet of things: Concept, architectural components and promises for person-centered healthcare,” in *2014 4th International Conference on Wireless Mobile Communication and Healthcare-Transforming Healthcare Through Innovations in Mobile and Wireless Technologies*, pp. 304–307, IEEE, 2014.
- [2] M. R. Yuce and J. Khan, *Wireless body area networks: technology, implementation, and applications*. CRC Press, 2011.
- [3] “Circulatory system.” <http://acescorers.com.sg>. Accessed October 11, 2019.
- [4] “EKG, ECG interpretation.” <https://ceufast.com>. Accessed October 11, 2019.
- [5] “Method and technique of ECG registration and coding.” <http://https://www.pcom.edu>. Accessed October 11, 2019.
- [6] “EKG interpretation.” <https://www.nurseslearning.com>. Accessed October 14, 2019.
- [7] “ECG placement.” <https://www.emtstudy.co.uk>. Accessed October 11, 2019.
- [8] “Holtor monitor.” <https://commons.wikimedia.org>. Accessed October 11, 2019.
- [9] M. H. Niemz, *Laser-tissue interactions: fundamentals and applications*. Springer, 1996.
- [10] E. Benfeldt, “In vivo microdialysis for the investigation of drug levels in the dermis and the effect of barrier perturbation on cutaneous drug penetration. studies in hairless rats and human subjects.,” *Acta dermato-venereologica. Supplementum*, vol. 206, pp. 1–59, 1999.
- [11] M. Lemay, M. Bertschi, J. Sola, P. Renevey, J. Parak, and I. Korhonen, “Application of optical heart rate monitoring,” in *Wearable Sensors*, pp. 105–129, Elsevier, 2014.
- [12] J. Allen, “Photoplethysmography and its application in clinical physiological measurement,” *Physiological measurement*, vol. 28, no. 3, p. R1, 2007.

- [13] J. Wang, G. Liu, K. Cham Fai Leung, R. Loffroy, P. X. Lu, X. J. Wang, *et al.*, “Opportunities and challenges of fluorescent carbon dots in translational optical imaging,” *Current pharmaceutical design*, vol. 21, no. 37, pp. 5401–5416, 2015.
- [14] A. A. Kamshilin and N. B. Margaryants, “Origin of photoplethysmographic waveform at green light,” *Physics Procedia*, vol. 86, pp. 72–80, 2017.
- [15] T. Persson and F. Nylund, “Development of a photoplethysmography based method for investigating changes in blood volume pulsations: for the purpose of pressure ulcer prevention,” 2017.
- [16] C. Fischer, B. Dömer, T. Wibmer, and T. Penzel, “An algorithm for real-time pulse waveform segmentation and artifact detection in photoplethysmograms,” *IEEE journal of biomedical and health informatics*, vol. 21, no. 2, pp. 372–381, 2016.
- [17] T. Tamura, Y. Maeda, M. Sekine, and M. Yoshida, “Wearable photoplethysmographic sensors—past and present,” *Electronics*, vol. 3, no. 2, pp. 282–302, 2014.
- [18] C. Holz and E. J. Wang, “Glabella: Continuously sensing blood pressure behavior using an unobtrusive wearable device,” *Proceedings of the ACM on Interactive, Mobile, Wearable and Ubiquitous Technologies*, vol. 1, no. 3, p. 58, 2017.
- [19] M.-Z. Poh, K. Kim, A. Goessling, N. Swenson, and R. Picard, “Cardiovascular monitoring using earphones and a mobile device,” *IEEE Pervasive Computing*, vol. 11, no. 4, pp. 18–26, 2010.
- [20] A. Solosenko and V. Marozas, “Automatic extrasystole detection using photoplethysmographic signals,” in *XIII Mediterranean Conference on Medical and Biological Engineering and Computing 2013*, pp. 985–988, Springer, 2014.
- [21] L. Van Dyk, “A review of telehealth service implementation frameworks,” *International journal of environmental research and public health*, vol. 11, no. 2, pp. 1279–1298, 2014.
- [22] S. P. Sood, S. Negash, V. W. Mbarika, M. Kifle, and N. Prakash, “Differences in public and private sector adoption of telemedicine: Indian case study for sectoral adoption,” *Studies in health technology and informatics*, vol. 130, p. 257, 2007.
- [23] S. M. Act, “Communication from the commission to the european parliament, the council, the economic and social committee and the committee of the regions,” 2012.

- [24] H. Akhlaghi and H. Asadi, *Essentials of telemedicine and telecare*. Chichester: Wiley, 2002.
- [25] A. Darkins, A. W. Darkins, M. A. Cary, and M. Cary, *Telemedicine and telehealth: principles, policies, performances and pitfalls*. Springer publishing company, 2000.
- [26] K. Deldar, K. Bahaadinbeigy, and S. M. Tara, “Teleconsultation and clinical decision making: a systematic review,” *Acta Informatica Medica*, vol. 24, no. 4, p. 286, 2016.
- [27] P. J. Choi, R. J. Oskouian, and R. S. Tubbs, “Telesurgery: past, present, and future,” *Cureus*, vol. 10, no. 5, 2018.
- [28] S. A. O. Ogirima, A. O. Afolabi, and A. A. Adigun, “An integrated framework for tediagnosis and prescriptions in herbal medicine,” *Int. J. Advanced Networking and Applications*, vol. 8, no. 04, pp. 3124–3143, 2017.
- [29] V. Nangalia, D. R. Prytherch, and G. B. Smith, “Health technology assessment review: Remote monitoring of vital signs-current status and future challenges,” *Critical Care*, vol. 14, no. 5, p. 233, 2010.
- [30] T. Gerber, V. Olazabal, K. Brown, and A. Pablos-Mendez, “An agenda for action on global e-health,” *Health affairs*, vol. 29, no. 2, pp. 233–236, 2010.
- [31] N. Nasiri and A. Tricoli, “Advances in wearable sensing technologies and their impact for personalized and preventive medicine,” *Wearable Technologies*, p. 1, 2018.
- [32] M. R. Yuce, “Implementation of wireless body area networks for healthcare systems,” *Sensors and Actuators A: Physical*, vol. 162, no. 1, pp. 116–129, 2010.
- [33] P. Abete, G. Testa, D. Della Morte, F. Mazzella, G. Galizia, D. D’ambrosio, C. Visconti, G. Gargiulo, F. Cacciatore, and F. Rengo, “La comorbilità nell’anziano: epidemiologia e caratteristiche cliniche,” *G Gerontol*, vol. 52, pp. 267–72, 2004.
- [34] A. L. Bui and G. C. Fonarow, “Home monitoring for heart failure management,” *Journal of the American College of Cardiology*, vol. 59, no. 2, pp. 97–104, 2012.
- [35] X. Zhu and A. Cahan, “Wearable technologies and telehealth in care management for chronic illness,” in *Healthcare Information Management Systems*, pp. 375–398, Springer, 2016.

- [36] G. Perolle, P. Fraisse, M. Mavros, and I. Etxeberria, “Automatic fall detection and activity monitoring for elderly,” *Proceedings of MEDETEL*, 2006.
- [37] G. Walraven, *Basic Arrhythmias*. Pearson Education, 2011.
- [38] E. N. Marieb and K. Hoehn, *Human anatomy & physiology*. Pearson Education, 2007.
- [39] K. Farzam and S. S. Bhimji, “Rhythm, premature ventricular contraction (pvc),” 2018.
- [40] M. W. Massing, R. J. Simpson Jr, P. M. Rautaharju, P. J. Schreiner, R. Crow, and G. Heiss, “Usefulness of ventricular premature complexes to predict coronary heart disease events and mortality (from the atherosclerosis risk in communities cohort),” *The American journal of cardiology*, vol. 98, no. 12, pp. 1609–1612, 2006.
- [41] W. N. Ribeiro, A. T. Yamada, C. J. Grupi, G. T. da Silva, and A. J. Mansur, “Premature atrial and ventricular complexes in outpatients referred from a primary care facility,” *PloS one*, vol. 13, no. 9, p. e0204246, 2018.
- [42] V. Lee, D. Perera, and P. Lambiase, “Prognostic significance of exercise-induced premature ventricular complexes: a systematic review and meta-analysis of observational studies,” *Heart Asia*, vol. 9, no. 1, pp. 14–24, 2017.
- [43] M.-S. Ahn, “Current concepts of premature ventricular contractions,” *Journal of lifestyle medicine*, vol. 3, no. 1, p. 26, 2013.
- [44] J. Marín-García, “Post-genomic analysis of dysrhythmias and sudden death,” in *Post-genomic cardiology*, pp. 563–611, Academic Press, 2014.
- [45] D. Zipes, A. Camm, M. Borggrefe, A. Buxton, B. Chaitman, M. Fromer, G. Gregoratos, G. Klein, A. Moss, R. Myerburg, *et al.*, “Guidelines for management of patients with ventricular arrhythmias and the prevention of sudden cardiac death. executive summary,” *Revista espanola de cardiologia*, vol. 59, no. 12, p. 1328, 2006.
- [46] J. G. Panizo, S. Barra, G. Mellor, P. Heck, and S. Agarwal, “Premature ventricular complex-induced cardiomyopathy,” *Arrhythmia & electrophysiology review*, vol. 7, no. 2, p. 128, 2018.

- [47] E. J. d. S. Luz, W. R. Schwartz, G. Cámara-Chávez, and D. Menotti, “ECG-based heartbeat classification for arrhythmia detection: A survey,” *Computer methods and programs in biomedicine*, vol. 127, pp. 144–164, 2016.
- [48] R. Kohno, H. Abe, and D. G. Benditt, “Ambulatory electrocardiogram monitoring devices for evaluating transient loss of consciousness or other related symptoms,” *Journal of arrhythmia*, vol. 33, no. 6, pp. 583–589, 2017.
- [49] M. Brignole, R. Sutton, C. Menozzi, R. Garcia-Civera, A. Moya, W. Wieling, D. Andresen, D. G. Benditt, and P. Vardas, “Early application of an implantable loop recorder allows effective specific therapy in patients with recurrent suspected neurally mediated syncope,” *European heart journal*, vol. 27, no. 9, pp. 1085–1092, 2006.
- [50] S. Mittal, E. Pokushalov, A. Romanov, M. Ferrara, A. Arshad, D. Musat, M. Pre-minger, T. Sichrovsky, and J. S. Steinberg, “Long-term ECG monitoring using an implantable loop recorder for the detection of atrial fibrillation after cavotricuspid isthmus ablation in patients with atrial flutter,” *Heart Rhythm*, vol. 10, no. 11, pp. 1598–1604, 2013.
- [51] F. Giada, E. Bertaglia, B. Reimers, D. Noventa, and A. Raviele, “Current and emerging indications for implantable cardiac monitors,” *Pacing and Clinical Electrophysiology*, vol. 35, no. 9, pp. 1169–1178, 2012.
- [52] H. Molitor and M. Kniazuk, “A new bloodless method for continuous recording of peripheral circulatory changes,” *Journal of Pharmacology and Experimental Therapeutics*, vol. 57, no. 1, pp. 6–18, 1936.
- [53] P. Hanzlik, F. DeEDS, and B. Terada, “A simple method of demonstrating changes in blood supply of the ear and effects of some measures,” *Journal of Pharmacology and Experimental Therapeutics*, vol. 56, no. 2, pp. 194–204, 1936.
- [54] A. B. Hertzman, “Observations on the finger volume pulse recorded photoelectrically,” *Am. J. Physiol.*, vol. 119, pp. 334–335, 1937.
- [55] A. B. Hertzman, “The blood supply of various skin areas as estimated by the photoelectric plethysmograph,” *American Journal of Physiology-Legacy Content*, vol. 124, no. 2, pp. 328–340, 1938.
- [56] A. B. Hertzman and L. W. Roth, “The vasomotor components in the vascular reactions in the finger to cold,” *American Journal of Physiology-Legacy Content*, vol. 136, no. 4, pp. 669–679, 1942.

- [57] L. Roth, "The reactions of the digital artery and minute pad arteries to local cold: Hertzman, ab, and roth, lw: Am. j. physiol. 136: 680, 1942," *American Heart Journal*, vol. 24, no. 6, pp. 866–867, 1942.
- [58] A. B. Hertzman and L. W. Roth, "The absence of vasoconstrictor reflexes in the forehead circulation. effects of cold," *American Journal of Physiology-Legacy Content*, vol. 136, no. 4, pp. 692–697, 1942.
- [59] A. B. Hertzman and J. B. Dillon, "Distinction between arterial, venous and flow components in photoelectric plethysmography in man," *American Journal of Physiology-Legacy Content*, vol. 130, no. 1, pp. 177–185, 1940.
- [60] A. B. Hertzman and J. B. Dillon, "Applications of photoelectric plethysmography in peripheral vascular disease," *American Heart Journal*, vol. 20, no. 6, pp. 750–761, 1940.
- [61] A. B. Hertzman and F. Flath, "Continuous simultaneous registration of sweating and blood flow in a small skin area," tech. rep., Saint Louis University MO, 1963.
- [62] J. Moraes, M. Rocha, G. Vasconcelos, J. Vasconcelos Filho, V. de Albuquerque, and A. Alexandria, "Advances in photoplethysmography signal analysis for biomedical applications," *Sensors*, vol. 18, no. 6, p. 1894, 2018.
- [63] V. V. Tuchin, "Tissue optics and photonics: light-tissue interaction," *Journal of Biomedical Photonics & Engineering*, vol. 1, no. 2, 2015.
- [64] D. W. Hahn, "Light scattering theory," *Department of Mechanical and Aerospace Engineering, University of Florida*, 2009.
- [65] L. G. Henyey and J. L. Greenstein, "Diffuse radiation in the galaxy," *The Astrophysical Journal*, vol. 93, pp. 70–83, 1941.
- [66] I. Hassaninia, R. Bostanabad, W. Chen, and H. Mohseni, "Characterization of the optical properties of turbid media by supervised learning of scattering patterns," *Scientific reports*, vol. 7, no. 1, p. 15259, 2017.
- [67] L. Yang and S. J. Miklavcic, "Revised kubelka–munk theory. iii. a general theory of light propagation in scattering and absorptive media," *JOSA A*, vol. 22, no. 9, pp. 1866–1873, 2005.
- [68] A. Ishimaru, "Diffusion of light in turbid material," *Applied optics*, vol. 28, no. 12, pp. 2210–2215, 1989.

- [69] A. Kienle and M. S. Patterson, "Determination of the optical properties of turbid media from a single monte carlo simulation," *Physics in Medicine & Biology*, vol. 41, no. 10, p. 2221, 1996.
- [70] W.-F. Cheong, S. A. Prahl, and A. J. Welch, "A review of the optical properties of biological tissues," *IEEE journal of quantum electronics*, vol. 26, no. 12, pp. 2166–2185, 1990.
- [71] V. V. Tuchin, "Light scattering study of tissues," *Physics-Uspekhi*, vol. 40, no. 5, p. 495, 1997.
- [72] A. Kamal, J. Harness, G. Irving, and A. Mearns, "Skin photoplethysmography—a review," *Computer methods and programs in biomedicine*, vol. 28, no. 4, pp. 257–269, 1989.
- [73] G. V. Baranoski and A. Krishnaswamy, "An introduction to light interaction with human skin," *Revista de Informática Teórica e Aplicada*, vol. 11, no. 1, pp. 33–62, 2004.
- [74] M. Geerligs, *In vitro mechanical characterization of human skin layers: stratum corneum, epidermis and hypodermis*. PhD thesis, PhD Thesis, 2006.
- [75] D. P. Jones, "Medical electro-optics: measurements in the human microcirculation," *Physics in Technology*, vol. 18, no. 2, p. 79, 1987.
- [76] P. Kyriacou, K. Budidha, and T. Y. Abay, "Optical techniques for blood and tissue oxygenation," *Encyclopedia of Biomedical Engineering*, ed R. Narayan (Oxford: Elsevier), pp. 461–472, 2019.
- [77] R. Anderson and J. Parrish, "Optical properties of human skin," in *The science of photomedicine*, pp. 147–194, Springer, 1982.
- [78] J. Lee, K. Matsumura, K.-i. Yamakoshi, P. Rolfe, S. Tanaka, and T. Yamakoshi, "Comparison between red, green and blue light reflection photoplethysmography for heart rate monitoring during motion," in *2013 35th annual international conference of the IEEE engineering in medicine and biology society (EMBC)*, pp. 1724–1727, IEEE, 2013.
- [79] Y. Maeda, M. Sekine, and T. Tamura, "The advantages of wearable green reflected photoplethysmography," *Journal of medical systems*, vol. 35, no. 5, pp. 829–834, 2011.

- [80] A. Reisner, P. A. Shaltis, D. McCombie, and H. H. Asada, “Utility of the photoplethysmogram in circulatory monitoring,” *Anesthesiology: The Journal of the American Society of Anesthesiologists*, vol. 108, no. 5, pp. 950–958, 2008.
- [81] S. Standring, *Gray’s anatomy e-book: the anatomical basis of clinical practice*. Elsevier Health Sciences, 2015.
- [82] A. N. Bashkatov, E. A. Genina, and V. V. Tuchin, “Optical properties of skin, subcutaneous, and muscle tissues: a review,” *Journal of Innovative Optical Health Sciences*, vol. 4, no. 01, pp. 9–38, 2011.
- [83] V. Roberts, “Photoplethysmography-fundamental aspects of the optical properties of blood in motion,” *Transactions of the Institute of Measurement and Control*, vol. 4, no. 2, pp. 101–106, 1982.
- [84] P. Agache and P. Humbert, *Measuring the skin*. Springer Science & Business Media, 2004.
- [85] J. Spigulis, “Optical noninvasive monitoring of skin blood pulsations,” *Applied optics*, vol. 44, no. 10, pp. 1850–1857, 2005.
- [86] M. Sherebrin and R. Sherebrin, “Frequency analysis of the peripheral pulse wave detected in the finger with a photoplethysmograph,” *IEEE Transactions on biomedical engineering*, vol. 37, no. 3, pp. 313–317, 1990.
- [87] N. Selvaraj, A. Jaryal, J. Santhosh, K. K. Deepak, and S. Anand, “Assessment of heart rate variability derived from finger-tip photoplethysmography as compared to electrocardiography,” *Journal of medical engineering & technology*, vol. 32, no. 6, pp. 479–484, 2008.
- [88] Y. Mendelson and B. D. Ochs, “Noninvasive pulse oximetry utilizing skin reflectance photoplethysmography,” *IEEE Transactions on Biomedical Engineering*, vol. 35, no. 10, pp. 798–805, 1988.
- [89] F.-H. Huang, P.-J. Yuan, K.-P. Lin, H.-H. Chang, and C.-L. Tsai, “Analysis of reflectance photoplethysmograph sensors,” *world academy of science, engineering and technology*, vol. 59, no. 241, pp. 1266–1269, 2011.
- [90] A. Gumiero, “Motion compensation in photoplethysmography-based heart rate monitoring,” Dec. 12 2017. US Patent 9,839,397.
- [91] Y. Zhang, S. Song, R. Vullings, D. Biswas, N. Simões-Capela, N. Van Helleputte, C. Van Hoof, and W. Groenendaal, “Motion artifact reduction for wrist-worn

photoplethysmograph sensors based on different wavelengths,” *Sensors*, vol. 19, no. 3, p. 673, 2019.

- [92] Z. Zhang, Z. Pi, and B. Liu, “Troika: A general framework for heart rate monitoring using wrist-type photoplethysmographic signals during intensive physical exercise,” *IEEE Transactions on biomedical engineering*, vol. 62, no. 2, pp. 522–531, 2014.
- [93] Y. Wang, Z. Liu, and B. Dong, “Heart rate monitoring from wrist-type PPG based on singular spectrum analysis with motion decision,” in *2016 38th Annual International Conference of the IEEE Engineering in Medicine and Biology Society (EMBC)*, pp. 3511–3514, IEEE, 2016.
- [94] Z. Zhang, “Photoplethysmography-based heart rate monitoring in physical activities via joint sparse spectrum reconstruction,” *IEEE transactions on biomedical engineering*, vol. 62, no. 8, pp. 1902–1910, 2015.
- [95] H.-W. Lee, J.-W. Lee, W.-G. Jung, and G.-K. Lee, “The periodic moving average filter for removing motion artifacts from PPG signals,” *International Journal of Control, Automation, and Systems*, vol. 5, no. 6, pp. 701–706, 2007.
- [96] K. A. Reddy, B. George, and V. J. Kumar, “Use of fourier series analysis for motion artifact reduction and data compression of photoplethysmographic signals,” *IEEE transactions on instrumentation and measurement*, vol. 58, no. 5, pp. 1706–1711, 2008.
- [97] L. Wang, B. P. Lo, and G.-Z. Yang, “Multichannel reflective PPG earpiece sensor with passive motion cancellation,” *IEEE transactions on biomedical circuits and systems*, vol. 1, no. 4, pp. 235–241, 2007.
- [98] K. Chan and Y. Zhang, “Adaptive reduction of motion artifact from photoplethysmographic recordings using a variable step-size lms filter,” in *SENSORS, 2002 IEEE*, vol. 2, pp. 1343–1346, IEEE, 2002.
- [99] B. Lee, J. Han, H. J. Baek, J. H. Shin, K. S. Park, and W. J. Yi, “Improved elimination of motion artifacts from a photoplethysmographic signal using a kalman smoother with simultaneous accelerometry,” *Physiological measurement*, vol. 31, no. 12, p. 1585, 2010.
- [100] C. Lee and Y. T. Zhang, “Reduction of motion artifacts from photoplethysmographic recordings using a wavelet denoising approach,” in *IEEE EMBS*

*Asian-Pacific Conference on Biomedical Engineering, 2003.*, pp. 194–195, IEEE, 2003.

- [101] Y.-s. Yan, C. C. Poon, and Y.-t. Zhang, “Reduction of motion artifact in pulse oximetry by smoothed pseudo wigner-ville distribution,” *Journal of NeuroEngineering and Rehabilitation*, vol. 2, no. 1, p. 3, 2005.
- [102] G. Drummond and G. Park, “Arterial oxygen saturation before intubation of the trachea: an assessment of oxygenation techniques,” *British Journal of Anaesthesia*, vol. 56, no. 9, pp. 987–993, 1984.
- [103] L. Short, R. B. Hecker, R. E. Middaugh, and E. J. Menk, “A comparison of pulse oximeters during helicopter flight,” *The Journal of emergency medicine*, vol. 7, no. 6, pp. 639–643, 1989.
- [104] N. Johnson, V. A. Johnson, J. Fisher, B. Jobbings, J. Bannister, and R. J. Lilford, “Fetal monitoring with pulse oximetry,” *BJOG: An International Journal of Obstetrics & Gynaecology*, vol. 98, no. 1, pp. 36–41, 1991.
- [105] P. Meier-Stauss, H. Bucher, R. Hürlimann, V. König, and R. Huch, “Pulse oximetry used for documenting oxygen saturation and right-to-left shunting immediately after birth,” *European journal of pediatrics*, vol. 149, no. 12, pp. 851–855, 1990.
- [106] A. R. Hovagim, S. A. Vitkun, G. R. Manecke, and R. Reiner, “Arterial oxygen desaturation in adult dental patients receiving conscious sedation,” *Journal of oral and maxillofacial surgery*, vol. 47, no. 9, pp. 936–939, 1989.
- [107] H. Trang, S. Boureghda, and V. Leske, “Sleep desaturation: comparison of two oximeters,” *Pediatric pulmonology*, vol. 37, no. 1, pp. 76–80, 2004.
- [108] M. Shafique, *Investigation of photoplethysmography and arterial blood oxygen saturation during artificially induced peripheral hypoperfusion utilising multimode photometric sensors*. PhD thesis, City University, 2011.
- [109] P. A. Kyriacou, “Pulse oximetry in the oesophagus,” *Physiological measurement*, vol. 27, no. 1, p. R1, 2005.
- [110] M. T. Islam, I. Zabir, S. T. Ahamed, M. T. Yasar, C. Shahnaz, and S. A. Fattah, “A time-frequency domain approach of heart rate estimation from photoplethysmographic (PPG) signal,” *Biomedical Signal Processing and Control*, vol. 36, pp. 146–154, 2017.

- [111] S. Fallet and J.-M. Vesin, “Adaptive frequency tracking for robust heart rate estimation using wrist-type photoplethysmographic signals during physical exercise,” in *2015 Computing in Cardiology Conference (CinC)*, pp. 925–928, IEEE, 2015.
- [112] B. Sun and Z. Zhang, “Photoplethysmography-based heart rate monitoring using asymmetric least squares spectrum subtraction and bayesian decision theory,” *IEEE Sensors Journal*, vol. 15, no. 12, pp. 7161–7168, 2015.
- [113] A. Garde, W. Karlen, P. Dehkordi, J. M. Ansermino, and G. A. Dumont, “Empirical mode decomposition for respiratory and heart rate estimation from the photoplethysmogram,” in *Computing in Cardiology 2013*, pp. 799–802, IEEE, 2013.
- [114] T. Shimazaki, S. Hara, H. Okuhata, H. Nakamura, and T. Kawabata, “Motion artifact cancellation and outlier rejection for clip-type PPG-based heart rate sensor,” in *2015 37th Annual International Conference of the IEEE Engineering in Medicine and Biology Society (EMBC)*, pp. 2026–2029, IEEE, 2015.
- [115] M. A. Kenfack, F. Lador, M. Licker, M. Christian, T. Enrico, C. Capelli, D. Morel, and G. Ferretti, “Cardiac output by modelflow® method from intra-arterial and fingertip pulse pressure profiles,” *Clinical science*, vol. 106, no. 4, pp. 365–369, 2004.
- [116] S. M. Romano and M. Pistolesi, “Assessment of cardiac output from systemic arterial pressure in humans,” *Critical care medicine*, vol. 30, no. 8, pp. 1834–1841, 2002.
- [117] M. P. Harms, K. H. Wesseling, P. Frank, M. Jenstrup, J. Van Goudoever, N. H. Secher, and J. J. Van Lieshout, “Continuous stroke volume monitoring by modelling flow from non-invasive measurement of arterial pressure in humans under orthostatic stress,” *Clinical Science*, vol. 97, no. 3, pp. 291–301, 1999.
- [118] A. Johansson and P. Öberg, “Estimation of respiratory volumes from the photoplethysmographic signal. part i: experimental results,” *Medical & biological engineering & computing*, vol. 37, no. 1, pp. 42–47, 1999.
- [119] L. Nilsson, A. Johansson, and S. Kalman, “Monitoring of respiratory rate in postoperative care using a new photoplethysmographic technique,” *Journal of clinical monitoring and computing*, vol. 16, no. 4, pp. 309–315, 2000.

- [120] J. Allen and A. Murray, "Age-related changes in the characteristics of the photoplethysmographic pulse shape at various body sites," *Physiological measurement*, vol. 24, no. 2, p. 297, 2003.
- [121] L. Mason, *Signal processing methods for non-invasive respiration monitoring*. University of Oxford Oxford, 2002.
- [122] J. Y. Kim, B. H. Cho, S. M. Im, M. J. Jeon, I. Y. Kim, and S. I. Kim, "Comparative study on artificial neural network with multiple regressions for continuous estimation of blood pressure," in *2005 IEEE Engineering in Medicine and Biology 27th Annual Conference*, pp. 6942–6945, IEEE, 2006.
- [123] F. S. Cattivelli and H. Garudadri, "Noninvasive cuffless estimation of blood pressure from pulse arrival time and heart rate with adaptive calibration," in *2009 Sixth international workshop on wearable and implantable body sensor networks*, pp. 114–119, IEEE, 2009.
- [124] D. B. McCombie, A. T. Reisner, and H. H. Asada, "Adaptive blood pressure estimation from wearable PPG sensors using peripheral artery pulse wave velocity measurements and multi-channel blind identification of local arterial dynamics," in *2006 International Conference of the IEEE Engineering in Medicine and Biology Society*, pp. 3521–3524, IEEE, 2006.
- [125] Y. Kurylyak, F. Lamonaca, and D. Grimaldi, "A neural network-based method for continuous blood pressure estimation from a PPG signal," in *2013 IEEE International instrumentation and measurement technology conference (I2MTC)*, pp. 280–283, IEEE, 2013.
- [126] J. Allen and A. Murray, "Development of a neural network screening aid for diagnosing lower limb peripheral vascular disease from photoelectric plethysmography pulse waveforms," *Physiological Measurement*, vol. 14, no. 1, p. 13, 1993.
- [127] P. Gizdulich, "On a non-invasive evaluation of pulse wave velocity in human peripheral arteries," *Clinical Physics and Physiological Measurement*, vol. 5, no. 1, p. 33, 1984.
- [128] A. Avolio, S.-G. Chen, R.-P. Wang, C.-L. Zhang, M.-F. Li, and M. O’rourke, "Effects of aging on changing arterial compliance and left ventricular load in a northern chinese urban community.," *Circulation*, vol. 68, no. 1, pp. 50–58, 1983.
- [129] A. Incze, I. Lazar, E. Abraham, M. Copotoiu, and S. Cotoi, "The use of light reflection rheography in diagnosing venous disease and arterial microcirculation.,"

*Romanian journal of internal medicine= Revue roumaine de medecine interne*, vol. 41, no. 1, pp. 35–40, 2003.

- [130] A. J. Camm, M. Malik, J. T. Bigger, G. Breithardt, S. Cerutti, R. J. Cohen, P. Coumel, E. L. Fallen, H. L. Kennedy, R. Kleiger, *et al.*, “Heart rate variability: standards of measurement, physiological interpretation and clinical use. task force of the european society of cardiology and the north american society of pacing and electrophysiology,” 1996.
- [131] S. Z. Rosero, V. Kutyifa, B. Olshansky, and W. Zareba, “Ambulatory ECG monitoring in atrial fibrillation management,” *Progress in cardiovascular diseases*, vol. 56, no. 2, pp. 143–152, 2013.
- [132] E. Richardson, A. Hall, and A. R. Mitchell, “Screening for atrial fibrillation and the role of digital health technologies,” in *Epidemiology and Treatment of Atrial Fibrillation*, IntechOpen, 2019.
- [133] A. Inc., *Using Apple Watch for Arrhythmia Detection*.
- [134] T. Schäck, Y. S. Harb, M. Muma, and A. M. Zoubir, “Computationally efficient algorithm for photoplethysmography-based atrial fibrillation detection using smart-phones,” in *2017 39th Annual International Conference of the IEEE Engineering in Medicine and Biology Society (EMBC)*, pp. 104–108, IEEE, 2017.
- [135] S. P. Shashikumar, A. J. Shah, Q. Li, G. D. Clifford, and S. Nemati, “A deep learning approach to monitoring and detecting atrial fibrillation using wearable technology,” in *2017 IEEE EMBS International Conference on Biomedical & Health Informatics (BHI)*, pp. 141–144, IEEE, 2017.
- [136] M. Voisin, Y. Shen, A. Aliamiri, A. Avati, A. Hannun, and A. Ng, “Ambulatory atrial fibrillation monitoring using wearable photoplethysmography with deep learning,” *arXiv preprint arXiv:1811.07774*, 2018.
- [137] A. G. Bonomi, F. Schipper, L. M. Eerikäinen, J. Margarito, R. M. Aarts, S. Babaeizadeh, H. M. de Morree, and L. Dekker, “Atrial fibrillation detection using photo-plethysmography and acceleration data at the wrist,” in *2016 Computing in Cardiology Conference (CinC)*, pp. 277–280, IEEE, 2016.
- [138] A. Tarniceriu, J. Harju, Z. R. Yousefi, A. Vehkaoja, J. Parak, A. Yli-Hankala, and I. Korhonen, “The accuracy of atrial fibrillation detection from wrist photoplethysmography. a study on post-operative patients,” in *2018 40th Annual International*

*Conference of the IEEE Engineering in Medicine and Biology Society (EMBC)*, pp. 1–4, IEEE, 2018.

- [139] D. Stankevičius, A. Petrėnas, A. Sološenko, M. Grigutis, T. Januškevičius, L. Rimševičius, and V. Marozas, “Photoplethysmography-based system for atrial fibrillation detection during hemodialysis,” in *XIV Mediterranean Conference on Medical and Biological Engineering and Computing 2016*, pp. 79–82, Springer, 2016.
- [140] A. Sološenko, A. Petrėnas, and V. Marozas, “Photoplethysmography-based method for automatic detection of premature ventricular contractions,” *IEEE transactions on biomedical circuits and systems*, vol. 9, no. 5, pp. 662–669, 2015.
- [141] A. L. Goldberger, L. A. Amaral, L. Glass, J. M. Hausdorff, P. C. Ivanov, R. G. Mark, J. E. Mietus, G. B. Moody, C.-K. Peng, and H. E. Stanley, “PhysioBank, PhysioToolkit, and PhysioNet: components of a new research resource for complex physiologic signals,” *Circulation*, vol. 101, no. 23, pp. e215–e220, 2000.
- [142] M. R. Yousefi, M. Khezri, R. Bagheri, and R. Jafari, “Automatic detection of premature ventricular contraction based on photoplethysmography using chaotic features and high order statistics,” in *2018 IEEE International Symposium on Medical Measurements and Applications (MeMeA)*, pp. 1–5, IEEE, 2018.
- [143] L. F. Polanía, L. K. Mestha, D. T. Huang, and J.-P. Couderc, “Method for classifying cardiac arrhythmias using photoplethysmography,” in *2015 37th Annual International Conference of the IEEE Engineering in Medicine and Biology Society (EMBC)*, pp. 6574–6577, IEEE, 2015.
- [144] G. B. Moody and R. G. Mark, “A database to support development and evaluation of intelligent intensive care monitoring,” in *Computer in Cardiology, 1996*, pp. 657–660, IEEE, 1996.
- [145] M. Saeed, M. Villarroel, A. T. Reisner, G. Clifford, L.-W. Lehman, G. Moody, T. Heldt, T. H. Kyaw, B. Moody, and R. G. Mark, “Multiparameter intelligent monitoring in intensive care ii (MIMIC-II): a public-access intensive care unit database,” *Critical care medicine*, vol. 39, no. 5, p. 952, 2011.
- [146] A. E. Johnson, T. J. Pollard, L. Shen, H. L. Li-wei, M. Feng, M. Ghassemi, B. Moody, P. Szolovits, L. A. Celi, and R. G. Mark, “MIMIC-III, a freely accessible critical care database,” *Scientific data*, vol. 3, p. 160035, 2016.

- [147] M. Elgendi, “Optimal signal quality index for photoplethysmogram signals,” *Bioengineering*, vol. 3, no. 4, p. 21, 2016.
- [148] N. Selvaraj, Y. Mendelson, K. H. Shelley, D. G. Silverman, and K. H. Chon, “Statistical approach for the detection of motion/noise artifacts in photoplethysmogram,” in *2011 Annual International Conference of the IEEE Engineering in Medicine and Biology Society*, pp. 4972–4975, IEEE, 2011.
- [149] L. M. Eerikäinen, A. G. Bonomi, F. Schipper, L. R. Dekker, R. Vullings, H. M. de Morree, and R. M. Aarts, “Comparison between electrocardiogram-and photoplethysmogram-derived features for atrial fibrillation detection in free-living conditions,” *Physiological measurement*, vol. 39, no. 8, p. 084001, 2018.
- [150] A. Shcherbina, C. M. Mattsson, D. Waggott, H. Salisbury, J. W. Christle, T. Hastie, M. T. Wheeler, and E. A. Ashley, “Accuracy in wrist-worn, sensor-based measurements of heart rate and energy expenditure in a diverse cohort,” *Journal of personalized medicine*, vol. 7, no. 2, p. 3, 2017.
- [151] F. Wadehn, Y. Zhao, and H.-A. Loeliger, “Heart rate estimation in photoplethysmogram signals using nonlinear model-based preprocessing,” in *2015 Computing in Cardiology Conference (CinC)*, pp. 633–636, IEEE, 2015.
- [152] P. Sedgwick, “Pearson’s correlation coefficient,” *Bmj*, vol. 345, p. e4483, 2012.
- [153] J. M. Bland and D. Altman, “Statistical methods for assessing agreement between two methods of clinical measurement,” *The lancet*, vol. 327, no. 8476, pp. 307–310, 1986.